SLAC-PUB-1873
January 1977
(T/E)

HADRON PRODUCTION IN e^+e^- ANNIHILATION*

Vera Lüth

Stanford Linear Accelerator Center
Stanford University, Stanford, California 94305

The diversity of phenomena that have been discovered in e^+e^- annihilation in recent years has greatly stimulated new ideas in elementary particle physics, in particular, theories on particle constituents and particle dynamics. These achievements are based on significant developments in the design and construction of e^+e^- storage rings and large solid angle particle detectors.

The production of hadrons by electron-positron collisions is particularly interesting because of the simplicity of the initial state. Its dynamics are well described by the theory of quantum electrodynamics (QED). All discrete additive quantum numbers, such as electric charge, baryon number, strangeness, charm, and lepton numbers, are zero. Furthermore, to first order in the fine structure constant α, the annihilation of electrons and positrons occurs via a single virtual photon, namely a state with spin one, negative parity, negative charge conjugation, and definite mass equal to the cm energy E_{cm}. Thus, the quantum numbers of the hadronic system are well defined, and the known electromagnetic force can be used to probe the unknown structure and dynamics of the final state. This is a nearly unique situation in hadron physics. In contrast, the situation is much more complicated at proton-proton storage rings, where the angular momentum, parity and charge conjugation are unknown, the baryon number is nonzero, and not even the energy of the produced hadrons is determined.

---

*Work Supported by the Energy Research and Development Administration

(Lectures presented at the X^{th} International School for High Energy Physics in Baku, USSR, September 25 - October 5, 1976.)

This series of lectures will concentrate on recent results on hadron production by e^+e^- annihilation. Following a brief description of colliding beam devices and detectors, we shall discuss the total hadronic cross section and scale invariance as applied to e^+e^- annihilation. The third and fourth lectures will summarize the present status of the ψ spectroscopy by studying the decay modes of the narrow resonances $\psi(3095)$ and $\psi(3684)$. In the final lecture we shall discuss the recent discovery of charmed mesons.

LECTURES I, II. Nonresonant Hadron Production at SPEAR

I. Experimental Setup

II. The Total Hadronic Cross Section

III. Mean Charged Multiplicity and Energy

IV. Inclusive Momentum Spectra

V. Angular Distributions

VI. Jet Structure

VII. Summary of General Features of Hadron Production

LECTURES III, IV. The ψ Spectroscopy

I. Total and Leptonic Width of the $\psi(3095)$ and $\psi(3684)$

II. J^{PC} Assignment of $\psi(3095)$ and $\psi(3684)$

III. Search for Narrow Resonances

IV. Decay Modes of the $\psi(3095)$

V. Hadronic Decay Modes of the $\psi(3684)$

VI. New States in Radiative Decays of the ψ States

VII. Summary of ψ Spectroscopy

LECTURE V. Charm in e^+e^- Annihilation

I. Introduction

II. Discovery of Narrow States Near 1.86 GeV

III. Recoil Mass Spectra

IV. Parity Violation in D-Meson Decay

V. Evidence for Semileptonic Decays

VI. Summary

Please note that these lectures are mostly tutorial and are not intended to be a complete review for specialists. Furthermore, there will be an over-emphasis on SPEAR results, as I am a member of the SLAC-LBL collaboration. I have attempted to include contributions from DESY and Frascati, but the presentation is clearly not as balanced as might be desirable. I apologize for this and refer to a review by B. Wiik[1] for a more complete presentation of recent experimental results.

LECTURES I, II. NONRESONANT HADRON PRODUCTION AT SPEAR

I. Experimental Setup

Before we discuss the physics of hadron production by e^+e^- annihilation let us digress for a while into some experimental details.

1. e^+e^- Storage Rings

Colliding beam facilities are in many ways the most intricate accomplishments of accelerator engineering. Since the first operation of ADA (Anello di Accumulatione),[2] the pioneering single ring device at Frascati, in 1963 enormous progress has been made in the understanding of these machines. A basic introduction to the physics of colliding beams has been presented by Sands;[3] for a more advanced discussion we refer to a review by Pellegrini.[4] Here only a very brief discussion of the essential parameters like energy, luminosity, and resolution will be given.

1.1 Kinematics

In colliding beam machines high energy particles collide head-on or at small angles and thus, as a consequence of elementary mechanics, permit a very efficient use of accelerator energy. For two particles of mass m_1 and m_2, momentum $\vec{p}_1$ and $\vec{p}_2$, and

and energy E_1 and E_2 the total c.m. energy $E_{c.m.}$ is defined as

$$E_{c.m.}^2 = (E_1+E_2)^2 - (\vec{p}_1+\vec{p}_2)^2 = m_1^2+m_2^2 + 2(E_1E_2-\vec{p}_1\vec{p}_2) \quad .$$

If they collide head-on with $\vec{p}_1 = -\vec{p}_2$, $E_1 = E_2 = E_0$, one obtains $E_{c.m.} = 2E_0$.

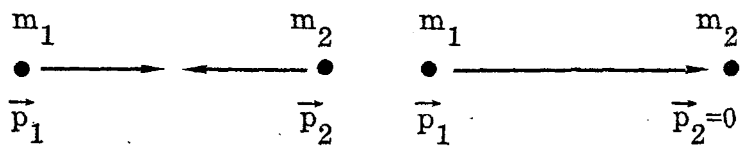

However, if the target is at rest, $\vec{p}_2 = 0$, we have

$$E_{c.m.}^2 = m_1^2 + m_2^2 + 2E_1m_2 \simeq 2E_1m_2 \quad .$$

For instance, to obtain the maximum of energy of the e^+e^- colliding beam facility SPEAR of $E_{c.m.} = 8$ GeV, it would require a 62,600 GeV e^+-beam striking a stationary target. Clearly, not a practical approach.

1.2 Luminosity

The enormous kinematic advantage provided by colliding beam devices is bought at the expense of intensity. The measure of beam intensity for a storage ring is the luminosity L. For a given reaction it is defined as the rate of interactions per unit cross section,

$$\text{Rate} = \sigma L$$

In terms of intrinsic machine parameters L is proportional to the product of the circulating beam currents I_1 and I_2, and inversely proportional to A, the cross section area of the beams

$$L \propto \frac{I_1 I_2}{A} \quad .$$

Existing storage rings have luminosities in the range of 10^{29} to 10^{31} cm^{-2} sec^{-1}. L is small compared to conventional targets because of the low density of particles stored. The maximum attainable luminosity is limited by electromagnetic forces between the particles and the ring components, the particles within the same bunch, and particles in different beams. In general, the maximum density of stored beams, and consequently L, are strongly dependent on the beam energy E_0, and may greatly vary among different machines of comparable energy. For example, at SPEAR L varies roughly as E_0^4, reaching a maximum of 10^{31} cm^{-2} sec^{-1} at $E_0 = 3.5$ GeV. For a typical cross section of 10 nb, this corresponds to interaction rates of several hundred events per hour.

1.3 e^+e^- facilities

The first high energy physics experiments with colliding beams were completed in 1965 at the 500 MeV Princeton-Stanford e^-e^- intersecting rings. Since then a variety of e^+e^- colliding beam facilities with increasing energy and luminosity has been built. A summary of some basic parameters for all e^+e^- storage rings presently in operation or under construction is given in Table I.

The highest energies have been reached by the Stanford colliding beam facility SPEAR. It is a single ring device circulating one bunch of positrons and one bunch of electrons. The bunches collide in two interaction regions that extend a few millimeters transverse and a few centimeters longitudinal to the beam. SPEAR operates at beam energies between 1.5 GeV and 3.8 GeV with luminosities in the range 10^{29} to 10^{31} cm^{-2} sec^{-1}. The energy resolution increases quadratically with energy E_0, and it is of the order of 1 MeV (standard deviation) at a beam energy of 1.5 GeV. It is dominated by quantum fluctuations in the emission of synchrotron radiation. The absolute energy of the machine is known to about 0.1%. The calibration is based on measurements of the magnetic field and particle orbits.

Two new storage-ring projects are well under way. At Orsay, space charge compensation will be used in a 4 beam device called DCI [10] that is designed to operate up to $E_0 = 1.8$ GeV with luminosities of 10^{32} cm^{-2} sec^{-1}. The Novosibirsk group is working on a project called VEPP-4 that should provide beam energies of up to 7 GeV. [5]

The next generation of colliding beam machines has reached the construction phase and is expected to begin operation in 1979. The two projects, PETRA at DESY[11] and PEP at SLAC[12] are designed for energies up to 15 GeV per beam.

Table I. e^+e^- storage rings presently in operation or under construction.

Storage Rings		Location	Start of Operation	Max. Energy per beam (GeV)	Max. Luminosity $cm^{-2}\ sec^{-1}$	Intersections	Type
VEPP II	(5)	Novosibirsk	1965	0.7	$(1-3)\times 10^{28}$	1	Single ring
ACO	(6)	Orsay	1966	0.5	5×10^{29}	4	Single ring
ADONE	(7)	Frascati	1969	1.5	$(3-6)\times 10^{29}$	4	Single ring
VEPP III	(5)	Novosibirsk	1972	2.2	2×10^{29}		Single ring
SPEAR	(8)	Stanford	1973	3.8	$10^{29} - 10^{31}$	2	Single ring
DORIS	(9)	Hamburg	1974	3.0	$10^{29} - 10^{30}$	2	Two rings, vertically superimposed
DCI	(10)	Orsay	1976	1.8	10^{32}	1	Two rings, 4 bunches space charge compensation
VEPP IV	(5)	Novosibirsk	1977	7.0	$10^{29} - 10^{32}$	1	Single ring
PETRA	(11)	Hamburg	1979	15.0	$10^{31} - 10^{32}$	6	Single ring
PEP	(12)	Stanford	1980	15.0	$10^{31} - 10^{32}$	6	Single ring

2. Detectors

The majority of results on hadron production by e^+e^- annihilation at high energies has been obtained in two large detectors.

a. The solenoidal magnetic detector at SPEAR.[13]

b. The double arm spectrometer at DORIS.[14]

These two detectors are sufficiently different in concept that it may be worthwhile to give a brief description of both of them here.

2.1 The solenoidal detector at SPEAR

The SLAC-LBL detector is schematically shown in Fig. 1. A solenoidal magnet provides a nearly uniform axial magnetic field of 4 kG in a volume 3 m long and 3 m in diameter. The detector inside covers a solid angle of 65% of 4π. The azimuthal acceptance is complete, and the subtended polar angle ranges from 50° to 130°. A particle leaving the interaction region in the center first traverses the 0.15 mm stainless steel vacuum pipe, then a pair of cylindrical scintillation counters and two proportional wire chambers that form an element of the trigger system. Continuing outwards, the particle enters 4 sets of cylindrical spark chambers, 2 gaps each, with magnetostrictive readout. Next, the trigger hodoscope provides time-of-flight measurements with a resolution of 0.4 nsec. Outside the 1 radiation length magnet coil an array of lead-scintillator shower counters (5 radiation lengths) identifies electrons. Most hadrons are absorbed in the 20 cm thick iron yoke and will not reach a set of spark chambers outside which aids muon identification. The hardware trigger requires at least two particles with momenta above 200 MeV/c in coincidence with the beams. The data analysis reconstructs tracks and vertices (momentum resolution $\Delta p/p \simeq 0.015\, p$ (GeV/c)) from the wire chamber information and selects three classes of events,

$$e^+e^- \rightarrow \text{hadrons} \tag{1}$$

$$e^+e^- \rightarrow e^+e^- \tag{2}$$

$$e^+e^- \rightarrow \mu^+\mu^- \tag{3}$$

Lepton pairs are required to have two oppositely charged prongs collinear within 10°, and each carrying more than 50% of the beam energy. Shower counter pulse heights are used to distinguish Bhabha scattering[2] from muon pair production.[3] A hadronic event is

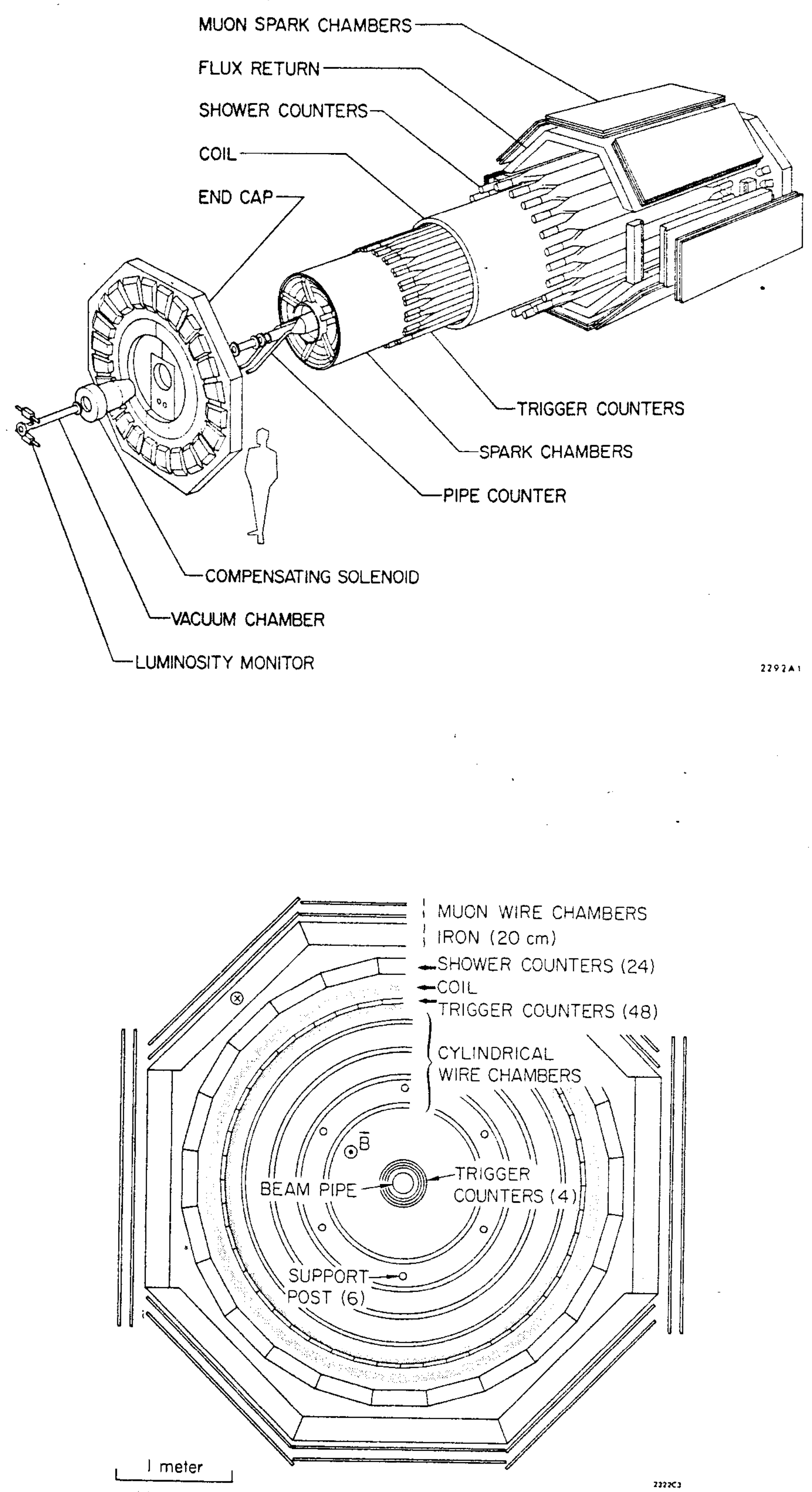

Fig. 1. The SLAC-LBL magnetic detector (a) telescoped view; (b) end view.

required to have three or more tracks forming a vertex within the luminous region of the machine. Two prong events are also included in the hadron event sample provided the tracks are acoplanar with the beams by at least 20° and have momenta exceeding 300 MeV/c. The purpose of these selection criteria is to eliminate various electromagnetic backgrounds.

2.2 The double-arm spectrometer at DORIS

One of the two interaction regions of DORIS is occupied by the double arm spectrometer DASP which was built by a collaboration of groups from Aachen, Hamburg, Munich, and Tokyo. DASP consists of a large aperture nonmagnetic detector surrounding the beam pipe, and a pair of identical magnetic spectrometers on either side of the interaction region covering a limited solid angle of 0.45 sterad each (Fig. 2a, b).

A charged particle emitted at the interaction point traverses the following detectors before reaching the magnet gap: a scintillation counter close to the beam pipe, a second scintillation counter that starts the time-of-flight measurement, a pair of proportional chambers, a third scintillator for triggering and a wire spark chamber. Behind the magnet the particle trajectory is measured by six enormous (5.6×1.7 m^2) double plane spark chambers with 1 mm wire spacing. For a maximum field of 11 kG a resolution of $\pm 0.7\%$ has been obtained for a particle of 1 GeV/c momentum.

Particles are identified using time-of-flight, shower and range information. The time-of-flight counters are mounted at an average distance of 4.7 m and have a resolution of 0.26 nsec. This allows to distinguish pions from kaons for momenta up to 1.8 GeV/c, and kaons from protons up to 3 GeV/c. Hadrons and muons are separated from electrons by 6.2 radiation length thick shower counters. An electron rejection level of 10^{-3} has been achieved by appropriate pulse-height cuts. Muons are positively identified by their range in a 90 cm thick, segmented iron absorber. Electron-hadron separation has recently been improved by the installation of freon filled threshold Cerenkov counters on either side of the beam pipe.

The inner detector shown in Fig. 2b is located in the free space between the magnets. It is made out of several layers of proportional chambers, scintillation counters, proportional tube counters, and shower counters. This part of the detector covers 70% of 4π and

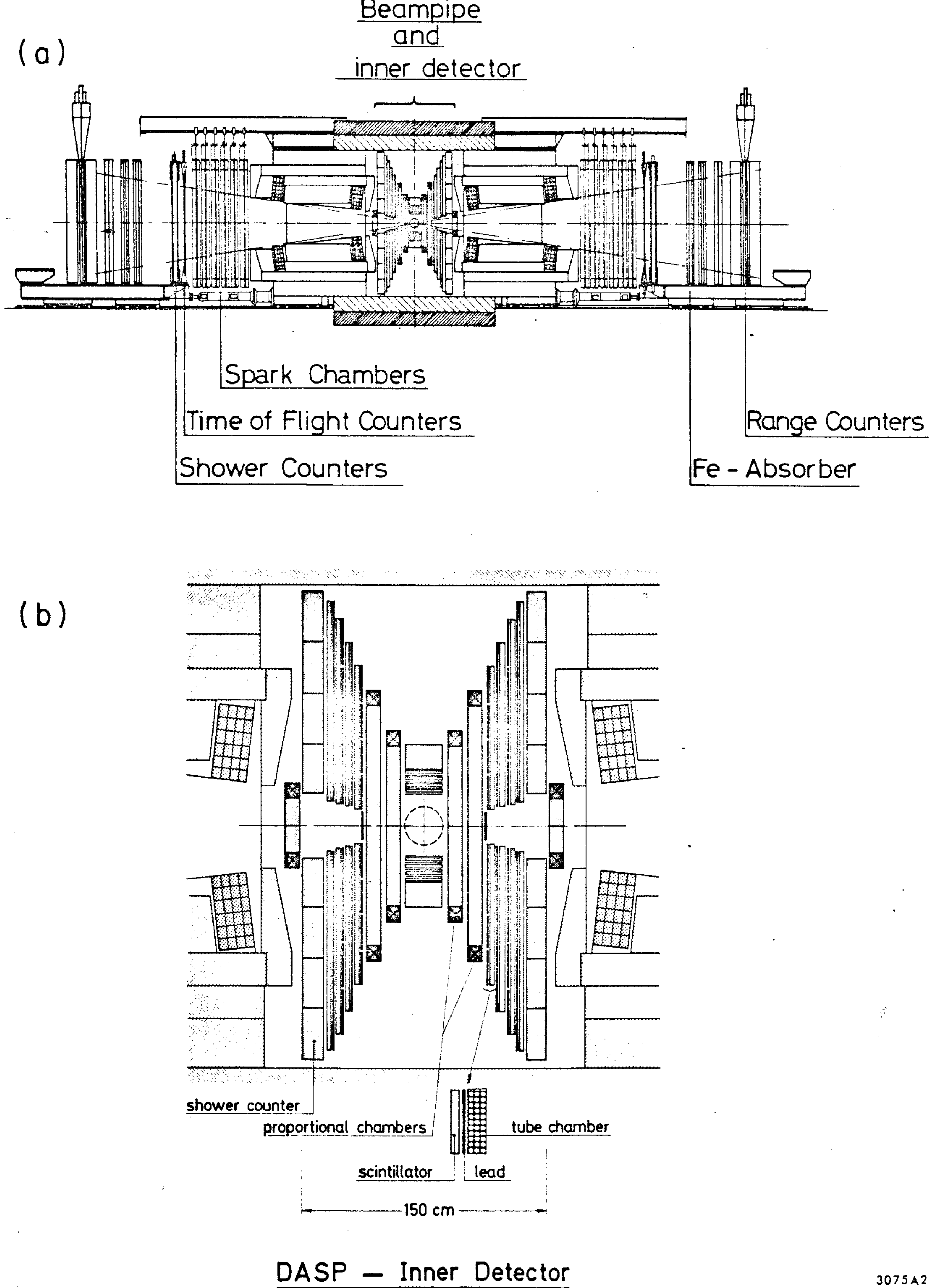

Fig. 2. The double arm spectrometer at DORIS (a) top view; (b) side view of the inner detector.

is well suited for photon detection. The direction of a shower is determined to about $\pm 2^{\circ}$, the energy resolution is around 30% for a 1 GeV photon. The detection efficiency for a 50 MeV photon is roughly 50%.

2.3 Comparison

The design concepts of the two big detectors are quite different. The large solid angle and good resolution makes the solenoidal detector well suited for measurements of total cross sections, charged multiplicity, exclusive final states. The strong features of DASP are good photon detection, and excellent identification of charged particles.

The major advantage of the SLAC-LBL group lies in the early start of operation of SPEAR in 1973, its good luminosity and large energy range.

II. The Total Hadronic Cross Section

The simplest property of hadron production by e^+e^- annihilation that can be studied experimentally is the total hadronic cross section σ_{had}. Accepting the traditional concept that the electron does not directly couple to hadrons, the reaction proceeds dominantly via the exchange of a single, timelike photon between the lepton and the hadron system (Fig. 3a). Higher order photon exchange processes will generally produce particles at small angles to the beam and are at present energies of limited importance to hadron production.

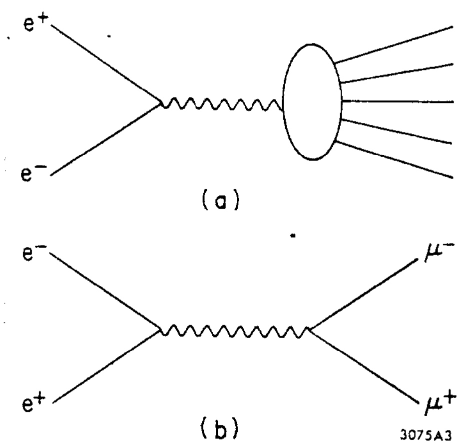

Fig. 3. Feynman diagrams for one-photon exchange
(a) $e^+e^- \to$ hadrons;
(b) $e^+e^- \to \mu^+\mu^-$.

If we restrict ourselves to the one-photon exchange as the main process for hadron production by e^+e^- annihilation (Fig. 3a), we see that all the ignorance is hidden in the cross hatched region of the photon-hadron vertex, whereas the lepton-photon vertex is well understood in terms of QED. A comparison with the diagram for muon pair production in Fig. 3b makes it obvious that a quantity of more direct interest than the total hadronic cross section, σ_{had} is R, the ratio of hadron production to muon pair production,

$$R = \frac{\sigma_{had}}{\sigma_{\mu\mu}} \qquad \text{with} \qquad \sigma_{\mu\mu} = \frac{4\pi\alpha^2}{3s} \quad .$$

Here s is the square of the mass of the virtual photon and α the fine structure constant.

1. Theoretical Predictions

The most fundamental theoretical idea in e^+e^- annihilation is that of scaling. It says that the hadronic cross section should vary like 1/s for large s or stated differently, the ratio R is expected to approach a constant value. What "large" means is not well specified; in general it means large compared to any mass or energy involved. The simplest argument to predict scaling is one of dimensional analysis. It says that at large energies the only unit of length remaining is $s^{-1/2}$, thus a cross section must behave like s^{-1}.

A by far more appealing, intuitive picture that arrives at the same answer is the parton model.[15, 16] In this picture hadrons are built out of constituents, the partons, which have point-like coupling to the electromagnetic current. As indicated schematically in Fig. 4, hadron production is viewed as the production of pairs of parton-antiparton that subsequently form hadrons. Partons of spin 1/2 couple to the virtual photon in the same way as muons, except for differences in electric charge. At high energies, where hadron masses can be neglected, the total hadronic cross section is equal to the sum of the individual parton pair cross sections which are proportional to $\sigma_{\mu\mu}$. The ratio $R = \sigma_{had}/\sigma_{\mu\mu}$ therefore depends only on the sum of the squares of the parton charges Q_i,[17]

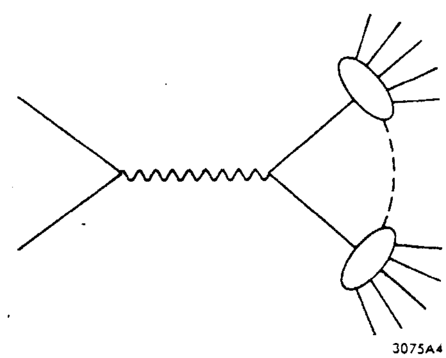

Fig. 4. Hadron production in the simple parton model.

$$R = \sum_{J=1/2} Q_i^2 + \frac{1}{4} \sum_{J=0} Q_j^2 \quad . \tag{1}$$

The summations run over spin-1/2 and spin-0 partons, respectively. Given a fixed number of partons having specified spin, mass, and charge, R is a constant, and hadron production is said to exhibit scaling. Whenever a threshold for the production of higher mass constituents is reached there should be an upward step in R proportional to Q_i^2 for the new parton. The value of R in any given energy range will provide information about the number and the properties of the partons. Up to now, the existence of partons is purely hypothetical, but like the ether in the 19th century, seemed to be necessary to explain the propagation of light, partons explain a great deal of high energy data. The ether was never found and nobody needs it anymore, so maybe someday we shall do without partons.

In this particular aspect partons are associated with quarks; their properties are listed in Table II. In the conventional Gell-Mann/Zweig(18) spin-1/2 quark model there are only 3 different flavors, u, d, s, and one obtains according to Eq. (1),

$$R_{uds} = (2/3)^2 + (1/3)^2 + (1/3)^2 = 2/3 \quad .$$

Table II. Quarks and their quantum numbers in SU_4

Quark	I_z	Q	B	S	C	Y
u(p)	+1/2	+2/3	1/3	0	0	+1/3
d(n)	-1/2	-1/3	1/3	0	0	+1/3
s(λ)	0	-1/3	1/3	-1	0	-2/3
c(p')	0	+2/3	1/3	0	+1	-2/3

I_z, Q, B, Y, S, and C stand for the third component of isotopic spin, charge, baryon number, hypercharge, strangeness and charm. Y and S are connected by Y=S+B-C and the Gell-Mann/Nishijima formula reads $Q=I_z+1/2\,(B+S+C)$.

More recently, a three-valued quantum number called color was introduced to correct the spin-statistics for three-quark baryons. The concept of color triples the number of quarks and

$$R_{uds,\,color} = 2 \quad .$$

The first suggestions of a fourth quark with an additional flavor, called charm, were based on an elegant lepton-quark symmetry. Later, their existence was shown to be necessary within the framework of a gauge theory of weak currents.(19) The charm quark with Q=2/3 helps to increase R to

$$R_{udsc} = 10/9 \qquad \text{or} \qquad R_{udsc,\,color} = 10/3 \quad .$$

2. Experimental Results

The very first measurements of hadron production in e^+e^- annihilation at the laboratories of Frascati,[21] Orsay[22] and Novosibirsk[23] indicated that the cross sections were relatively large, i.e., comparable to μ-pair production. In Fig. 5

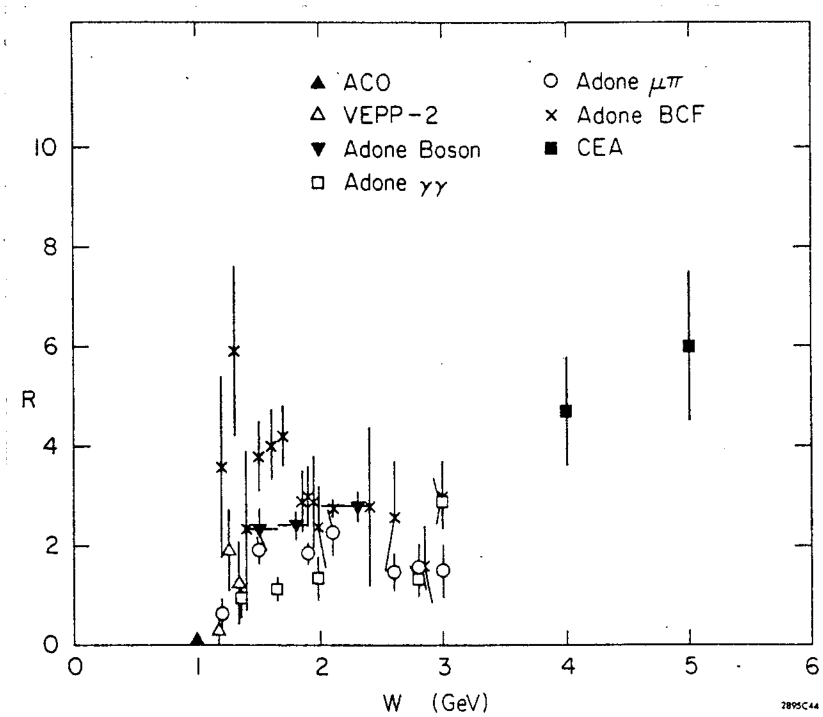

Fig. 5. Early results on R versus c.m. energy.[21]

measurements of the variable R, the ratio of the total hadronic cross section σ_{had} to the μ-pair cross section $\sigma_{\mu\mu}$, are presented for data available at the 1973 Conference at Bonn. The two high energy points of the CEA group[24] were, at first, met with considerable skepticism, and it took another year until the SLAC-LBL collaboration at SPEAR confirmed the observation that R is significantly higher above $E_{c.m.} = 4$ GeV. The large solid angle and good statistical accuracy of this most recent experiment have substantially reduced the experimental uncertainties. In the following, we shall discuss these measurements in some detail.[26, 25]

The total cross section for hadron production σ_{had} is obtained as the sum of all detected hadronic events divided by the time-integrated luminosity $\int Ldt$ (Bhabha scattering observed in the detector is used for normalization) and corrected for the average detection efficiency,

$$\sigma_{had} = \frac{\sum_i M_i}{\bar{\epsilon} \int L dt} \quad . \tag{2}$$

M_i denotes the number of observed events with i charged tracks, and is related to the number of events produced N_j with j charged prongs by

$$M_i = \sum_j \epsilon_{ij} N_j \quad , \tag{3}$$

where ϵ_{ij} is the efficiency for detecting an event with i prongs when it was produced with j charged particles. The ϵ_{ij} are usually computed by Monte Carlo techniques. Known properties of the detector such as solid angle, trigger biases, cuts in the data analysis, and a plausible model of the final states are necessary ingredients to the simulation. The parameters of the model are adjusted to obtain agreement with the observed charged multiplicity and the observed angular and momentum distributions. Knowing the coefficients ϵ_{ij}, Eq. (3) can be inverted by a maximum likelihood method to obtain the produced multiplicity distribution N_j. The average detection efficiency $\bar{\epsilon}$ is then evaluated as

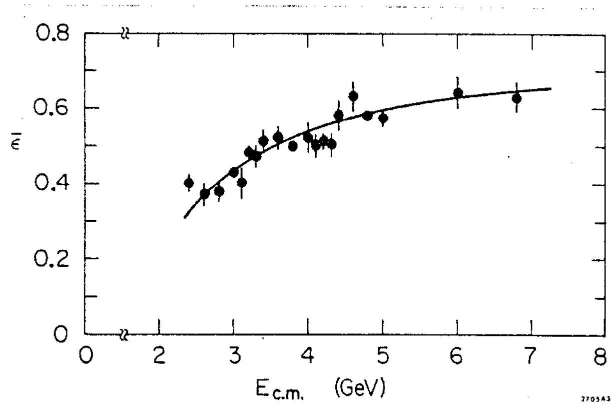

Fig. 6. Average detection efficiency for multihadronic final states vs. c.m. energy. The points are determined by the "unfold" procedure, the curve is an analytic fit to the points.(25)

$$\bar{\epsilon} = \sum_i M_i / \sum_j N_j \quad . \tag{4}$$

The above procedure makes optimum use of the experimental data, thus minimizing the model dependence. $\bar{\epsilon}$ as a function of c.m. energy is given in Fig. 6. The curve represents a smooth fit to the results obtained from the unfold. $\bar{\epsilon}$ varies from 40% at 2.5 GeV to 65% near 7 GeV.

The complete measurement of the hadronic cross section σ_{had} over the whole c.m. energy range of the SPEAR machine from 2.4 GeV to 7.8 GeV as first presented at the 1976 Lepton-Photon Symposium(25) is shown in Fig. 7. The data have been corrected for background from beam-gas interactions (<5%) and contamination from two photon processes (< 2%). Radiative corrections have been applied to remove the tails of the narrow

ψ resonances. The errors include statistical errors and systematic point-to-point errors (8-10%). There is an overall uncertainty of ±10% in the normalization and there could be an additional variation of up to 10% from the lowest to the highest energy due to incorrect modeling in the Monte Carlo.

The energy dependence of the hadron production rate is more clearly displayed in the variable R, the ratio of hadron to μ-pair production cross section (Fig. 8). Below 3.5 GeV,

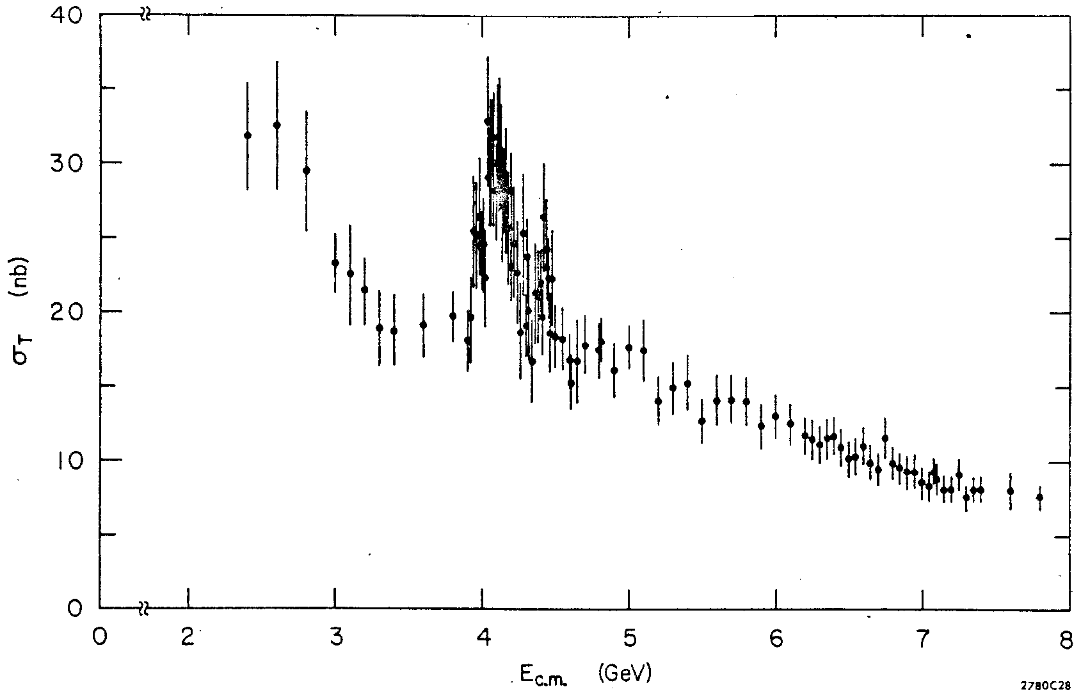

Fig. 7. Total hadronic cross section versus c.m. energy.[25]

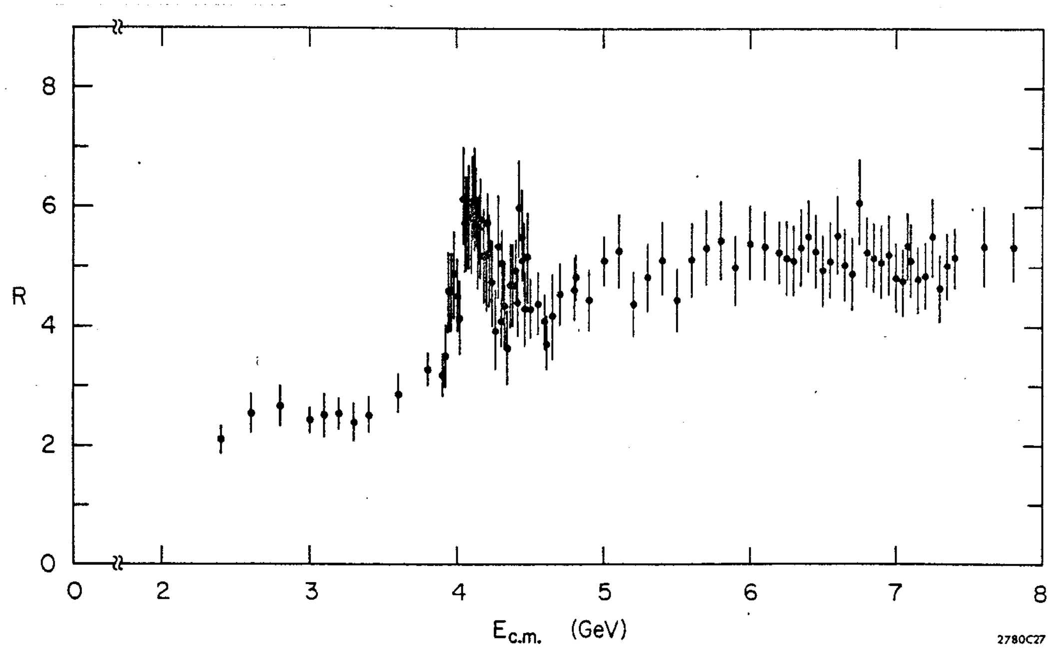

Fig. 8. The ratio of the hadronic to μ-pair production cross sections versus c.m. energy.[25]

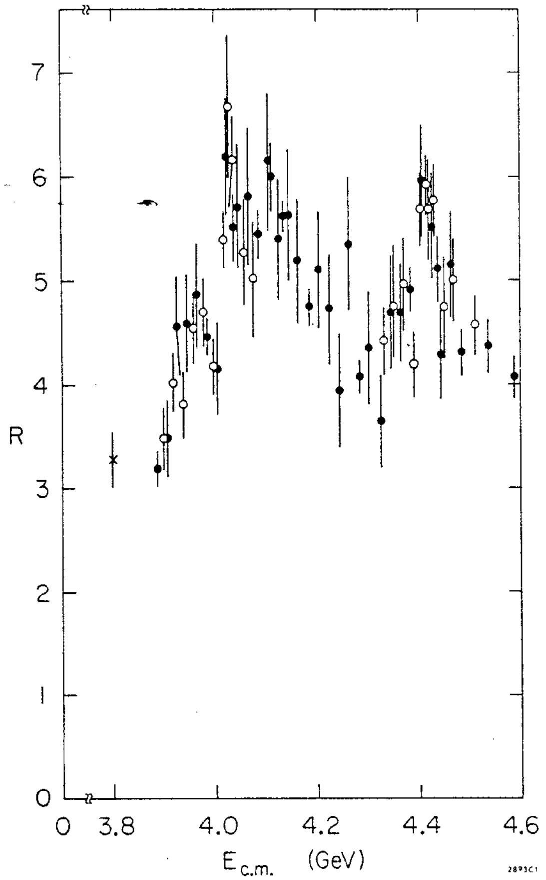

Fig. 9. R vs. c.m. energy including more recent data.(24)

R is approximately constant with a value around 2.5. Above 5 GeV, R is approximately constant with a value about twice that of the lower energy region. In between, around 4 GeV, there is a rather complex structure which we are only beginning to resolve.

During the last year a considerable effort was made to obtain a more detailed picture of this transition region (Fig. 9). What at first looked like a broad enhancement at 4.15 GeV, has now been resolved into a resonance at 4.4 GeV, a broad shoulder near 3.95 GeV, an extremely sharp rise just above 4.0 GeV and possibly several narrow peaks near 4.1 GeV. Though there exist more data now, considerably more will be required to determine the details of this threshold region. For a number of reasons it is very difficult to tell the number of states and obtain the widths and integrated cross sections. First, the shape of the nonresonant background is not known and there may be interference with this background. Secondly, the resonance may strongly interfere with each other, and thirdly, in the transition region between the low and high energy plateaus threshold production of new particles may badly distort the Breit-Wigner shapes. The 4.1 region is most likely not a single state; the peak at 4.4 GeV can be well fit to a Breit-Wigner function.(27) Resonances in e^+e^- annihilation will be discussed in Lecture III.

The data are consistent with the parton model if new degrees of freedom, such as heavier quarks, are being excited in the 4 GeV region. Above 5 GeV the experimental value of R is roughly 5 compared to the prediction of 3-1/3 by a four quark (u, d, s, c) model including color. Thus almost 2 units of R are unaccounted for. In the lower energy region the value of R is approximately 2.5 and compatible with quark model predictions of R=2 for 9 quarks with 3 "flavors" and 3 "colors". But even if we take these data at face value and assume that the prediction of this conventional quark set is uniformly too low by 20%, then we would get a value of R=4.2 above threshold for charmed particles and have still one unit of R unexplained. In the parton model this means that additional fermions, either quarks or leptons, must be present above 4 GeV, leading to $\Delta R \sim 1$-2.

A present, two possibilities are being discussed. (1) An additional unit of R could be added for any heavy lepton that would contribute to the multiprong events. The anomalous $e\mu$-events(28) may be responsible for such an increase in R, if their parent particles are leptons. (2) Additional quarks could be excited in the c.m. energy range between 4 GeV and 5.5 GeV causing several small increases in R. The present data are not accurate enough to exclude any of these hypotheses.

III. Mean Charged Multiplicity and Energy

The mean charged multiplicity $\langle n_{ch} \rangle$ of the hadronic final state is obtained from the observed multiplicity as a by-product of the Monte Carlo analysis that was used to determine $\bar{\epsilon}$. The data from experiments at ADONE, (21) CEA, (24) and SPEAR(25) are presented in Fig. 10. The energy dependence is consistent with the logarithmic rise of the form

$$\langle n_{ch} \rangle = a + b \ln(s)$$

where a=1.93 and b=0.75 and s is the square of the c.m. energy in units of GeV^2. A similar

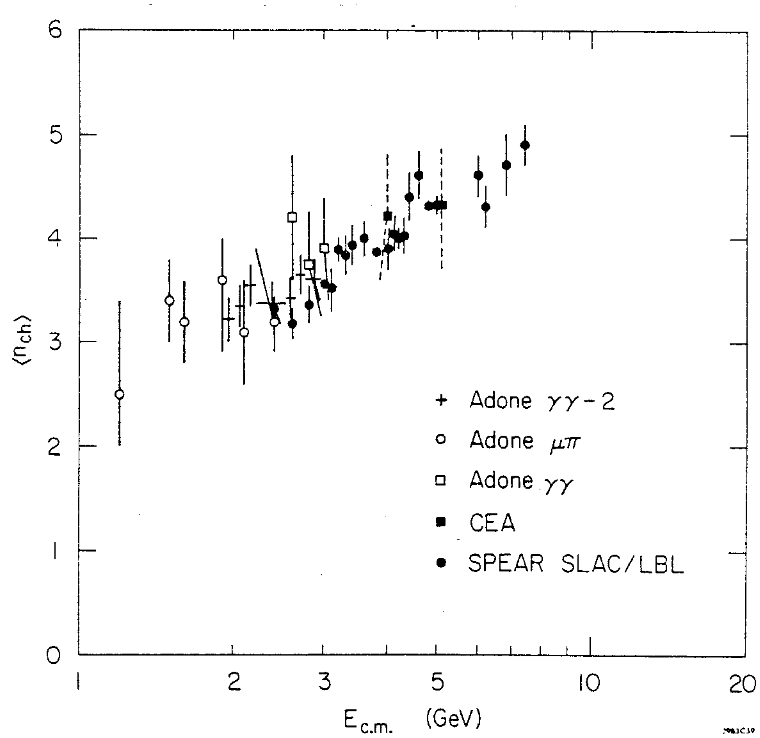

Fig. 10. Mean charged multiplicity $\langle n_{ch} \rangle$ vs. c.m. energy. Data from ADONE,(21) CEA,(24) and SPEAR.(25)

parametrization fits multiplicity growth in hadron-hadron interactions.[29] There is very little evidence for any break in the distribution around 4 GeV, although the errors are rather large.

The mean fraction of the c.m. energy carried by charged particles in the hadronic final state is shown in Fig. 11. Pion masses have been assigned to all tracks. The data have been corrected for losses of charged particles due to acceptance and trigger biases. The charged energy fraction decreases from 60% to 50% over the measured energy range. The fact that it is 60% rather than 2/3 at the lowest energy is probably a consequence of the production of kaons, nucleons, etas, etc. in addition to pions, though the difference is somewhat bigger than expected. It is, however, not understood why the fraction of energy appearing in charged particles should fall with c.m. energy. Decays of heavy leptons should not influence this distribution appreciably, since they are expected to contribute primarily two charged prongs; and only three or more prong events were considered in this analysis.

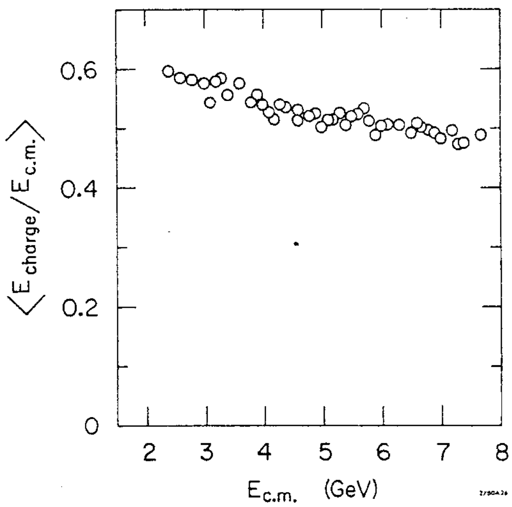

Fig. 11. Ratio of energy carried by charged particles to total energy. All particles are assumed to be pions.[25]

IV. Inclusive Momentum Spectra

The inclusive process

$$e^+e^- \rightarrow h + \text{anything} \,, \tag{1}$$

where h is any hadron, can be related to deep inelastic electron scattering

$$e^-p \rightarrow e^- + \text{anything} \tag{2}$$

by crossing as illustrated in Fig. 12. In the approximation that the annihilation proceeds via one-photon exchange the most general form for reaction (2) can be written as

$$\frac{d^2\sigma}{dx d\Omega} = \frac{\alpha^2 \beta}{4s} \left[W_1(x,s) \left\{ 1 + \cos^2\theta \right\} + W_0(x,s) \sin^2\theta \right] \tag{3}$$

where

$$x = 2p_h \cdot q/s = 2E_h/E_{c.m.} \qquad \beta = p_h/E_h$$

and θ is the angle between the outgoing hadron and the incident positron, q is the four-momentum of the photon, and p_h and E_h are respectively the momentum and the energy of the detected hadron, β is the velocity of the hadron. Such a decomposition is convenient because all possible information is contained in the structure functions W_0 and W_1. To understand the meaning of this parametrization let us recall the basic properties of the annihilation process at high energies.

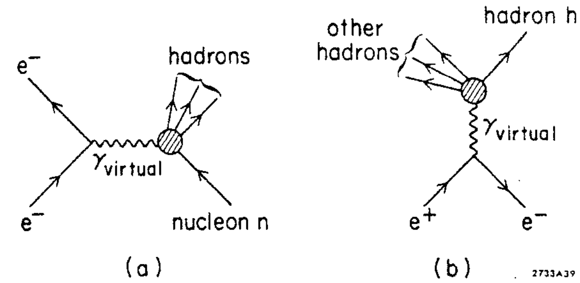

Fig. 12. (a) Diagram for $e^-p \to e^- +$ anything by exchange of a space-like photon. (b) Diagram for $e^+e^- \to$ hadrons + anything by single time-like photon annihilation.

For a storage ring experiment the kinematics are very simple if one neglects radiative losses. Electrons and positrons have equal, but opposite momenta, so the laboratory and the center-of-mass system coincide. The mass of the time-like photon $\sqrt{s}$ equals the total energy $E_{c.m.}$. Since a fermion-antifermion pair have opposite intrinsic parity, the e^+e^- pair must be in an angular momentum state ℓ=0 or ℓ=2, and therefore be in a triplet state with aligned spins $\left({}^{2s+1}L_j = {}^3S_1\right)$ to form a virtual photon with the quantum numbers $J^{PC} = 1^{--}$. In the ultra-relativistic limit, $m_e/E_0 \to 0$, electron and positron spins are aligned with the momentum either in the same or the opposite direction, and an electron of a given helicity will only couple to a positron of opposite helicity. Consequently,

the electromagnetic current is completely confined to the plane perpendicular to the beam line, i.e., it has no component parallel to the beam.

With this in mind, we can write the inclusive angular distribution for a particle h in reaction (1) as

$$\frac{d\sigma}{dz} \sim \sum_{\lambda\mu} |A_{\lambda\mu} d^1_{\lambda\mu}(z)|^2 \qquad z = \cos\theta \tag{4}$$

here $d^J_{\lambda\mu}$ are the helicity functions, λ and μ the helicities of the initial and final states, respectively, and $A_{\lambda\mu}$ some complex amplitudes. Using the properties of the $d^J_{\lambda\mu}$ and the fact that the photon couples only to helicity ± 1, Eq. (4) can be reduced to

$$\frac{d\sigma}{dz} \sim \left(A^2_{11} + A^2_{-1-1}\right) |d^1_{11}(z)|^2 + A^2_{10} |d^1_{10}(z)|^2$$
$$+ \left(A^2_{1-1} + A^2_{-11}\right) |d^1_{1-1}(z)|^2 .$$

Parity conservation implies that terms linear in $\cos\theta$ must vanish, and one obtains

$$\frac{d\sigma}{d\cos\theta} \sim W_1\left\{|d^1_{11}|^2 + |d^1_{1-1}|^2\right\} + W_0 |d^1_{10}|^2$$
$$\sim W_1\left\{1 + \cos^2\theta\right\} + W_0 \sin^2\theta$$

where the real functions W_1 and W_0 represent the probability that the final state has net helicity one and zero, respectively, along the direction of momentum. Let us consider as an example two different two-body final states: The production of μ-pairs proceeds (in the limit $m_\mu/E \to 0$) entirely with the spin aligned with the muon momentum, i.e., $W_0=0$ and only W_1 contributes to the cross section

$$\frac{d\sigma_{\mu\mu}}{d\cos\theta} = \frac{\pi\alpha^2}{2s}(1+\cos^2\theta)$$

For the production of two spin-0 particles like pions or kaons, the component of angular momentum along the direction of motion is zero, hence $W_1=0$. The unknown charge structure is contained in the form factor $F(s)$ and the cross section becomes

$$\frac{d\sigma_{\pi\pi}}{d\cos\theta} = \frac{\pi\alpha^2}{4s} |F_\pi(s)|^2 \sin^2\theta$$

The decomposition of the differential cross section into two structure functions is completely analogous to deep inelastic scattering, where we replace s by $-q^2$ in the definition of x, and h corresponds to the target proton rather than an outgoing particle. The major result of experiments on deep inelastic scattering was the observation that for large q^2 the structure functions merely depend on x rather than x and s. This is the manifestation of scaling as suggested by Bjorken.[30] The similarity between deep inelastic electron scattering and e^+e^- annihilation is very appealing, though the structure functions for space-like and time-like photons are not necessarily simply related. If at sufficiently high energy W_0 and W_1 become functions of only one dimensionless quantity x, the cross section $d\sigma/dx$ will decrease like $1/s$ with energy; the ratio R will be constant (Eq. (3)).

Single particle inclusive momentum distributions have been studied at SPEAR for large samples of multihadron final states recorded at different c.m. energies. The data are presented in terms of the scaling variable x defined as

$$x = 2p/E_{c.m.} \tag{5}$$

This particular definition was chosen because the momentum p of a particle, not its energy is measured. The results are presented for the quantity $s\,d\sigma/dx$ (we use $s = E^2_{c.m.}$) which is expected to scale at high energies. The integral for this function can be written as

$$\int s \frac{d\sigma}{dx}\, dx = \langle n_{ch} \rangle \cdot s \cdot \sigma_{had} \tag{6}$$

So the area under $s\,d\sigma/dx$ must increase with s, because both the mean charged multiplicity and $s \cdot \sigma_{had}$ increase.

The data are presented in Fig. 13. The errors given are purely statistical, systematic errors could be as large as 20% for the highest and the lowest values of x varying smoothly with x. The spectra for all three energies rise sharply at small values of x, peak below x=0.2, and then fall with increasing x. The areas under the curve grow significantly with $E_{c.m.}$ as expected from Eq. (6), but almost all of the increase is in the low x region. Above x=0.5 the spectra are equal within the experimental errors, and thus are consistent with Bjorken scaling. To study scaling more critically $s\,d\sigma/dx$ is plotted versus $E_{c.m.}$ for several intervals in x in Fig. 14. Near x=0.1, i.e., for small β, there is no scaling; above x=0.2, however, the data for fixed values of x are roughly independent of the c.m. energy for $E_{c.m.}$ greater than 4 GeV. For $x \geq 0.4$, the data scale to within 20% over the entire energy

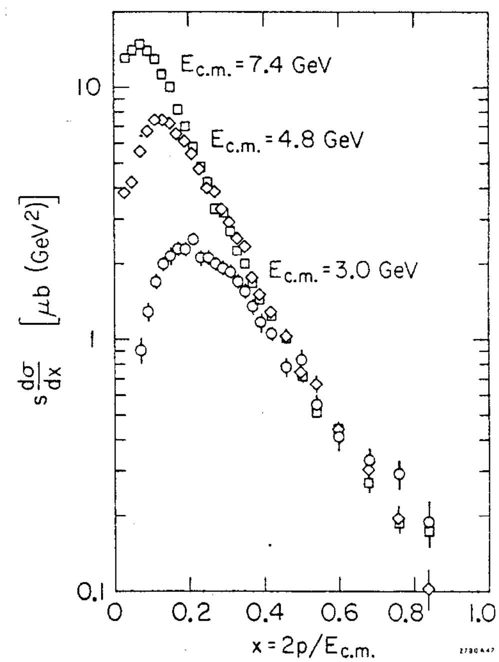

Fig. 13. Test of scaling. $s\,d\sigma/dx$ for various c.m. energies.[25]

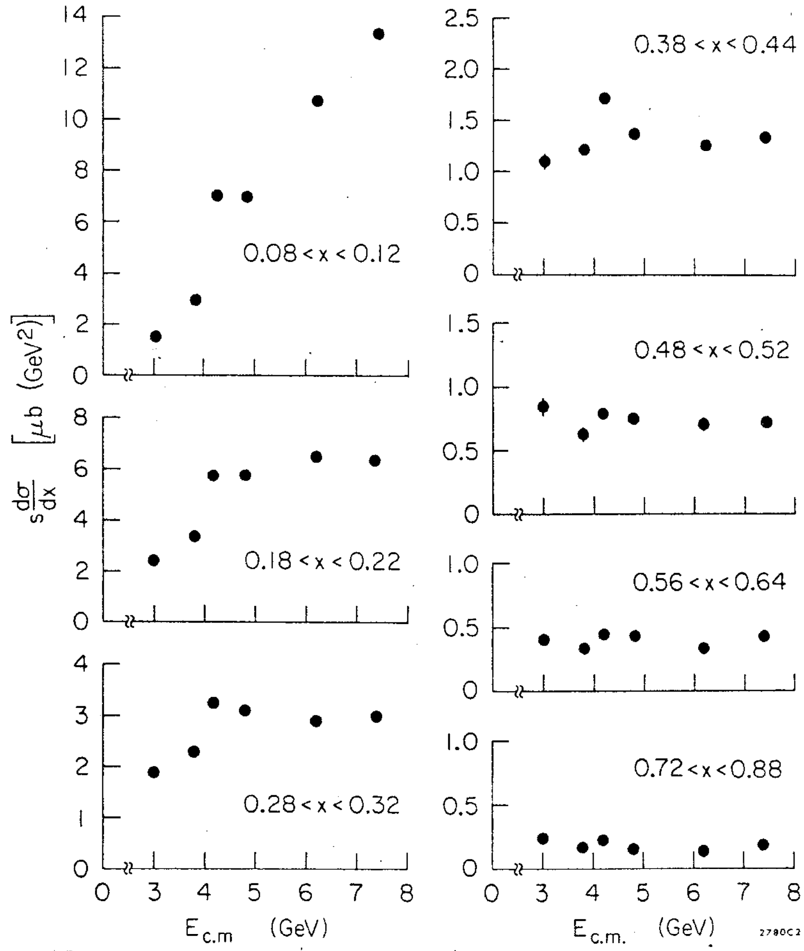

Fig. 14. Test of scaling. $sd\sigma/dx$ vs. c.m. energy for various regions of x.[25] Bjorken scaling implies that $sd\sigma/dx$ is independent of $E_{c.m.}$ for fixed values of x.

range. This is rather remarkable considering that the ratio R changes dramatically around 4 GeV. It suggests that the "new physics" is confined to relatively small values of x.

V. Angular Distributions

Let us return to the structure functions W_1 and W_0, as they contain all information obtainable from a single particle inclusive measurement. In principle, W_0 and W_1 can be separated because of the different angular dependence; W_1 goes with $1+\cos^2\theta$ and W_0 goes with $\sin^2\theta$, where θ is the angle between particle momentum and the incident positron. In practice, this is not easy because of the limited coverage of the detector with $|\cos\theta|<0.6$. The inclusive polar angle distributions for multiprong events as observed by the magnetic detector is shown in Fig. 15. The tracks are quite uniformly distributed for $E_{c.m.}=4.8$ GeV; at 7.4 GeV prongs with $x>0.3$ indicate some evidence for a $\cos^2\theta$ term while the low x prongs do not.

Fortunately, there is another means of studying $\vec{W}_1$ and W_0, namely through polarization of the beams. In high energy storage rings electrons and positrons will become polarized due to the emission of synchrotron radiation. A complete discussion of this phenomenon, far beyond the scope of these lectures, was first given by Baier;[31] a more pedagogical treatment can be found in a recent review by Jackson.[32] In the absence of depolarizing effects, the polarization of each beam builds up in time according to

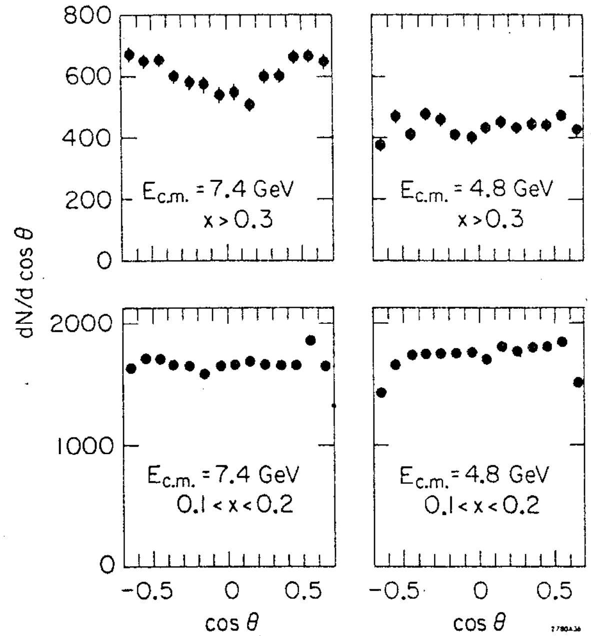

Fig. 15. Angular distributions in $\cos\theta$ for final state hadrons in ≥ 3-prong events for two intervals of x at different c.m. energies.[25]

$$P(t) = P_0(1-e^{t/\tau}) \quad , \tag{1}$$

where P_0 is the maximum polarization, theoretically $P_0=0.925$. The characteristic time τ depends on the radius and magnetic bending field of the storage ring. For SPEAR τ (in minutes) is given by

$$\tau = 15\left[\frac{7.4}{E_{c.m.}}\right]^5 \quad . \tag{2}$$

The positrons (electrons) are polarized parallel (antiparallel) to the magnetic guide field. At low energies, P can be neglected, but at high energies τ is short compared to typical storage times, and polarization effects become important.

To calculate the inclusive angular distribution for polarized beams lets use an elegant, "labor saving trick for theorists".[33] This trick is based on the insight that given the one-photon approximation the cross section for any specific final state for completely polarized beams can be obtained from measurements with unpolarized incident beams. Thus, there is no new information obtainable. The algorithm is as follows: Suppose one knows the analytic form for a cross section $\sigma_f(z)$ for unpolarized beams along the z-axis.

Then the cross section for the final state f for beams polarized along the y-axis may be calculated according to

$$\sigma_f(z, 1) = \sigma_f(z, 0) + \sigma_f(x, 0) - \sigma_f(y, 0) \quad . \tag{3}$$

The first argument specifies the direction of the beam, the second indicates the polarization. The result for an arbitrary polarization P for each beam is easily derived

$$\sigma_f(z, P) = \sigma_f(z, 0) + P^2 \left\{\sigma_f(x, 0) - \sigma_f(y, 0)\right\} \quad . \tag{4}$$

If we apply to Eq. (IV. 3) the prescription given in (4), we obtain for the inclusive cross section

$$\frac{d^2\sigma}{dx d\Omega} = \frac{\alpha^2 \beta}{4s} \left[(W_1 + W_0) + (W_1 - W_0) \left\{\cos^2\theta + P^2 \sin^2\theta \cos 2\phi\right\}\right] \tag{5}$$

Thus, by measuring the azimuthal distribution and the beam polarization P, one can determine the coefficient of the $\cos^2\theta$ term,

$$a = \frac{W_1 - W_0}{W_1 + W_0} \qquad -1 < a < +1 \quad .$$

Going back to the two extreme examples mentioned before we get with a=1

$$\frac{d\sigma_{\mu\mu}}{d\Omega} \sim 1 + \left\{\cos^2\theta + P^2 \sin^2\theta \cos 2\phi\right\}$$

and with a=-1

$$\frac{d\sigma_{\pi\pi}}{d\Omega} \sim \sin^2\theta \left\{1 - P^2 \cos 2\phi\right\}$$

Thus, in μ-pair production we expect a maximum at $\phi=\pi/2$ and a minimum at $\phi=0$ and π. For the spin-0 case exactly the opposite is true, namely the ϕ distribution is maximum at $\phi=0$ and π, but minimum at $\phi=\pi/2$. All other possibilities are intermediate between the two extremes. For example, when $W_0=W_1$ and therefore a=0, the angular distribution is isotropic.

The inclusive azimuthal distribution for particles with $x > 0.3$ and $|\cos\theta < 0.6|$ are given in Fig. 16 for two different c.m. energies. At 7.4 GeV the data show evidence for a strong $\cos 2\phi$ term, at 6.2 GeV the azimuthal distribution is completely flat. At this energy no polarization is expected due to a spin precession resonance of the machine.[34]

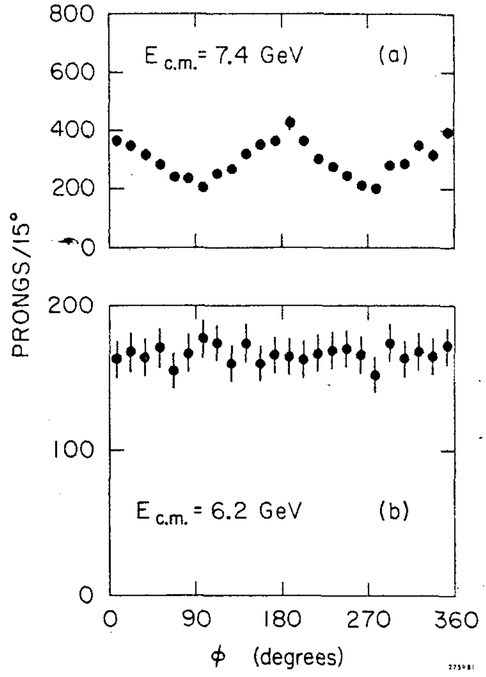

Fig. 16. Azimuthal distribution of hadrons with $x > 0.3$ and $|\cos\theta| < 0.6$. $\phi=0$ is the horizontal plane. [25]

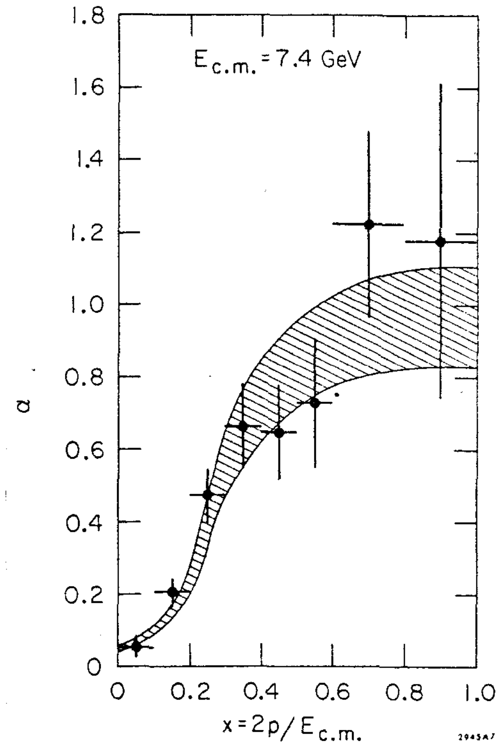

Fig. 17. Parameter α vs. x at 7.4 GeV. The shaded area represents the prediction of the jet model. [34]

The inclusive angular distribution in ϕ and θ at 7.5 GeV have been fitted to the function given by Eq. (6) to determine the structure functions W_0 and W_1. The average value of P^2 is obtained from the μ-pair data that had been recorded simultaneously, $P^2=0.46\pm0.05$. The values of a as a function of x are given in Fig. 17. Particles with low x are produced isotropically, a=0, while hadrons of large x are produced predominantly in a helicity 1 state, a=1, i.e., through a transverse coupling to the virtual photon. This transverse coupling displayed by hadrons is characteristic of the production of pairs of spin 1/2 particles and is expected in the spin 1/2 parton model where hadrons are produced via a parton-antiparton state.

VI. Jet Structure

With the mean charged multiplicity increasing slowly with the c.m. energy, like ln(s), and with momentum distributions scaling for large x, hadrons produced in e^+e^- annihilation seem to resemble hadrons produced in hadron-hadron interactions. This suggests that like in conventional hadron physics the inclusive cross section may be factorizable into a scaling part for the longitudinal momenta and part limiting the transverse momenta.

In contrast to hadron-hadron collisions where the principle axis is given by the beam particles, e^+e^- annihilation proceeds via an intermediate photon and the "jet" axis cannot be along the beam direction but must follow an angular distribution of the form given by Eq. (5), Section V.

Jet structure in hadron final states is one of the important predictions of the parton model.[16] An intuitive picture of hadron production by partons was given in Fig. 4. A pair of partons is produced and subsequently emits hadrons. At sufficiently high energies a jet-like structure arises due to limited transverse momenta of the hadrons relative to the parton direction of motion.

Experimentally the jet axis is defined as the direction that minimizes the sum of the squares of the transverse momenta. The procedure for finding jets was developed by G. Hanson[34] following a suggestion by Bjorken and Brodsky.[35] For each event, a parameter called sphericity S is computed as a measure of the jet-like character. It is defined as

$$S = \frac{3\sum_i p_{\perp i}^2}{2\sum_i p_i^2} \qquad 0 < S < 1 \quad ,$$

where the summations run over all measured charged particles in the event, p_i is the particle momentum, $p_{\perp i}$ the momentum perpendicular to the jet axis. S is small for jet-like events and approaches 1 for events with isotropic particle distributions. Sphericity distributions for data taken at different c.m. energies are given in Fig. 18.

Since the SLAC-LBL detector has a limited solid angle and neutral particles are not detected, the experimentally determined jet axis is usually not correct and Monte Carlo simulations are needed to interpret the experimental results. Two models are used for this analysis, (a) a Lorentz invariant phase space model and (b) a jet model in which the transverse momenta are limited by a matrix element of the form

$$M^2 = e^{-\sum_i p_{\perp i}^2/2b^2}$$

Here $b = 315$ MeV/c is a free parameter, that is chosen to reproduce the mean transverse momentum relative to the jet axis. In both models only charged and neutral pions are

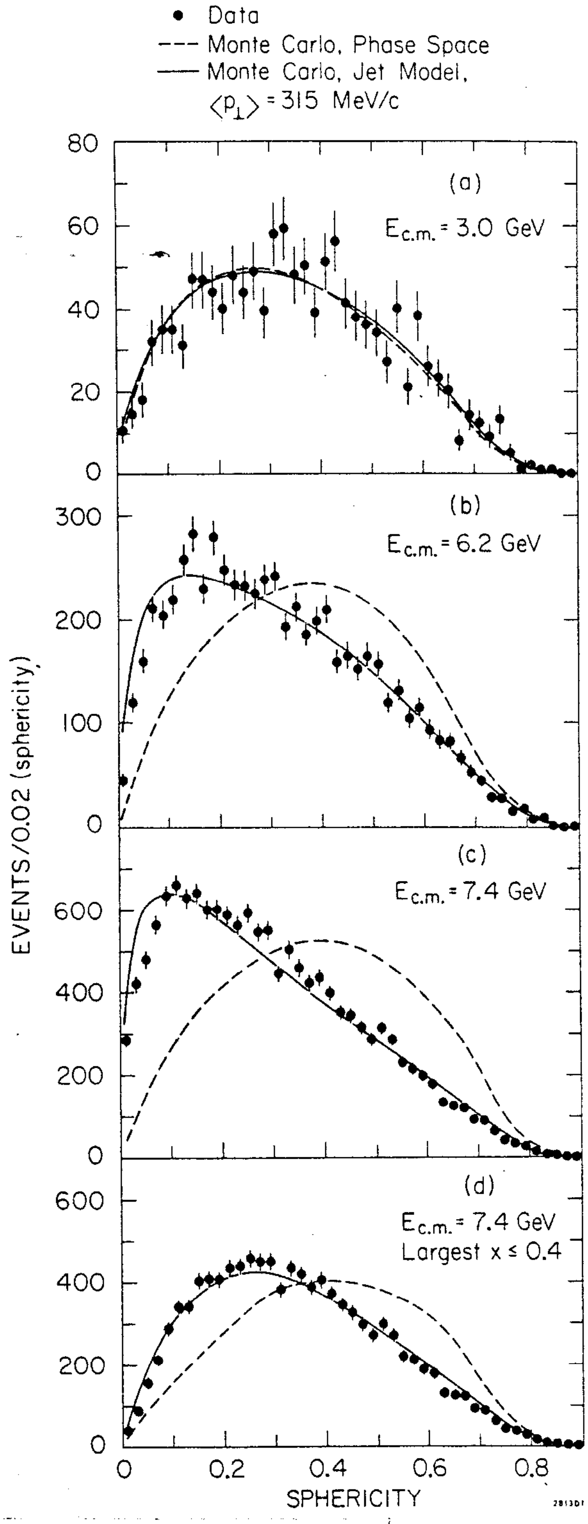

Fig. 18. Sphericity distributions for > 3-prong hadronic final states. The solid curves are the predictions of the jet model, the dashed lines give the phase-space predictions. In (d) only events with no high momentum particle (x>0.4) were included (Ref. (34)).

produced. Calculations including η's, kaons and nucleons give basically the same result. Free parameters of the model like the average multiplicity and the ratio of charged to neutral pions have been adjusted to best fit the observed properties of the final state.

The observed sphericity distributions are compared with the model calculations in Fig. 18. At 3 GeV both models agree with the data because the limit on the transverse momentum distributions has little effect. At the higher energies the phase space model reproduces the data very poorly, while the jet model gives good agreement. Likewise, the inclusive x distribution of 7.4 GeV does not agree with the predictions of the phase-space model as demonstrated in Fig. 19. The question arises whether the existence of high momentum particles is sufficient to produce a jet-like effect. To answer this question the sphericity distribution has been evaluated for events in which none of the observed particles has $x < 0.4$. Again, the phase-space model fails to describe the data, while the jet model agrees reasonably well (Fig. 18d).

The difference between the two models is clearly marked in Fig. 20, where the average observed sphericity is shown as a function of the c.m. energy. Below 4 GeV both models

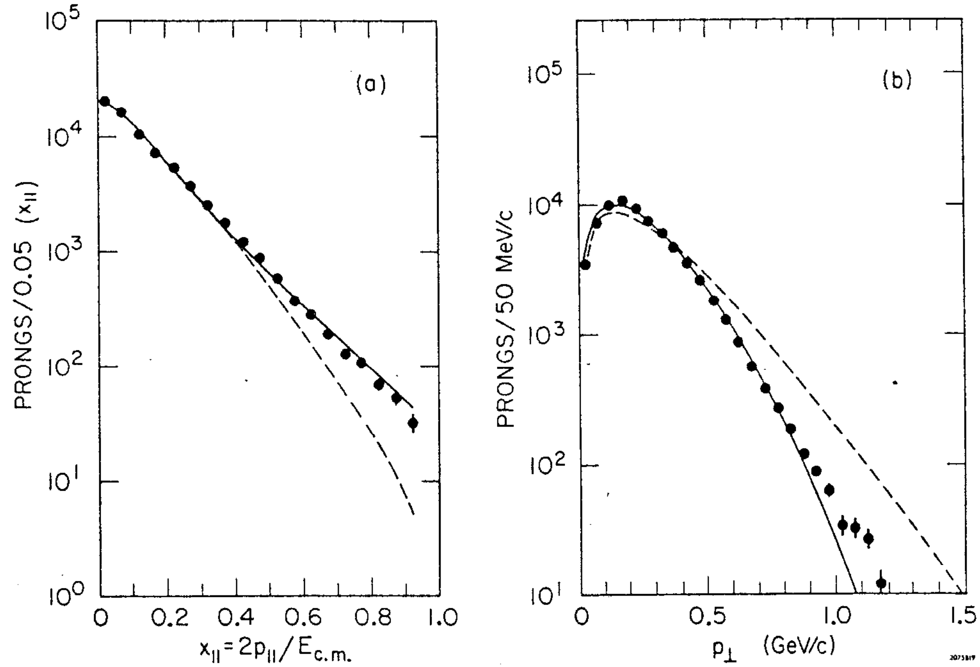

Fig. 19. Comparison of the observed longitudinal and transverse momentum distributions with the predictions of model calculations at 7.4 GeV.

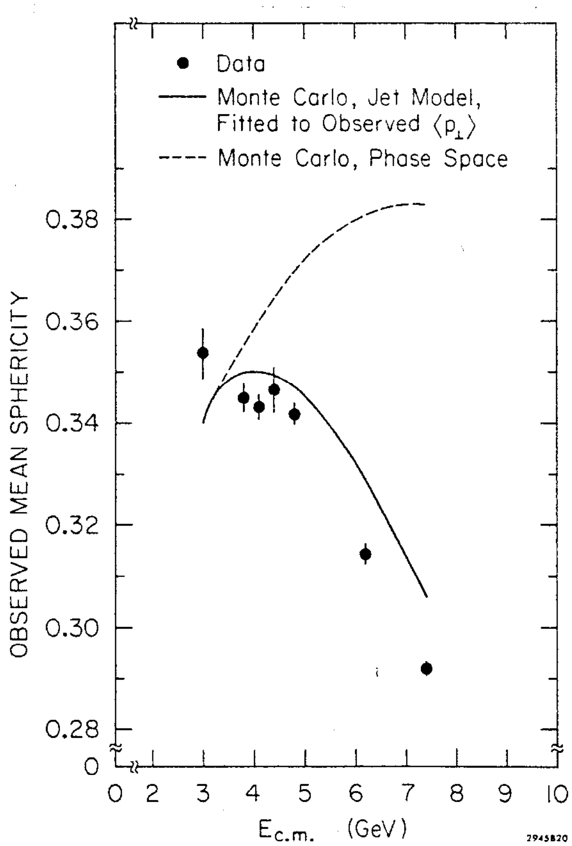

Fig. 20. Comparison of the observed mean sphericity as a function of c.m. energy with jet model (solid line) and the invariant phase-space model (broken line).(34)

are consistent with the data, at higher energies the phase-space model predicts that the mean S should increase, whereas the jet model predicts that it should decrease, in agreement with the data.

Supporting evidence for a nonisotropic emission of hadrons is obtained from angular correlations between any pair of particles in an event. The distributions peak more strongly in forward and backward direction than expected by phase space. An alternative explanation for the appearance of jet-like structure could be the production of two heavy particles which subsequently decay. No support for this hypothesis has been found. Figure 21 shows the observed jet masses, where the jet mass is defined as the effective mass of all particles on either side of a plane perpendicular to the reconstructed axis. Most jet masses are less than 2 GeV/c^2, we observe a small K_S^0 peak and a shoulder at the ρ^0 mass above a smooth continuum. f and A mesons are not evident.

The angular distribution of the jet axis at 7.4 GeV shows the same azimuthal asymmetry as the inclusive hadron (Fig. 22) and the μ-pair data. (Since the jet axis is a symmetry axis, the angles $\phi + 180^{\circ}$ are equivalent to ϕ.) The measured beam polarization P^2 and the observed ϕ distribution can be used to determine the coefficient a for the jet axis, $a = 0.97 \pm 0.14$. The quoted error is purely statistical, systematic errors due to inadequacy in the model calculations are difficult to evaluate. In terms of W_1 and W_0 this value of a corresponds to $W_0/W_1 = 0.02 \pm 0.07$. Hadrons produced in jets with this angular distribution would display momentum dependent values of a as shown by the shaded area in Fig. 17. This prediction of the jet model is in excellent agreement with the observed angular distribution of hadrons as discussed above. The change from isotropic particle production (a=0) at low x to muon-like distributions at high x is well reproduced.

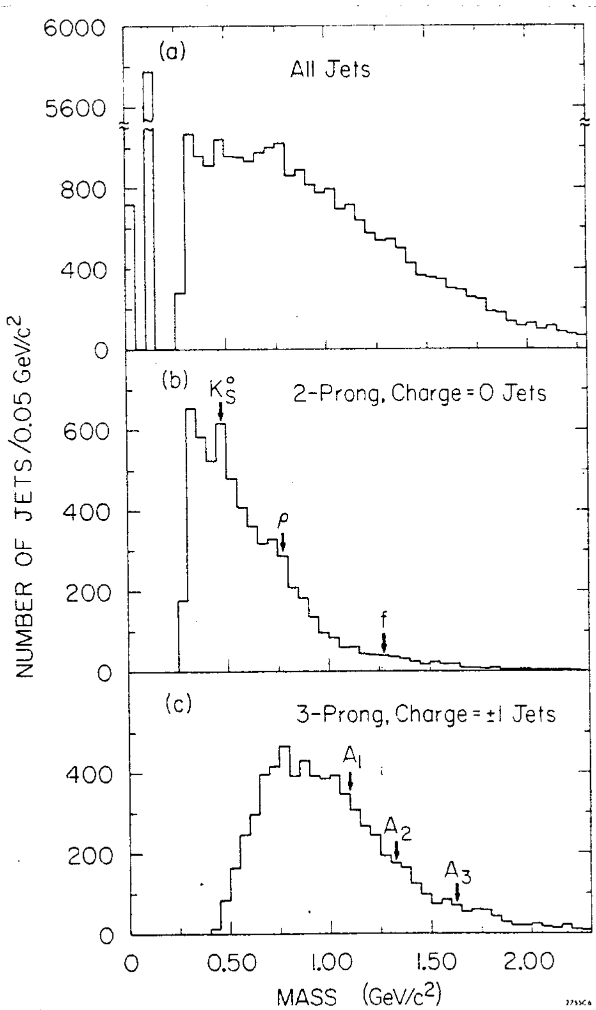

Fig. 21. Effective mass of jets as observed at 7.4 GeV for different multiplicity.(34)

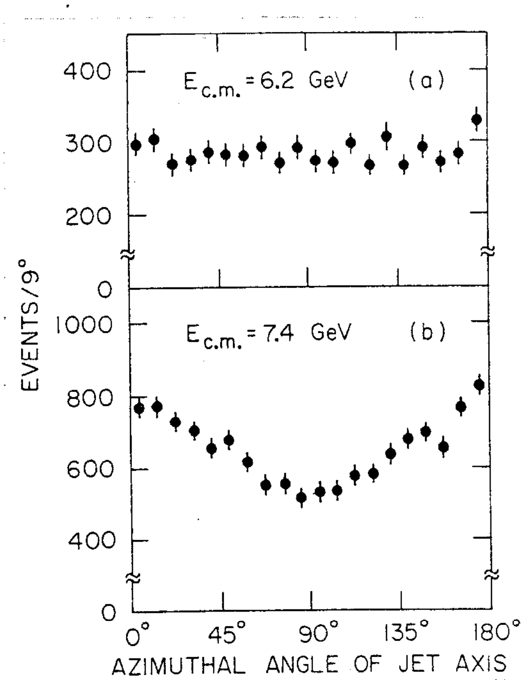

Fig. 22. Azimuthal distribution of the reconstructed jet axis > 3-prong events for (a) 6.2 GeV and (b) 7.4 GeV c.m. energy.(34)

The angular distribution for the jet axis is very similar to the μ-pair distribution with a=1. Thus, jets are produced with helicity ±1 along their axis, and this strongly implies that if partons are responsible for jets, then the parton spin is 1/2.

VII. Summary of General Features of Hadron Production

Hadron production by e^+e^- annihilation has developed into an extremely rich and interesting field. These two lectures have centered on results from the SLAC-LBL experiment at SPEAR;

1. Aside from the very narrow resonances $\psi(3095)$ and $\psi(3684)$ the variable R, the ratio of hadron to μ-pair production, is approximately constant at a value of 2.5 below 3.5 GeV, and at a value of 5 above 5 GeV. A complicated transition region connects these two scaling regions.
2. The mean charged particle multiplicity increases slowly ($\sim \ln s$) with energy, the mean fraction of c.m. energy appearing in charged hadrons decreases as the c.m. energy increases.
3. Within the experimental errors of ±20% single particle inclusive spectra exhibit Bjorken scaling for $x > 0.4$ over the energy range from 3.0 GeV to 7.4 GeV.
4. The inclusive angular distributions of hadrons at 7.4 GeV vary from isotropic for small x to nearly $1+\cos^2\theta$ for particles with large x.
5. There is jet-like structure in multihadronic final states, the transverse momentum distribution of hadrons relative to the jet axis is approximately constant for all energies. The angular distribution of the jet axis is of the form $1+\cos^2\theta$, thus jets couple to the virtual photon similar to μ pairs.

In summary, qualitative features of hadron production by e^+e^- annihilation are well described by the parton model. The constant value of R, scaling of inclusive momentum spectra, and jets are a direct consequence of the parton picture. The angular distributions are strong evidence for a value of 1/2 for the spin of the partons.

LECTURES III, IV. THE ψ SPECTROSCOPY

The discovery of two extremely narrow resonances, $\psi(3095)$ and $\psi(3684)$, at BNL and SLAC, in early November 1974 has recently been referred to as the "November Revolution" in particle physics. This may be somewhat exaggerated, nevertheless, since then our view on particle constituents in general, and hadron production by e^+e^- annihilation, in particular, has changed dramatically. The experimental evidence was unmistakable from the very first day. By now a large number of experiments has verified the existence of these particles and is searching for other particles that may be related to them. The following two lectures will summarize the present experimental status of the "ψ-spectroscopy".

I. Total and Leptonic Width of the $\psi(3095)$ and $\psi(3684)$

Extensive measurements of the cross sections for the production of hadrons, μ-pairs, and e-pairs have been made as a function of the c.m. energy near both ψ resonances. The SPEAR data are presented in Figs. 23 and 24.[36, 37] Contrary to the hadron data the lepton data are not corrected for the loss of events with $|\cos\theta| > 0.6$, where θ is the angle between the outgoing positive lepton and the incident positron. This was done because the angular distribution for lepton pairs and thereby their detection efficiencies are sensitive to the spin-parity assignment, whereas the acceptance for multihadron events is largely independent of this assignment. The relatively large nonresonant cross section for the e^+e^- final states arises from t-channel scattering which is of course absent for the $\mu^+\mu^-$ final state. It is this nonresonant small angle (25 mrad) elastic e^+e^- scattering that is used to monitor the luminosity

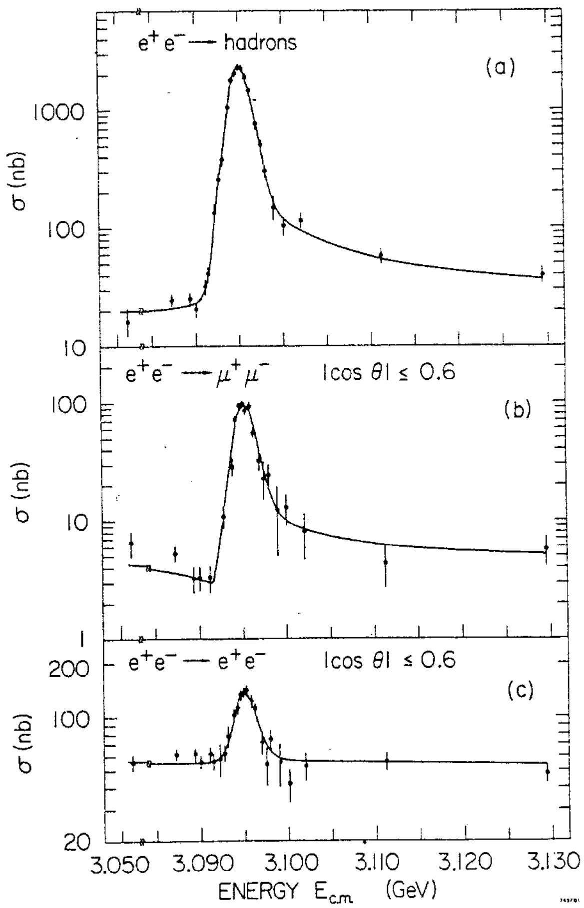

Fig. 23. Cross sections in the region of the $\psi(3095)$ resonance.

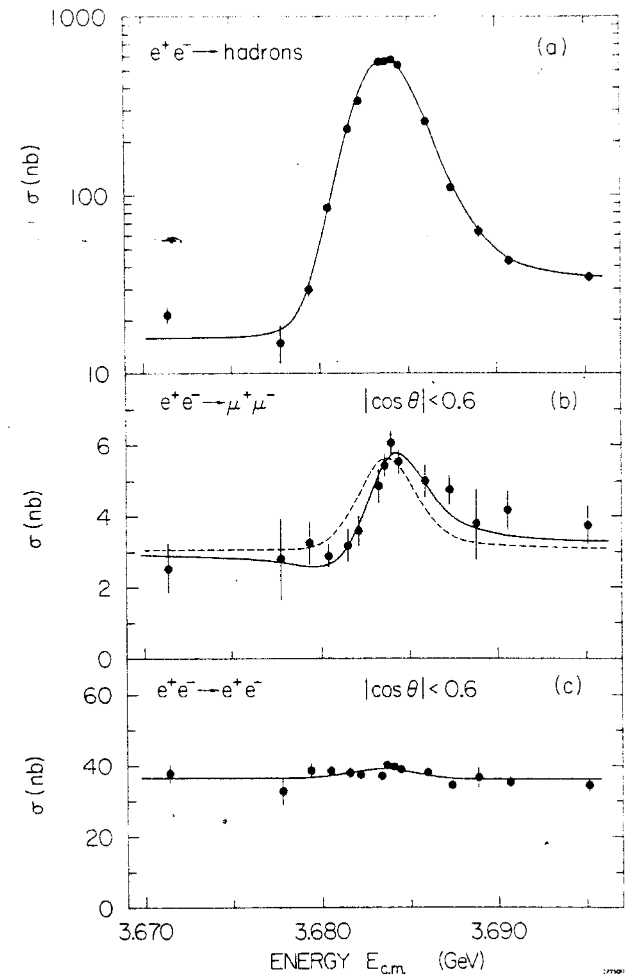

Fig. 24. Cross sections in the region of the $\psi(3684)$ resonance.

of the machine and normalize the counting rates. The most striking feature of the data is the copious production of hadrons, the sizable lepton pair production at the $\psi(3095)$, and the widths of the distributions, which are fully compatible with the resolution of the storage ring. This means that the measured cross section is a convolution of the Breit-Wigner resonance with the energy spectrum of the incident e^+e^- beams. The effect of this convolution is a redistribution of events, i.e., a change in the shape of the cross section leaving the integral unchanged.

In order to determine the exact mass m, and Γ_e, Γ_μ, Γ_{had}, the partial width to electrons, muons, and hadrons, respectively, the three data sets for each resonance are fitted simultaneously. The total width is defined as $\Gamma = \Gamma_e + \Gamma_\mu + \Gamma_{had}$, thus assuming no unobserved decay modes. Assuming further that the ψ's have Breit-Wigner shape, then for any decay mode f the cross section σ_f for the reaction $e^+e^- \to \psi \to f$ may be written as follows:

$$\sigma_f(E_{c.m.}) = \frac{(2J+1)\pi}{E^2_{c.m.}} \frac{\Gamma_e \Gamma_f}{(m-E_{c.m.})^2 + \Gamma^2/4} \tag{1}$$

Here, J is the spin and Γ is the total width of the resonance, Γ_f is the partial decay width to the state f and $E_{c.m.}$ is the c.m. energy. This formula is simply a consequence of unitarity and time-reversal invariance. Since the experimental resolution is large compared to Γ, the experiment is sensitive to the integral

$$\Sigma_f = \int \sigma_f(E_{c.m.}) dE_{c.m.} = \frac{2\pi^2}{m^2}(2J+1)\frac{\Gamma_e \Gamma_f}{\Gamma} \tag{2}$$

From this we can see intuitively that Γ_e and the branching ratios into hadrons, muons, and electrons can be determined simply by comparing the integrated cross sections for the three channels. The sum of the three directly determines Γ_e,

$$\Gamma_e = \frac{m^2}{2\pi^2(2J+1)} \int \sigma_{tot}(E_{c.m.})\, dE_{c.m.} = \frac{m^2}{2\pi^2(2J+1)} \Sigma_{tot}$$

and

$$\Gamma = \Gamma_e \frac{\int \sigma_{tot}(E_{c.m.})\, dE_{c.m.}}{\int \sigma_e(E_{c.m.})\, dE_{c.m.}} = \Gamma_e \frac{\Sigma_{tot}}{\Sigma_e} \tag{3}$$

Obviously, to obtain these integrals one must subtract the nonresonant backgrounds.

In practice, the integrals are evaluated by a simultaneous fit to the three distributions for each resonance, treating m, Γ_e, Γ_μ, Γ_{had}, the nonresonant hadron cross section, the energy spread of the machine and an overall luminosity calibration constant as free parameters. The QED cross sections are well-known and fixed. Because of the small branching ratio to leptons, μe-universality has been used in the $\psi(3684)$ analysis, i.e., $\Gamma_\mu = \Gamma_e$. The fit assumes (and this will be justified later) that the resonance like the photon is a $J^{PC}=1^{--}$ state. Consequently it must take into account the interference between the Breit-Wigner and the nonresonant amplitude. For the lepton channels this is well understood (and will be discussed below), for the hadron channels, the situation is not clear, some channels couple to the ψ directly, some only via an intermediate photon. Fortunately the final answer is rather insensitive to such interference effects in the hadron channels.

The theoretical cross sections are folded over the energy distribution of the colliding beams which itself is treated as an analytic fold of a Gaussian resolution function and radiative energy losses in the initial state. Radiative effects like vertex corrections and vacuum polarization as well as final state radiation are included.[38] Point-to-point errors typically include a 2% systematic uncertainty and take into account a ±50 keV error in the setting of the c.m. energy. The results of the fits are given in Table III. The errors on the decay widths are dominated by a 15% overall uncertainty in the hadron detection efficiency. Measurements from DESY[39] and Frascati[40] are in remarkably good

Table III. Properties of the ψ-particles as obtained from fit to cross sections σ_{had}, $\sigma_{\mu\mu}$, and σ_{ee}.(36, 37)

	$\psi(3095)$	$\psi(3684)$
mass	3.095 ± 0.004 GeV	3.684 ± 0.005 GeV
J^{PC}	1^{--}	1^{--}
$\Gamma_e = \Gamma_\mu$	4.8 ± 0.6 keV	2.1 ± 0.3 keV
Γ_H	59 ± 14 keV	224 ± 56 keV
Γ	69 ± 15 keV	228 ± 56 keV
Γ_e/Γ	0.069 ± 0.009	0.0093 ± 0.0016
Γ_H/Γ	0.86 ± 0.02	0.981 ± 0.003
Γ_μ/Γ_e	1.00 ± 0.05	0.89 ± 0.16
$\Gamma_{\gamma H}/\Gamma$	0.17 ± 0.03	0.029 ± 0.004

agreement with the SLAC results. It is interesting to compare the properties of the $\psi(3684)$ relative to those of the $\psi(3095)$. The total width of the $\psi(3684)$ is roughly a factor three larger, the leptonic branching ratio is down by a factor of seven. This circumstance makes it relatively hard to detect the $\psi(3684)$ in processes other than annihilation.

Assuming that there is no direct coupling of the resonances to μ-pairs, one can derive the fraction of the hadronic decays that proceeds via an intermediate photon rather than directly. To obtain it one has to assume that the ratio of hadron to μ-pair production via an intermediate photon is the same at the resonance as elsewhere, thus $B_{\gamma H} = B_\mu \cdot R$(off resonance). For the $\psi(3095)$ with $R \simeq 2.8$ this relation predicts $B_{\gamma H} = 0.17 \pm 0.03$ compared to a total hadronic branching ratio of $B_H = 0.86 \pm 0.02$. For the $\psi(3684)$ the numbers are $B_{\gamma H} = 0.029 \pm 0.004$ compared to $B_H = 0.981 \pm 0.003$. So the decays to hadrons via 2nd order electromagnetic interaction are small relative to the direct decays.

II. J^{PC} Assignment of $\psi(3095)$ and $\psi(3684)$

The fact that the ψ resonances are produced in e^+e^- annihilation suggests that they couple directly to photons and thus have the same spin, parity, and charge conjugation, $J^{PC} = 1^{--}$. The most compelling way to check if the ψ resonances and the photon share the same quantum numbers is to search for interference effects in the energy dependence of the cross section for μ-pair production near the resonance. The $\mu^+\mu^-$ final state is chosen rather than the e^+e^- final state which is dominated by the t-channel QED amplitude. Let A and R represent the QED and the resonance amplitudes for production of μ-pairs, respectively, then we have

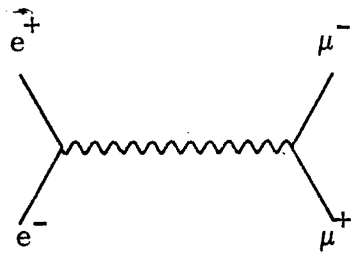

$$A = \left(\frac{3\pi}{E^2_{c.m.}}\right)^{1/2} \left(-\frac{2\alpha}{3}\right) .$$

and

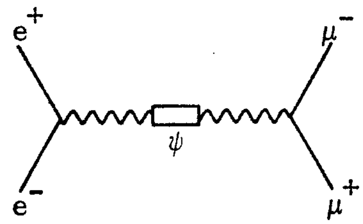

$$R = \left(\frac{(2J+1)\pi}{E^2_{c.m.}}\right)^{1/2} \frac{\Gamma_e}{m - E_{c.m.} - i\Gamma/2}$$

If the ψ's have $J^{PC} = 1^{--}$, these two amplitudes will interfere yielding a cross section of the form

$$\frac{d\sigma}{d\cos\theta} = \frac{9\pi}{8E^2_{c.m.}} (1+\cos^2\theta) \left| -\frac{2}{3}\alpha + \frac{\Gamma_e}{m - E_{c.m.} - i\Gamma/2} \right|^2 .$$

The addition of the amplitudes is shown in Fig. 25; there will be destructive interference below the resonant energy and constructive interference above. Because of the radiative tail for $E_{c.m.} > m$, it is the region below the resonance which is most useful in this study. The maximum interference will occur for $|A| = |R|$, i.e., for

$$m - E_{c.m.} = \frac{3\Gamma_e}{2\alpha} \begin{cases} 1 \quad \text{MeV for } \psi(3095) \\ 0.5 \text{ MeV for } \psi(3684) \end{cases}$$

This estimate ignores the energy spread of the machine, in practice one will observe an effect as long as m-E is not large compared to Γ_e/α.

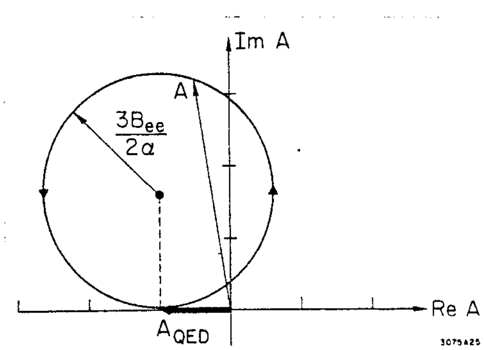

Fig. 25. Addition of interfering amplitudes for μ-pair production by QED and resonant processes.

To exhibit the interference effects it is most convenient to study the ratio of $\mu^+\mu^-$ to e^+e^- yields as a function of c.m. energy. This ratio minimizes normalization problems in the data and is most sensitive to the interference, because the electron amplitudes interfer constructively where the muon amplitudes are expected to show destructive interference. The data for both resonances are presented in Fig. 26 and compared to calculations involving maximum interference, i.e., a pure $J^{PC} = 1^{--}$ state, and no interference, e.g., J=0. The data are fully compatible with the prediction of maximum interference. The $\psi(3095)$ measurements disagree with the hypothesis of no interference by 2.7 standard deviations, and the $\psi(3684)$ data deviate by 4.9σ from the no interference curve.

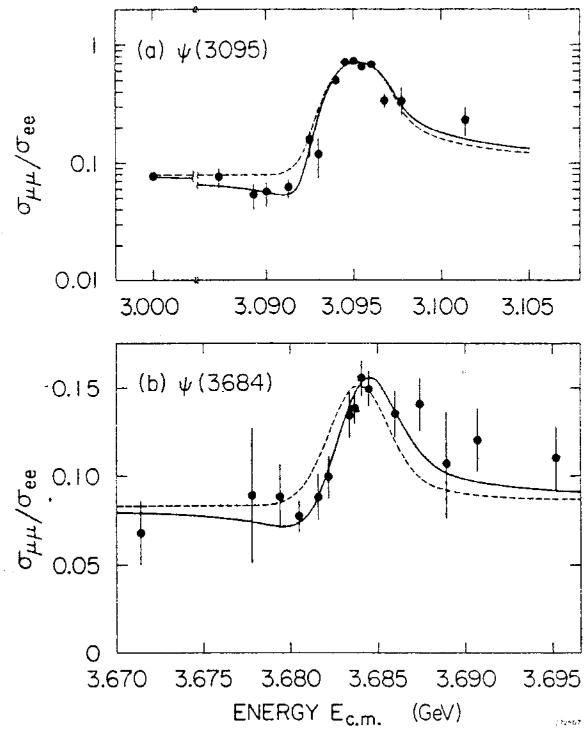

Fig. 26. Ratio of μ-pair yield to e-pair yield vs. c.m. energy for the ψ resonances. The dashed line gives the expected ratio for no interference, the solid line gives full interference (Refs. (36,37)).

The observation of destructive interference in μ-pair production provides an unambiguous determination of the quantum numbers of the ψ-states only if the detector covers the complete solid angle with uniform efficiency. The SLAC-LBL solenoid detector subtends a limited angular range,

$$-0.6 \leq \cos\theta < +0.6 \qquad 0 \leq \psi \leq 2\pi \quad ,$$

where θ and ψ are polar and azimuthal angles relative to the beam direction. Since the detector is symmetric in $\cos\theta$, the interference term between the two amplitudes can only be nonzero, if the parities of the ψ and the photon are equal, i.e., both negative. Likewise, the fact that the detector is symmetric with respect to charge implies equal charge conjugation quantum numbers for the photon and the resonance, namely C=-1.

In order to discriminate against higher spins one has to study the angular dependence of the interference term in more detail. Again, a decomposition in terms of helicity amplitudes $d^J_{\lambda\mu}$ will prove useful.

$$f(z) = \sum_{\lambda\mu} |A_{\lambda\mu} d^1_{\lambda\mu}(z) + R_{\lambda\mu} d^J_{\lambda\mu}(z)|^2 \qquad z = \cos\theta$$

is the complete angular distribution, $A_{\lambda\mu}$ and $R_{\lambda\mu}$ are the QED and resonance amplitudes for initial state helicity λ and final state helicity μ. The photon only couples to helicities ± 1, i.e., $A_{\lambda\mu} \neq 0$ only for $\lambda, \mu = \pm 1$. Consequently the interference term can be written as

$$I(z) = 2 \,\mathrm{Re}\left\{ \sum_{\substack{\lambda=\pm 1 \\ \mu=\pm 1}} A_{\lambda\mu} R_{\lambda\mu} d^1_{\lambda\mu}(z)\, d^J_{\lambda\mu}(z) \right\} .$$

Using the properties of the $d^J_{\lambda\mu}$ functions

$$d^J_{-1-1} = d^J_{+1+1} \qquad d^J_{-1+1} = d^J_{+1-1} \qquad d^J_{-1+1}(z) = (-1)^{J+1}\, d^J_{+1+1}(-z)$$

and parity conservation one can relate the four helicity amplitudes to a single independent amplitude. Since the $A_{\mu\lambda}$ are real, the interference is determined by the real part of one independent helicity amplitude times an angular overlap integral that is completely determined by the value of J and the angular range of the detector;

$$\int_{-z'}^{+z'} I(z, J)\,dz = 8\, A_{11}\, \mathrm{Re}\, R_{11} \int_{-z'}^{+z'} d^1_{11}(z)\, d^J_{11}(z)\, dz \; .$$

Time reversal invariance, μe universality, unitarity, and causality specify the sign of the real part of the resonance amplitude. Integrated over the complete solid angle the overlap integral vanishes for any $J \neq 1$. Within the limited acceptance of the detector, amplitudes for spins greater than 3 can only contribute very little to the overlap integral. Below the resonance J=1 produces a <u>destructive</u> interference, while J=2 and J=3 with both produce a <u>constructive</u> interference. In conclusion, even with the finite angular acceptance of the SLAC-LBL detector, the observation of <u>destructive</u> interference below the resonance implies that both the $\psi(3095)$ and $\psi(3684)$ resonances share the quantum numbers of the photon, $J^{PC} = 1^{--}$.

The assumption that the resonances are eigenstates of P and C may be tested by studying the front-back asymmetry in the leptonic decays. The measured asymmetry for μ-pairs versus c.m. energy is shown in Fig. 27. The data are consistent with zero asymmetry which argues against the resonances being degenerate mixtures of opposite P and C.

The angular distributions of μ-pair and e-pairs confirm the interference test (Fig. 28). After subtraction of the QED contributions, both angular distributions are consistent with

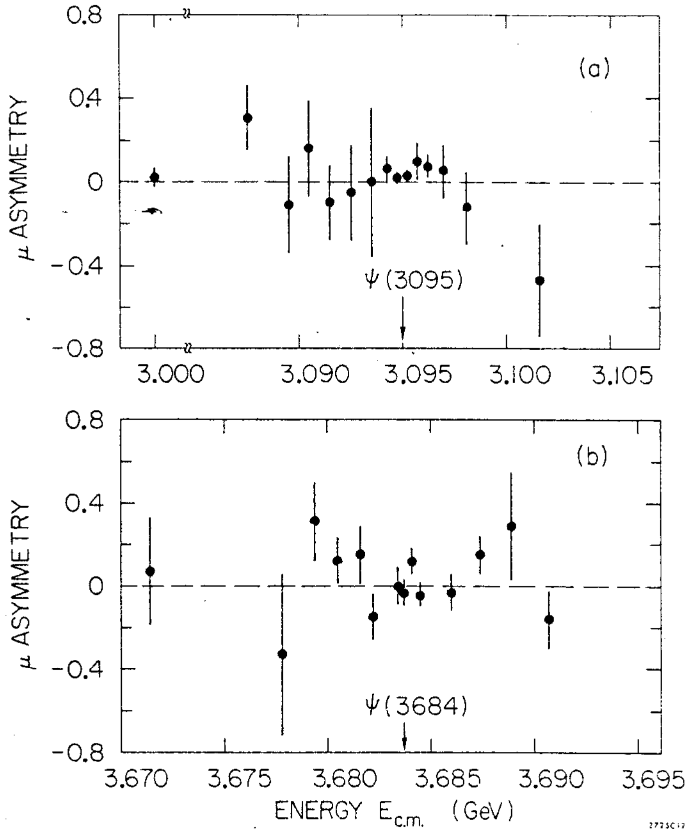

Fig. 27. Front-back asymmetry for μ-pairs vs. c.m. energies near ψ resonances. The errors are statistical only, systematic uncertainties are 1-2%.

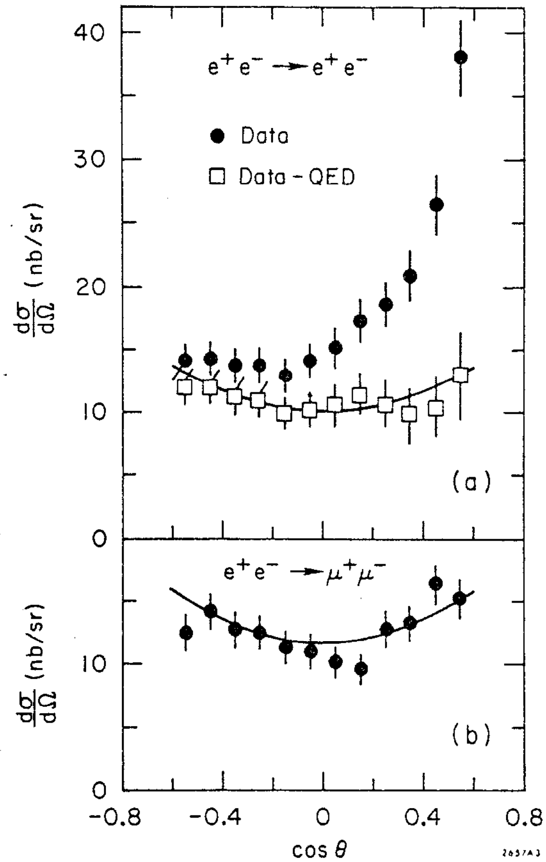

Fig. 28. The angular distributions for e-pairs and μ-pairs at the center of the ψ(3095) resonance. The line represents a fit to $1+\cos^2\theta$.[36]

the $f(\theta) \sim 1+\cos^2\theta$ as expected for a simple 1^{--} state populating only helicity ±1, but are inconsistent with 2^{--} and 3^{--} states for the same helicity coupling.

III. Search for Narrow Resonances

The production of hadrons by e^+e^- annihilation proceeds mainly via a single time-like photon, i.e., a state with the quantum numbers $J^{PC}=1^{--}$ and all additive quantum numbers equal to zero. Consequently any particle coupled to the photon with the same quantum numbers can be observed as an enhancement in the total hadronic cross section if the c.m. energy equals the mass of the particle. The "standard" vector mesons ρ, ω, and φ with masses up to 1 GeV have been known for some time, and e^+e^- annihilation was believed to have reached asymptopia above 2 GeV. The discovery of the two enormous, narrow resonances above 3 GeV destroyed this simple picture. It became imperative to perform a systematic search for other such states.

Shortly after the discovery of the $\psi(3095)$ several groups of various laboratories began such searches by measuring the total hadronic cross section in very fine energy intervals. Scanning procedures were developed whereby the c.m. energy of the machine could be automatically increased by approximately 2 MeV energy every few minutes, allowing for average of 2-3 hadronic events per step. Since the step size is chosen to be comparable to the energy spread of the beams, even resonances that are narrow compared to the energy resolution will show as enhancements over several bins and the integrated cross section can be measured.

During the first run of this search at SPEAR, the $\psi(3684)$ was discovered.[41] Since then similar fine scans covering a broad energy range have been reported from Novosibirsk[42] and Frascati.[43] Results of a typical fine mesh scan are presented in Fig. 29. A summary of upper limits for the existence of a narrow vector meson is given in Table IV. For most of the energy intervals covered these limits on the integrated

Table IV. Search for narrow resonances in e^+e^--annihilation. Upper limits (90% confidence level) for the integrated cross section and for the leptonic width Γ_e of a possible narrow resonance with spin J=1.

Storage Ring	Mass Range (GeV)	$\int \sigma_{had} dE_{c.m.}$ (nb MeV)	Γ_e (keV)
Novosibirsk[42]	0.78 - 1.34	2300	0.10
ADONE[43]	1.910 - 2.20	950	0.17
	2.20 - 2.545	660	0.16
	2.97 - 3.09	830	0.33
SPEAR[41]	3.2 - 3.5	970	0.47
	3.5 - 3.68	780	0.44
	3.72 - 4.0	850	0.55
	4.0 - 4.4	620	0.47
	4.4 - 4.9	580	0.54
	4.9 - 5.65	780	0.95
	5.65 - 6.00	90	0.13
	6.00 - 6.45	100	0.17
	6.45 - 6.95	65	0.13
	6.95 - 7.45	35	0.07

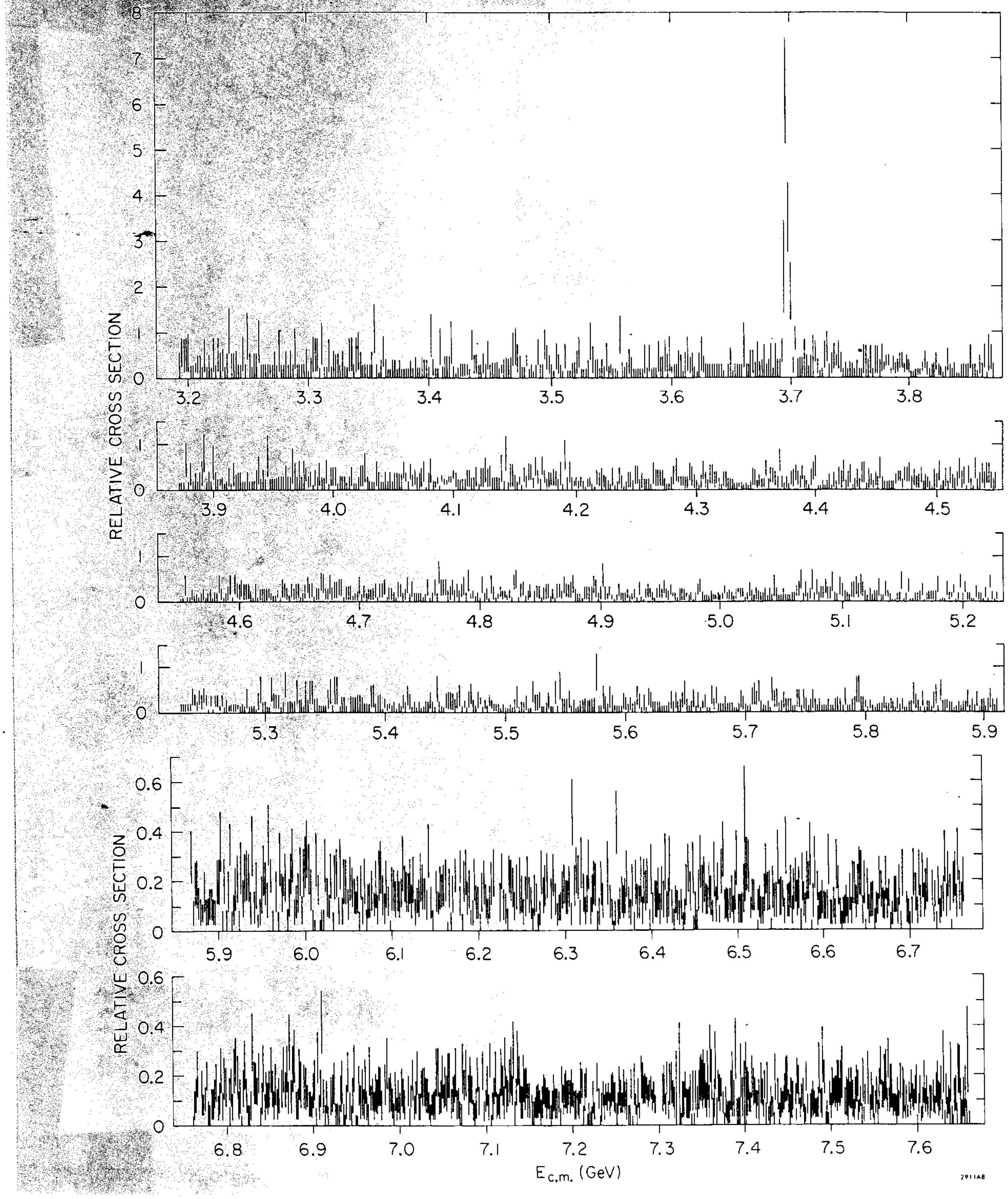

Fig. 29. Relative cross section for $e^+e^- \to$ hadrons as obtained from the fine mesh scan at SPEAR.(41) The $\psi(3684)$ stands out clearly, it was first seen in the process of this scan.

cross section and the partial width to electrons are more than an order of magnitude smaller than those for well-known vector mesons.

Recently, the observation of high mass e^+e^--pairs in high energy p-Be interactions and possible new resonances at 6.0 GeV and 7.2 GeV were reported.(44) In order to

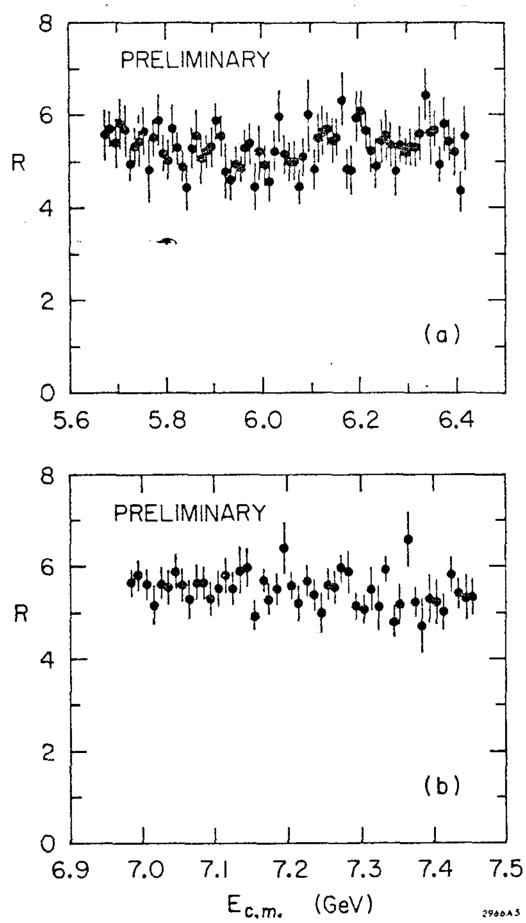

Fig. 30. Search for narrow high mass resonances; R vs. c.m. energy.

investigate these new states in e^+e^--annihilation, the SPEAR group repeated the scan between 5.65 GeV and 7.45 GeV with increased statistical accuracy. No sign of a narrow peak near 6.0 GeV or anywhere else has been found (Fig. 30). Quantitatively these measurements can be translated to a leptonic width of $\Gamma_e \lesssim 170$ eV for a narrow state, or to a leptonic branching ratio of $B_e \leq 10^{-5}$ for a resonance wide enough to be resolved. These limits are rather stringent for vector mesons which typically have leptonic widths of several keV. The $\psi(4414)$, however, has $\Gamma_e = 440$ eV, indicating that such small coupling to leptons is not unthinkable. On the other hand, the limit of $B_e \leq 10^{-5}$ and the quoted value of $(\sigma \cdot B_e) = (5.2 \pm 2.0) \times 10^{-36}$ cm^2 per nucleon for the product of the hadronic production cross section and the branching ratio to electrons leads to the production cross section of about 5×10^{-31} cm^2. This is more than three times the ψ production measured in the same experiment.(45) A rather surprising result!

It is interesting to compare some of the properties of the ψ particles with those of the well-known vector mesons. In Table V, in addition to the $\psi(3095)$ and $\psi(3684)$, the 4.4 GeV enhancement has been listed, although its spin and parity have not been measured. While the total widths of the vector mesons vary over several orders of magnitude, their partial widths to electrons agree to within a factor of ten.

In the vector dominance model (Fig. 31a) the photon-meson coupling constants f_v are related to Γ_e, the decay rate to e-pairs, by

$$\Gamma_e = \frac{1}{3} \alpha^2 \frac{4\pi}{f_v^2} M_v \quad , \tag{1}$$

Table V. Comparison of vector mesons

Particle	Mass (GeV)	Γ (MeV)	Γ_e (keV)	$\left(\frac{f^2}{4\pi}\right)^{-1}$
ρ	0.770 ± 0.010	150 ± 10	6.5 ± 0.5	0.48 ± 0.04
ω	0.7827 ± 0.0006	10 ± 0.4	0.76 ± 0.17	0.055 ± 0.012
ϕ	1.0197 ± 0.0003	4.2 ± 0.2	1.34 ± 0.08	0.074 ± 0.004
$\psi(3095)$	3.095 ± 0.004	0.069 ± 0.015	4.8 ± 0.6	0.09 ± 0.01
$\psi(3684)$	3.684 ± 0.005	0.228 ± 0.056	2.1 ± 0.3	0.032 ± 0.005
$\psi(4414)$	4.414 ± 0.007	33 ± 10	0.44 ± 0.14	0.006 ± 0.002

where M_V is the meson mass. From the observed leptonic widths one finds for the relative magnitude of the coupling constants

$$f^{-2}(\rho):f^{-2}(\omega):f^{-2}(\phi):f^{-2}(\psi):f^{-2}(\psi') = 8.7:1.0:1.4:1.6:0.6$$

as compared to the SU_3 prediction of

$$e_\rho^2:e_\omega^2:e_\phi^2:e_\psi^2:e_{\psi'}^2 = 9:1:2:8:4 \quad .$$

Here e_V are the average charges of the quark constituents of the vector mesons. The relative magnitude is roughly correct for $\psi(3095)$ and $\psi(3684)$, but the coupling of the two relative to other vector mesons is at least a factor of four too small.

Alternatively, the rate of decay may be explained in terms of a bound state picture as illustrated in Fig. 31b. The quark-antiquark state annihilates into a virtual photon. The decay rate to leptons is given as

$$\Gamma_e = 16\pi \frac{\alpha^2 e_V^2}{M_V^2} |\psi(0)|^2 \tag{2}$$

Here $\psi(0)$ is the bound state wave function. The experimental ratio

$$\Gamma_e(\rho) \quad : \quad \Gamma_e(\omega) \quad : \quad \Gamma_e(\phi) \quad : \quad \Gamma_e(\psi) \quad : \quad \Gamma_e(\psi')$$

$$= (8.5 \pm 1.2) : (1.0 \pm 0.1) : (1.8 \pm 0.2) : (6.8 \pm 0.6) : (2.8 \pm 0.4)$$

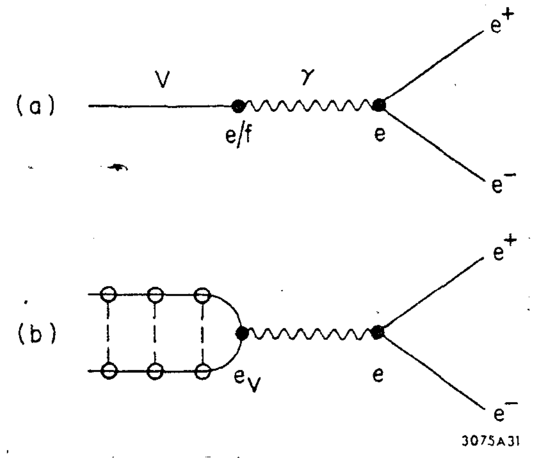

Fig. 31. Decay of a vector meson to e^+e^-. (a) Vector dominance diagram; (b) Bound state annihilation picture.

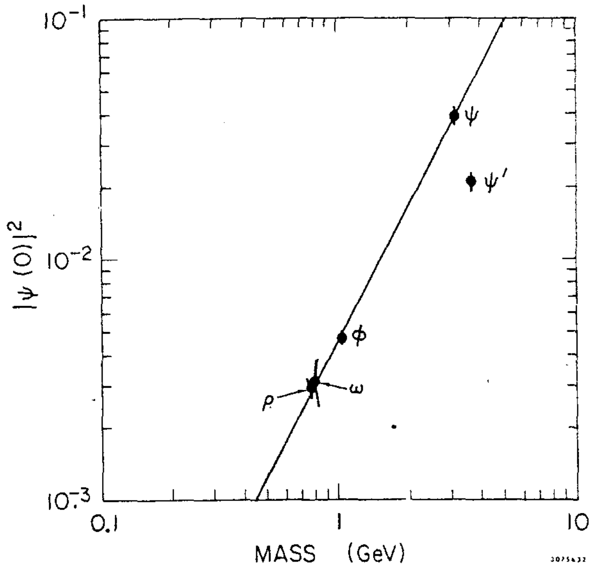

Fig. 32. $|\psi(0)|^2$ vs. mass for vector mesons. The straight line has a slope of 1.89 ± 0.15. [46]

indicates that $|\psi(0)|^2$ is roughly proportional to M_V^2. This can be verified in Fig. 32, where $|\psi(0)|^2$ as obtained from Eq. (2) is plotted versus the mass M_V. The solid line corresponds to a fit to M^n with $n = 1.89 \pm 0.15$.

IV. Decay Modes of the ψ(3095)

Detailed analysis of exclusive hadronic final states has been under way for a long time and has proven to be a rich field of research, leading to the determination of the G-parity and the isospin of the ψ(3095) and to tests of the SU_3 character of this state. Table VI gives a list of updated values for various identified decay modes.

1. G-Parity of the ψ(3095)

The all-pion decays are the final states that are most copious and easily identifiable. Using the measured momenta and directions of the charged tracks in the detector (and the directions of the neutral particles if available) the conservation of energy and momentum is tested for each event. Clear signals in states of 2, 3, 4, 5, 6, 7, and 9 pions have been observed.[47, 48, 49] Thus, there is an apparent violation of G-parity; the ψ(3095) decays into both even and odd numbers of pions. However, this violation can be accounted for by second order electromagnetic effects.

Table VI. Decay modes of $\psi(3095)$†

Mode	Fraction (%)	Reference	Mode	Fraction (%)	Reference
e^+e^-	6.9 ± 0.9	36			
$\mu^+\mu^-$	6.9 ± 0.9	36			
$\gamma \to$ hadrons	17 ± 3	36 [a]			
$\pi^+\pi^-$	0.01 ± 0.007	48 [b]	$\phi\pi^+\pi^-$	0.21 ± 0.09	52
$\pi^+\pi^-\pi^o$	1.6 ± 0.6	47	ωK^+K^-	0.03 ± 0.02	52
$2\pi^+2\pi^-$	0.4 ± 0.1	47 [a]	ϕK^+K^-	0.09 ± 0.04	52
$2\pi^+2\pi^-\pi^o$	0.43 ± 0.45	47	$\phi\eta$	0.07 ± 0.04	52
$3\pi^+3\pi^-$	0.4 ± 0.2	47 [a]	$\phi\eta'$	0.05 ± 0.04	52
$3\pi^+3\pi^-\pi^o$	2.9 ± 0.7	47	$\phi f'$	0.08 ± 0.05	52
$4\pi^+4\pi^-\pi^o$	0.9 ± 0.3	47	$p\bar{p}$	0.21 ± 0.13	48,50 [e]
$\rho\pi$	1.1 ± 0.15	47,48,49	$p\bar{n}\pi^-$	0.38 ± 0.08	50
$\omega\pi^+\pi^-$	0.68 ± 0.19	52	$p\bar{p}\pi^o$	0.10 ± 0.02	50
$A_2^{\mp}\pi^{\pm}$	< 0.43	48 [a]	$p\bar{p}\eta$	0.19 ± 0.04	50
K^+K^-	0.015 ± 0.011	48,52 [c,d]	$p\bar{p}\pi^+\pi^-$	0.41 ± 0.08	54
K_SK_L	< 0.008	52 [d]	$p\bar{p}\pi^+\pi^-\pi^o$	0.11 ± 0.04	54
$K^+K^-\pi^+\pi^-$	0.72 ± 0.23	52	$p\bar{p}\omega$	0.05 ± 0.01	54
$2K^+2K^-$	0.07 ± 0.03	52			
			$\Lambda\bar{\Lambda}$	0.16 ± 0.08	50
$K^+K^-2\pi^+2\pi^-$	0.31 ± 0.13	52			
K^+K^{-*}	0.34 ± 0.05	48,52	$\gamma\gamma$	< 0.3	1 [f]
$K^o\bar{K}^{o*}$	0.27 ± 0.06	52	$\gamma\pi^o$	< 0.016	1
K^+K^{-**}	< 0.15	52 [d]	$\gamma\eta$	0.10 ± 0.018	49,54
$K^o\bar{K}^{o**}$	< 0.20	52 [d]	$\gamma\eta'$	0.24 ± 0.06	49
$K^{o*}\bar{K}^{o*}$	< 0.05	52 [d]	$\gamma\chi(2850)$	< 5	1
$K^{o*}\bar{K}^{o**}$	0.67 ± 0.26	52	$\gamma\chi(2850) \to 3\gamma$	0.015 ± 0.004	49,54
$K^{o**}\bar{K}^{o**}$	< 0.29	52 [d]	$\gamma\chi(2850) \to \gamma p\bar{p}$	< 0.004	50

†The resonance contributions are included in the general mode—i.e., $\rho\pi$ is included in $\pi^+\pi^-\pi^o$. The branching ratio listed is the sum of the mode and its charge conjugate state. Limits refer to 90% confidence level. K(890) ≡ K*, K(1420) ≡ K**.

[a] Violates G-parity and proceeds via second order electromagnetic interaction.

[b] Two $\pi^+\pi^-$ pairs with an estimated background of 0.24 events were found. The rate implies $|F_\pi(q^2 = 3.1\ \mathrm{GeV}^2)|^2 = (5.6 \pm 4.0) \times 10^{-3}$.

[c] Two events observed, one at DORIS, one at SPEAR, implies $|F_K(q^2 = 3.1\ \mathrm{GeV}^2)|^2 = (8.0 \pm 5.6) \times 10^{-3}$.

[d] Forbidden for SU_3 singlet state.

[e] Angular distribution $f(\theta) \sim 1 + \cos^2\theta$ assumed, consistent with experimental results.

[f] Forbidden for spin 1 particle.

To understand this, it is convenient to consider the diagrams involved in hadron production at the $\psi(3095)$ and outside the resonance region,

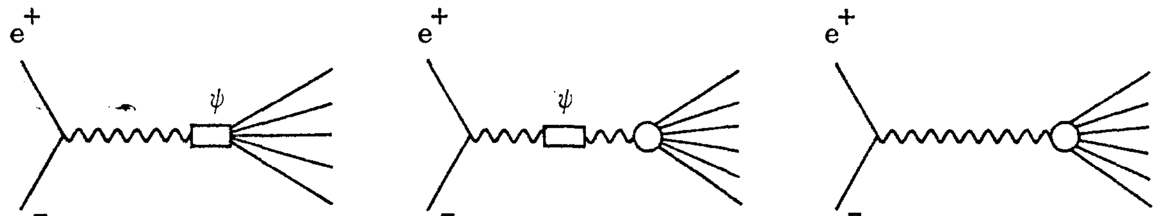

(1) (2) (3)

and compare them to the diagrams for μ-pair production

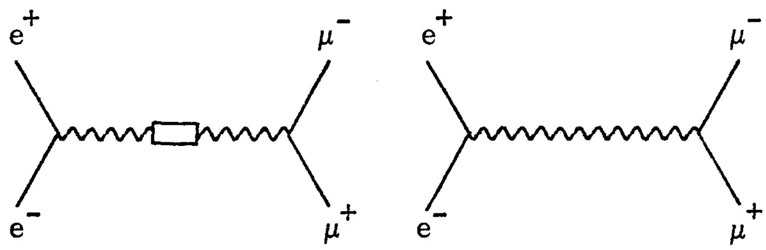

(4) (5)

Graph (1) describes the direct decay of the ψ to hadrons, whereas (2) and (3) show the production of hadrons via an intermediate photon. The final states in (2) must be the same as the nonresonant final states in (3). These states need not conserve G-parity and may be different from states produced by (1). Furthermore, the ratio of hadron to μ-pair production for diagrams (3) and (5), i.e., <u>off</u> resonance, must be the same as for diagrams (2) and (4), i.e., <u>on</u> resonance. Thus, if the hadronic decays observed are due to the second order electromagnetic process (2) <u>only</u>, the following relation holds,

$$R_{on} = \frac{\sigma^{on}_{had}}{\sigma^{on}_{\mu\mu}} = \frac{\sigma^{off}_{had}}{\sigma^{off}_{\mu\mu}} = R_{off}$$

To test this hypothesis, the ratio of all-pion cross sections to μ-pair cross sections are compared for data at 3.0 GeV and at the $\psi(3095)$. The ratio of ratios $\alpha = R_{on}/R_{off}$ is presented in Fig. 33 for different pion multiplicities. The production of an even number of pions is consistent with $\alpha=1$ as expected for decays proceeding entirely via electromagnetic interaction, whereas $\alpha >> 1$ for any odd number of pions. Thus most of the odd pion states come from direct decays of the $\psi(3095)$. The purity of the G-parity selection

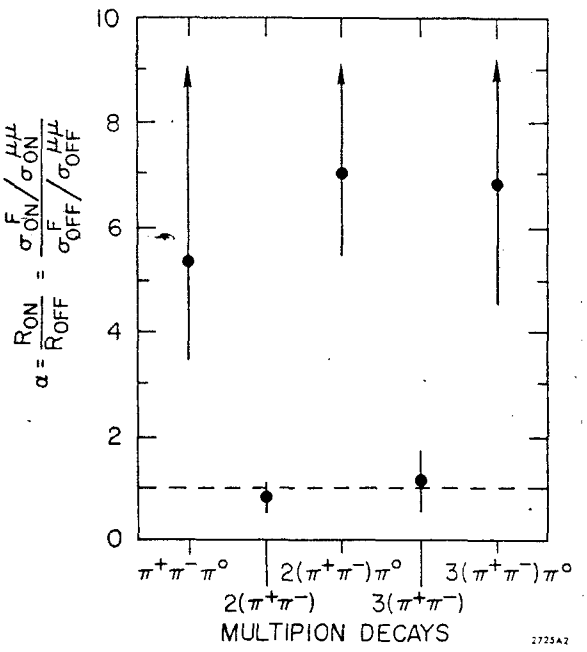

Fig. 33. Test on G-parity in all-pion decays of the $\psi(3095)$.[47] The ratio of multipion to $\mu^+\mu^-$ pair production as a function of pion multiplicity is compared at the ψ resonance (ON) and at 3.0 GeV (OFF).

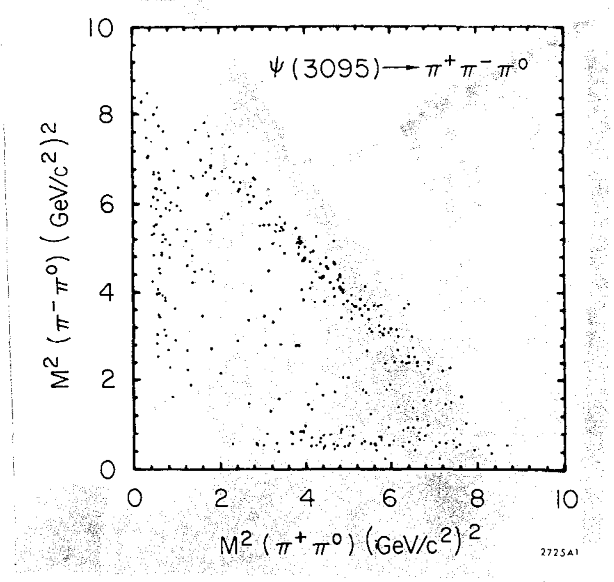

Fig. 34. Dalitz plot for the $\pi^+\pi^-\pi^0$ decay of the $\psi(3095)$.[47]

is striking and argues that the decay is hadronic, since strong interaction is the only one known to conserve G-parity. Consequently, the $\psi(3095)$ must have odd G-parity. One can turn the above argument around and use the fact that the decays to four and six pions are consistent with the second order electromagnetic decay as evidence that the $\psi(3095)$ couples to leptons only through the photon rather than directly.

2. Isospin of the $\psi(3095)$

The fact that the G-parity and charge conjugation of the $\psi(3095)$ are odd implies that the isospin has to be even, since $G=C(-1)^I$. There are several pieces of evidence indicating that I=0. (1) The analysis of the $\pi^+\pi^-\pi^0$ decay, which is mostly a hadronic decay, reveals that this state is dominantly produced as $\rho\pi$.[47,49] This can be verified from the Dalitz plot in Fig. 34. There are three different bands corresponding to ρ^+, ρ^-, and ρ^0; the branching ratio into the three charge modes are roughly equal,

$$\frac{\Gamma(\rho^0\pi^0)}{\Gamma(\rho^+\pi^-) + \Gamma(\rho^-\pi^+)} = 0.59 \pm 0.17$$

An I=0 state should produce equal rates, $\Gamma(\rho^0\pi^0) : \Gamma(\rho^+\pi^-) : \Gamma(\rho^-\pi^+) = 1:1:1$, while an I=2 state should have the ratios 4:1:1. Thus I=0 is clearly favored. (2) An even stronger argument for I=0 is derived from the measurement of the decay $\psi(3095) \to p\bar{p}$ with a branching ratio of $(0.22 \pm 0.02)\%$ at SLAC[50] and DESY.[48] This rate is far

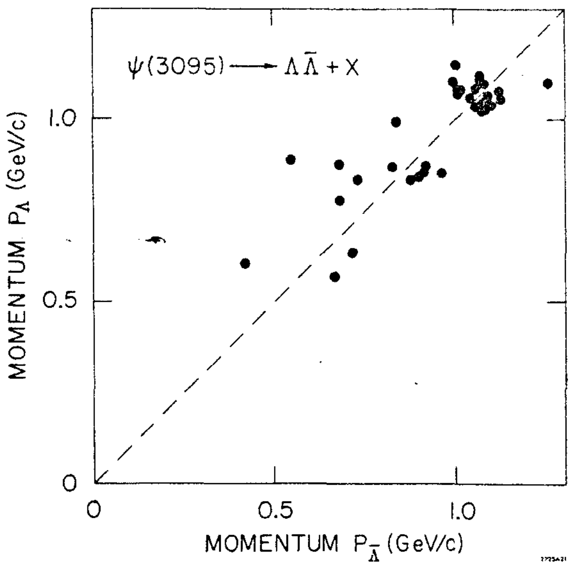

Fig. 35. Momentum of the Λ vs. the momentum of the $\bar{\Lambda}$ for four-prong events compatible with $\psi \rightarrow \Lambda\bar{\Lambda}+X$.[50]

above the electromagnetic rate, and must therefore be hadronic. Since a $p\bar{p}$ state can only be in an I=0 or I=1 state, the $\psi(3095)$ must be I=0. (3) The observation of the decay $\psi(3095) \rightarrow \Lambda\bar{\Lambda}$ directly selects I=0. For events with identified decays of Λ and $\bar{\Lambda}$, the momentum of the Λ versus the momentum of the $\bar{\Lambda}$ is given in Fig. 35. There is a cluster of 19 ± 5 events at 1.07 GeV, consistent with Λ pair production.[50]

3. SU_3 Classification of the $\psi(3095)$

Since the $\psi(3095)$ decays like a non-strange meson with I=0, the question arises whether or not the resonance is an SU_3 singlet, the eighth component of an octet or a mixture of the two, such as the physical ω and ϕ states. Information relevant to this classification can be obtained from the study of branching ratios into various channels, provided that the decay process itself conserves SU_3. An SU_3 singlet with odd charge conjugation is forbidden to decay into two mesons belonging to the same SU_3 multiplet, or more generally, to decay into two members of multiplets whose I_3=Y=0 members have the same charge conjugation.[51] Accordingly, SU_3 symmetry forbids the decay of such singlets into $K\bar{K}$, $K^*\bar{K}^*$, $K^{**}\bar{K}^{**}$ and KK^{**}, while it allows modes such as $K\bar{K}^*$ and $K^*\bar{K}^{**}$. This is generally not true for other SU_3 assignments.

A detailed study of the decays into two strange mesons seems to support the hypothesis that the $\psi(3095)$ is an SU_3 singlet.[52] The results are completely compatible with the predicted pattern of forbidden and allowed modes, as can be seen from Table VI. The most stringent limit has been set on the branching ratio for $\psi(3095) \rightarrow K_L K_S$. Four events, possibly background, lead to a 90% confidence limit of 9×10^{-5}. This suppression by more than an order of magnitude relative to the allowed decays rates, strongly indicates that SU_3 is operative and that the $\psi(3095)$ behaves like a singlet.

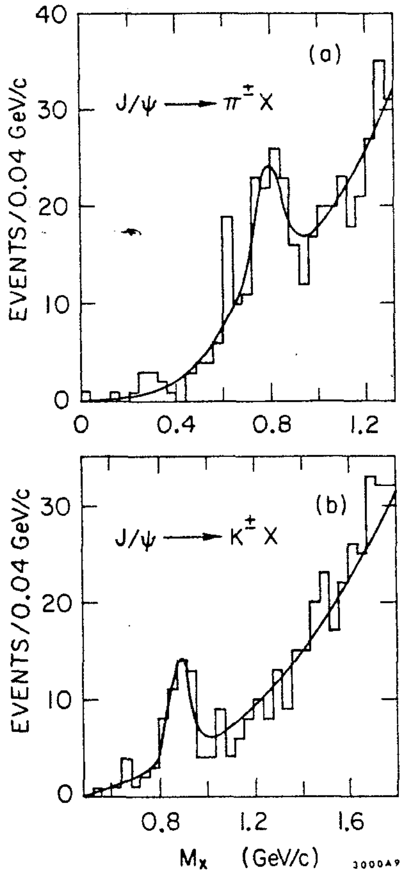

Fig. 36. Measurement of two-body decays of the $\psi(3095)$ in DASP.[48] Effective mass recoiling against a single charged particle.

Further tests of a possible SU_3 singlet assignment involve the comparison of branching ratios for observed decays to different members of the same two multiplets. A pure SU_3 singlet couples equally to $\pi^-\rho^+$, $\pi^o\rho^o$, $\pi^+\rho^-$, K^+K^{*-}, $K^o\bar{K}^{*o}$, K^-K^{*+}, $\bar{K}^oK^{*o}$, and equally to $p\bar{p}$ and $\Lambda\bar{\Lambda}$. Zero isospin for the $\psi(3095)$ requires equality for the three different charge states of the $\pi\rho$ mode and for the four KK^* modes; this is in agreement with the data. Experimentally, one measures $\Gamma(p\bar{p})/\Gamma(\Lambda\bar{\Lambda}) = 1.8 \pm 0.7$ and $\Gamma(\pi^-\rho^+)/\Gamma(K^-K^{*+}) = 1.9 \pm 0.7$ compared to the phase space corrected predictions of 1.5 and 1.2 by the SU_3 singlet hypothesis. Results from DASP[48] on the $\pi^+\rho^-$ and K^*K^{*-} branching ratios have been obtained by a very different technique illustrated in Fig. 36 and agree well with the SPEAR data. In general, one must take into account the possibility of interference with the second order electromagnetic decay of the ψ proceeding through a virtual photon. But in the case of $\pi^+\rho^-$ and $K^+\bar{K}^{*-}$ the same relative amplitudes are predicted for decays through one photon and direct decays of a singlet state. The ratio of $\pi^+\rho^-$ to $K^+\bar{K}^{*-}$ is thus unchanged by such an interference. Furthermore, the observed equality of the rates for $K^{\pm}K^{*\mp}$ and K^oK^{*o} argues against a substantial contribution from the second order electromagnetic process.

The disagreement of the relative branching ratio for $\pi^+\rho^-$ to that for $K^{*+}\bar{K}^{*-}$ with the prediction for a singlet ψ is at the one standard deviation level. If we assume that SU_3 is broken in the decay process with a resulting admixture of a small octet amplitude, A_8, to the dominant singlet amplitude, A_1, for the pseudoscalar-vector final state, the relative rates for K^+K^{*-} and $\pi^+\rho^-$ are proportional to $|A_1-A_8|^2$ and $|A_1+2A_8|^2$, respectively. The measured branching ratio yields

$$\mathrm{Re}\,(A_8/A_1) = 0.12 \pm 0.05 \quad .$$

Such a magnitude of symmetry breaking at the 10 to 20% level in the amplitude is consistent with that found in the decays of other mesons and baryons.

4. The Okubo-Zweig-Iizuka Rule

In models that consider the $\psi(3095)$ to be a bound state of a charmed quark and antiquark, all decays into noncharmed hadrons correspond to disconnected quark diagrams. According to the Okubo-Zweig-Iizuka rule[53] such processes are suppressed. This rule was originally invoked for the ϕ decays to "explain" the relative suppression of $\phi \to 3\pi$ compared to $\phi \to K\bar{K}$ as illustrated by the quark diagrams in Fig. 37. It has also been applied to explain the extremely small widths of the $\psi(3095)$ and $\psi(3684)$. The inhibition of the $\phi \to 3\pi$ relative to $\omega \to 3\pi$ is roughly a factor of 100 in rate, while ψ decays are suppresed by roughly a factor of 5×10^{-3}.

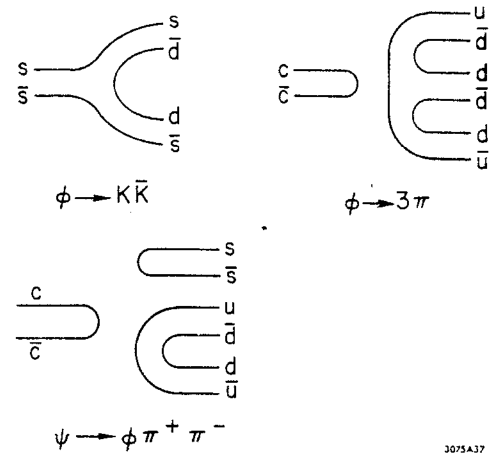

Fig. 37. Quark diagrams to illustrate the Zweig rule.

In order to obtain further quantitative information on this selection rule, ψ decays involving ϕ mesons have been studied by the SPEAR group.[52] Taking the ϕ as a pure $(s\bar{s})$ state such decays are described by quark diagrams with a second disconnection, provided no additional strange quarks appear in the final state. A comparison of the decay rates for $\psi \to \phi\pi^+\pi^-$ and $\psi \to \omega\pi^+\pi^-$ shows a rather mild inhibition,

$$\frac{\Gamma(\psi \to \phi\pi^+\pi^-)}{\Gamma(\psi \to \omega\pi^+\pi^-)} = 0.21 \pm 0.10 \quad .$$

However, the dynamics of the two decays are strikingly different as demonstrated in Fig. 38. While the effective mass of the $\pi^+\pi^-$ pair peaks in the region of the f(1270) for the final state $\omega\pi^+\pi^-$, the same region is empty for $\phi\pi^+\pi^-$, and all events accumulate below 1 GeV. One

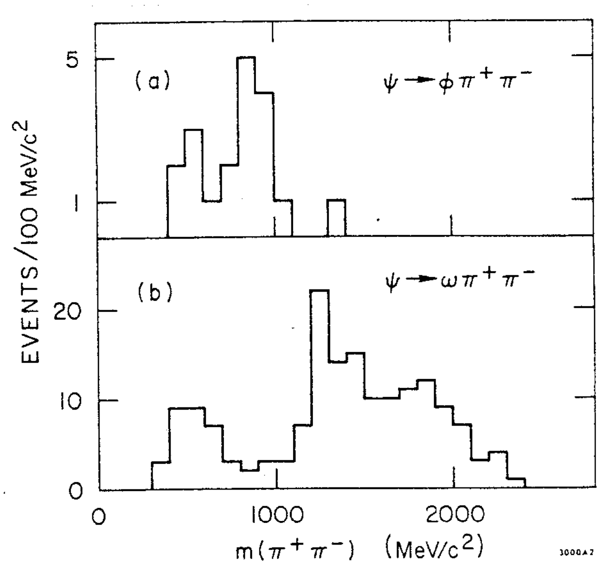

Fig. 38. Comparison of the $\pi^+\pi^-$ invariant mass distributions in the decays (a) $\psi(3095) \to \phi\pi^+\pi^-$ and (b) $\psi(3095) \to \omega\pi^+\pi^-$.[52]

possible explanation for these spectra is the assumption that the ϕ meson is preferentially produced in association with the state containing an $s\bar{s}$ component like the s* meson. Such a state would only decay to $\pi^+\pi^-$ if its mass is below the $K\bar{K}$ threshold. The decay $\psi \rightarrow \phi s^*$ would correspond to a once disconnected diagram, just like the $\psi \rightarrow \omega\pi^+\pi^-$, and consequently there should be no relative suppression due to the Zweig rule.

5. Radiative Decays of the $\psi(3095)$

Radiative decays of the ψ resonances are of particular interest to color models which predict large radiative branching ratios. In this context it is crucial that final states π^o can be clearly distinguished from photons. The selection by missing mass only is subject to uncertainty, however, clear signals for $\rho^{\pm}$ and ω in the multipion final states make it unlikely that the π^o could be a γ in disguise.

Recently two experimental groups at DORIS have reported measurements of radiative decays of the $\psi(3095)$. Both groups, the DESY-Heidelberg(49) and the DASP(54) collaboration, use a nonmagnetic setup with elaborate systems of shower detectors to measure the directions of photons.

The DESY-Heidelberg group has observed(49) the decay $\psi(3095) \rightarrow \eta'\gamma \rightarrow \rho\gamma\gamma \rightarrow \pi^+\pi^-\gamma\gamma$. The nonmagnetic setup with a large system of NaI and lead glass detectors measures the directions of all final state particles, charged and neutral, allowing the determination of particle momenta by kinematic fitting. Background from $\rho^o\pi^o$ can be easily eliminated, leaving a clean signal of 57 ± 13 events. This corresponds to a branching ratio of $(2.4 \pm 0.7) \times 10^{-3}$, in a agreement with preliminary data from the DASP group.

A detailed study of three photon final states has been in progress for quite some time, and earlier data have shown some evidence for a new state with a mass around 2.85 GeV decaying into two photons.(54) This will be discussed in chapter V.4. The DASP group has used the same data to derive an upper limit for the branching ratio to $\pi^o\gamma$ of 1.6×10^{-4}, and detected the mode $\psi(3095) \rightarrow \eta\gamma$ with a branching ratio of $(1.0 \pm 0.2) \times 10^{-3}$.

A comparison of the above rates can shed some light on the possible admixture of charmed quarks in the neutral pseudoscalar mesons. If η and η' contain only light quarks the radiative decay must proceed according to the two graphs in Fig. 39a,b. In the first diagram the photon is emitted from the light quarks. From SU_3 coupling one would

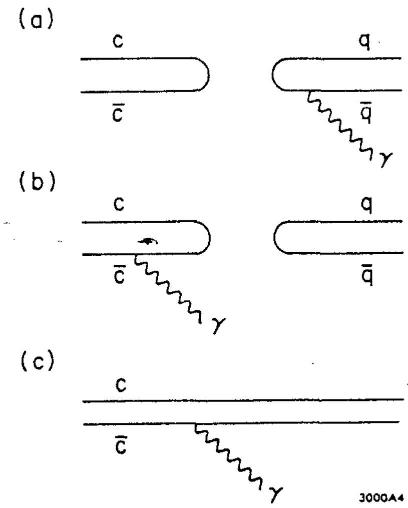

Fig. 39. Quark diagrams for radiative decays of the $\psi(3095)$ resonance.

expect $\Gamma(\pi^o\gamma) > \Gamma(\eta\gamma) > \Gamma(\eta'\gamma)$. This clearly is in contraction to the very small branching ratio to $\gamma\pi^o$. The second mechanism is for the photon to be emitted from the charmed quark pair. This diagram should be dominated by the process $\gamma\eta'$ because η' is almost a pure SU_3 singlet, while η is dominantly an octet state. This diagram predicts $\Gamma(\pi^o\gamma) = 0$ and $\Gamma(\eta'\gamma)/\Gamma(\eta\gamma) \simeq 25$, whereas experimentally the ratio is (2.4 ± 0.7). If this diagram was the correct description of the decay process it would imply a large SU_3 breaking. As an alternative explanation it has been suggested(55) that the η and η' contain a small $c\bar{c}$ component such that the radiative decay of the $\psi(3095)$ could proceed without suppression from the Zweig rule (Fig. 39c).

6. Summary of the Decays of the $\psi(3095)$

The study of decay modes of the $\psi(3095)$ has revealed a vast number of different decays with a fairly small branching ratio for any particular mode. Of all hadronic final states listed in Table VI the $2\pi^+ 2\pi^- \pi^o$ mode has the largest branching ratio, namely $(4 \pm 1)\%$. An obvious question is (1) how large a fraction of the ψ decays can be clearly reconstructed as exclusive decay channels, and (2) what can be inferred from any specific observed state about the total decay rate into states with the same particle multiplicity, but different charge configurations, many of which are unmeasureable with the existing detectors. For example, the measurement of the $2\pi^+ 2\pi^- \pi^o$ decay rate can be used to estimate the decay rate for all 5π final states. For this purpose one can make use of isotopic spin symmetry following a procedure by Shumchkevich.(56) This calculation will in general not give a definite answer, but set limits for decay rates, because the relative population of different isospins for higher multiplicity states is unknown and will strongly depend on the formation of resonances among the decay products. The following lower limits can be set; 13% for all pion decays, 8% for decays involving kaons, and probably 4% for decays involving baryons. If one assumes statistically equal population of all possible isospin states one obtains branching ratios of roughly 20%, 13%, and 5%, respectively, leading to a total of 38%. This number is to be compared to 69%, the total branching ratio for decays that do not arise from second-order electromagnetic processes. The difference of roughly 30% is presumably due to large uncertainties in the estimates, contributions from higher multiplicities, decays that are hard to detect like those involving η's, and/or photons, baryons, etc. One can certainly not rule out some 20% of the total decays involving many neutrals.

V. Hadronic Decay Modes of the $\psi(3684)$

The decays of the $\psi(3684)$ have proven to be quite different from the $\psi(3095)$ decays, primarily because they are dominated by a cascade to the $\psi(3095)$.

1. Decays $\psi(3684)$ to $\psi(3095)$

The presence of the $\psi(3095)$ among the decay products of the $\psi(3684)$ is detectable in many ways.(58) The study of μ-pairs reveals two well separated peaks in the invariant mass distribution, as shown in Fig. 40a, one corresponding to the μ-pairs produced at full energy, i.e., direct production plus decays $\psi(3684) \to \mu^+\mu^-$, and one around 3.1 GeV from the process

$$\psi(3684) \to \psi(3095) + \text{anything} \quad . \\ \quad \llcorner\!\to \mu^+\mu^-$$

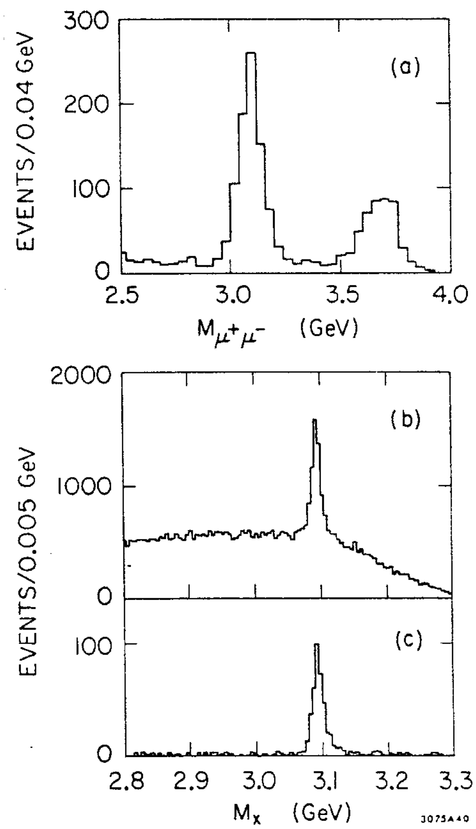

Fig. 40. Decays $\psi(3684) \to \psi(3095)\pi^+\pi^-$. (a) Inclusive $\mu^+\mu^-$ mass spectrum. Missing mass recoiling against all pairs of oppositely charged particles, (b) for all multiprong events, (c) for 4-prong events in which the measured particles conserved energy and momentum.(58)

A similar structure is observed in 3-prong and 4-prong events. Taking into account the leptonic branching ratio of the $\psi(3095)$, the data yield

$$\frac{\Gamma(\psi(3684) \to \psi(3095) + \text{anything})}{\Gamma(\psi(3684) \to \text{all})} = 0.57 \pm 0.08 \quad .$$

Alternatively, one observes the $\psi(3095)$ in the reaction

$$\psi(3684) \to \psi(3095)\pi^+\pi^- \quad .$$

where the identification of the $\psi(3095)$ is obtained from a sharp peak in the mass recoiling against any pair of oppositely charged particles (Fig. 40b). The observed rates, corrected for all known inefficiencies, lead to the branching ratio

$$\frac{\Gamma(\psi(3684) \to \psi(3095)\pi^+\pi^-)}{\Gamma(\psi(3684) \to \text{all})} = 0.33 \pm 0.03 \quad .$$

A particularly clean sample of events can be obtained for events that have both a lepton pair from decay of the $\psi(3095)$ and the recoil pion pair. This subset is selected by kinematics and plotted in Fig. 40c. Individual events as observed in the SLAC-LBL detector uniquely confirm the choice of the Greek letter ψ as a name for these particles (Fig. 41).

The ratio of the two branching fractions measures

$$\frac{\Gamma(\psi(3684) \to \psi(3095)\pi^+\pi^-)}{\Gamma(\psi(3684) \to \psi(3095) + \text{anything})} = 0.56 \pm 0.03 \quad .$$

If the cascade decay of $\psi(3684)$ to $\psi(3095)$ proceeds entirely via the reaction $\psi(3684) \to \psi(3095)\pi\pi$, the above ratio would have roughly the values 2/3, 1, or 1/3 for $\pi\pi$ states of definite isospin 0, 1, or 2, respectively. Isospin zero is clearly preferred. If one assumes that the $\psi(3684)$ like the $\psi(3095)$ decays to a pure isoscalar state, the difference between the measured and the expected value suggests the presence of decay modes to $\psi(3095)$ + neutrals other than $\psi(3095)\pi^0\pi^0$. The presence of $\psi(3684) \to \psi(3095)\gamma\gamma$ [59] does not completely account for the difference. However, the observation of the final state $\psi(3095)\eta$ with a branching ratio of $(4.3 \pm 0.8)\%$ [60] adds to a full balance between the expected and measured $\psi(3095)\pi\pi$ rates. It independently demonstrates that the $\psi(3684)$ is an isoscalar, and consequently has negative G-parity.

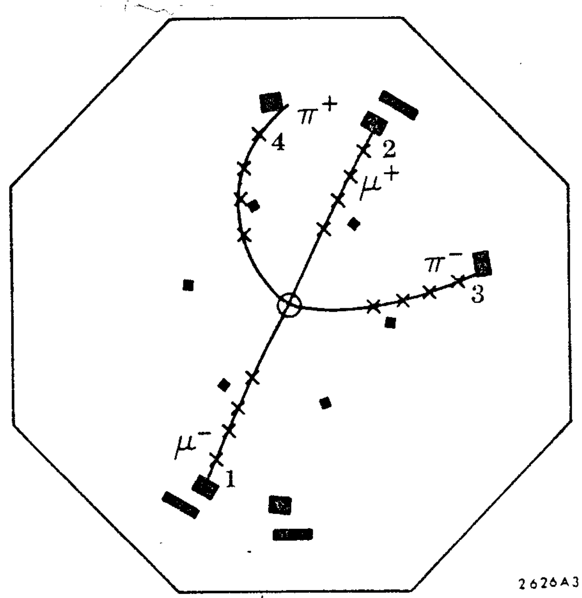

Fig. 41. An example of the decay $\psi(3684) \to \psi(3095)\pi^+\pi^-$ with $\psi(3095) \to e^+e^-$, as seen in the SLAC-LBL magnetic detector. Tracks 1 and 2 are leptons, tracks 3 and 4 are pions. [58]

2. Direct Hadronic Decays of the $\psi(3684)$

Only very few direct decays of the $\psi(3684)$ to "ordinary" hadrons have been observed so far. Branching ratios are listed in Table VII. For any specific channel the measured partial widths for the $\psi(3684)$ is about a factor of 2-3 smaller than for $\psi(3095)$.

Table VII. Decay modes of the $\psi(3684)$

Mode	Fraction (%)	Reference	Mode	Fraction (%)	Reference
e^+e^-	0.93 ± 0.16	37	$\gamma\gamma$	<0.5	72
$\mu^+\mu^-$	0.93 ± 0.16	37	γ	<0.7	49, 72
$\gamma \rightarrow$ hadrons	2.9 ± 0.4	37	$\gamma\eta$	<0.13	49
$\psi\pi^+\pi^-$	33.0 ± 3.3	58	$\gamma\eta'$	<0.11	49
$\psi\pi^0\pi^0$	17.2 ± 2.6	60	$\gamma\chi(2850)$	<1.1	61
$\psi\eta$	4.2 ± 0.7	60	$\gamma\chi(2850) \rightarrow 3\gamma$	<0.037	54
$\psi\gamma + \psi\pi^0$	<0.15	60	$\gamma\chi(3415)$	8.2 ± 2.2	61, 62 [a]
$2\pi^+2\pi^-$	0.08 ± 0.02	65	$\gamma\chi(3450)$	<5	62 [b]
$2\pi^+2\pi^-\pi^0$	0.35 ± 0.15	50	$\gamma\chi(3500)$	9 ± 3	62 [b]
$\rho^0\pi^0$	<0.1	49	$\gamma\chi(3550)$	8 ± 3	62 [b]
$K^+K^-\pi^+\pi^-$	0.14 ± 0.04	65			
$p\bar{p}$	0.023 ± 0.007	50			

[a] Angular distribution $f(\theta) \sim 1 + \cos^2\theta$ assumed.

[b] Values for an isotropic angular distribution of the photon. $f(\theta) \sim 1 + \cos^2\theta$ would increase the quoted fraction by a factor of 1.3.

If this relation holds for any direct decay as for the leptonic widths, this may be a support for the idea that decay rates are proportional to the wave function at the origin, $|\psi(0)|^2$.

If one tries to make up an account for the known decays of the $\psi(3684)$, it shows that there are about 30% of all decays still missing,

$\psi' \rightarrow \psi$ + anything	57%
$\rightarrow \gamma_V \rightarrow$ hadrons	3%
$\rightarrow$ leptons	2%
$\rightarrow$ "direct" hadrons $\lesssim$	10%

The limit of 10% for "direct" decays refers to an estimate derived from all $\psi(3095)$ decays other than those proceeding via an intermediate photon. This estimate takes into account the ratio of the total widths, and the suppression factor in the individual rates mentioned above.

The remaining 30% of all decays are no longer a serious problem. A variety of radiative transitions to several hitherto unobserved, high mass states has been discovered and will be discussed in the following.

VI. New States in Radiative Decays of the ψ States

If one accepts the hypothesis that the $\psi(3095)$ as well as the $\psi(3684)$ are bound states of a pair of new heavy quarks ($c\bar{c}$) then in analogy to the usual quark model one expects a whole family of such states. They would have parity $P=-(-1)^L$ and charge conjugation $C=(-1)^{L+S}$, where L is the orbital angular momentum and S the total spin of the pair. The lowest mass states would have zero orbital momentum between the quark and antiquark, and hence be $J^{PC}=0^{-+}$ and 1^{--} states. The L=1 states, triplet 0^{++}, 1^{++}, 2^{++} and singlet 1^{+-}, should be several hundred MeV higher. At even higher masses there would be L=2 states and radially excited L=0 and L=1 states.

The $\psi(3095)$ with $J^{PC}=1^{--}$ is associated with the L=0, S=1 ground state, the $\psi(3684)$ is assumed to be the first radial excitation, with the same spin configuration. Likewise the broader structures above 4.0 GeV, which are directly formed in e^+e^- annihilation, have most likely the quantum number of photon and could be interpreted as higher radial excitations. In addition to these states, others should exist that could be reached by radiative transitions from $\psi(3095)$ and from $\psi(3684)$ as indicated in Fig. 42. In the following these C-even states will be referred to by the generic name χ. These new states could be either pseudoscalar or P-wave states and they could decay into $\psi(3095)$ by the emission of a second photon or they could decay directly into ordinary hadrons.

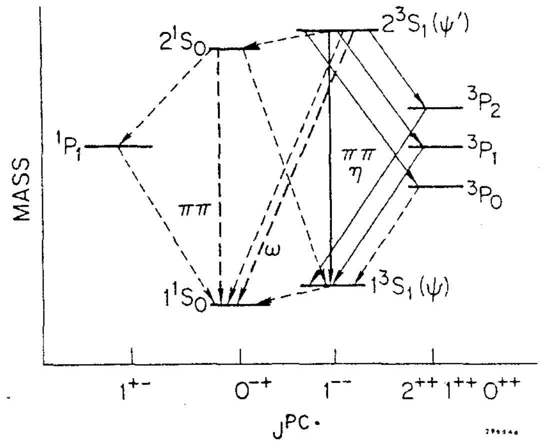

Fig. 42. Expected radiative and hadronic transitions in the spectroscopy of ($c\bar{c}$) states.

1. Inclusive Photon Spectra

The most direct way to look for C=+1 states among the decay products of $\psi(3095)$ and $\psi(3684)$ is to study the energy spectrum of photons observed in their decays. The SLAC-LBL group used some 150,000 decays of the $\psi(3095)$, and some 350,000 decays of the $\psi(3684)$ to search for monochromatic photons.[61] In their setup photons are detected by their conversion to e^+e^- pairs in the 5% radiation length material of the vacuum pipe and the surrounding scintillation counters. Though the conversion rates are very low and lead to a detection efficiency of the order of 1%, the rms energy resolution of 3-4% is very good. The shape of the inclusive photon spectra as shown in Fig. 43 is largely given by production and subsequent decay of neutral pions.

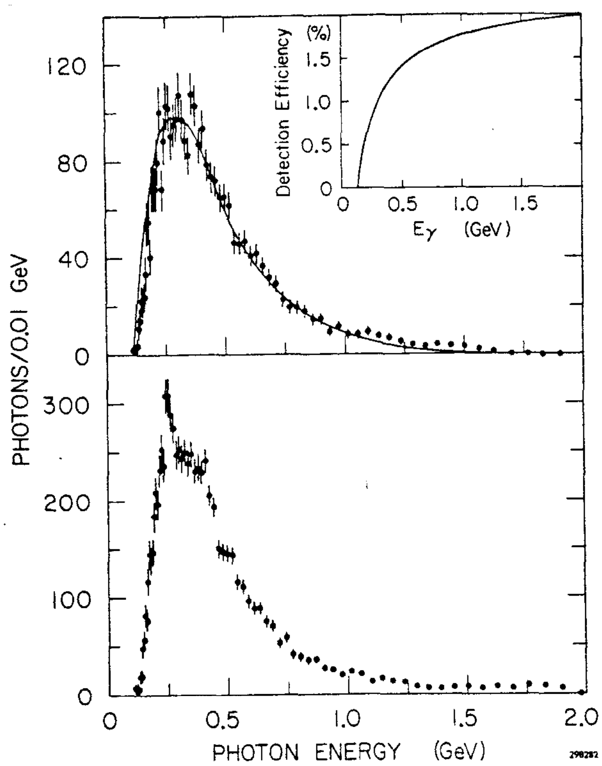

Fig. 43. Inclusive photon spectra measured at $\psi(3095)$ and $\psi(3684)$.[61]

The γ spectrum of the $\psi(3684)$, however, has a 5σ peak at 261 ± 5 MeV with a width consistent with the resolution. This photon line identifies the decay $\psi(3684) \rightarrow \gamma\chi(3415)$. The branching fraction for this decay is 0.063 ± 0.022 for an isotropic angular distribution and 0.075 ± 0.026 for a distribution $f(\theta) \sim 1 + \cos^2\theta$ of the polar angle θ of the photon (compare Section 3). The relatively large error is dominated by systematics.

There are no other significant monochromatic signals in either of the two spectra. Below 250 MeV, the small and rapidly varying acceptance makes it extremely difficult to find a signal. At higher energies the lines are expected to be broadened due to the motion of the decaying state. This Doppler broadening enlarges the widths by more than a factor of two and may cause an overlap of different lines. Upper limits have been evaluated under the assumption that the photon lines are well separated. They are typically about 4% at 400 MeV and 1% at 1 GeV (90% C.L.). The decay of the $\psi(3684)$ into a state with a mass of about 2850 MeV would lead to a monochromatic photon line at 750 MeV; no such line is observed. Likewise the $\psi(3095)$ data show no indication of such a state, however, the sensitivity for observing a low energy photon line depends strongly on the energy of the photon.

A collaboration of the universities of Maryland, Pavia, Princeton, San Diego and Stanford has recently[62] reported a measurement of the photon spectra using two sets of segmented NaI crystals mounted above and below the SPEAR interaction region. The apparatus is operated in conjunction with four layers of proportional tubes surrounding the beam pipe (Fig. 44). The energy resolution varies between 2.5% at 1500 MeV and 5% at 200 MeV. The intrinsic resolution of the crystals is degraded primarily by shower leakage to the sides, losses in the stainless steel walls between the crystals, and to a lesser extent by the readout electronics. The spectra of photons recorded in coincidence with at least two charged particles are presented in Fig. 45. While the spectrum observed at the $\psi(3095)$ appears structureless, the $\psi(3684)$ data show several bumps superimposed on a large background. Photon lines centered at 121 MeV, 168 MeV, and 256 MeV correspond to intermediate states with masses of 3561 MeV, 3512 MeV and

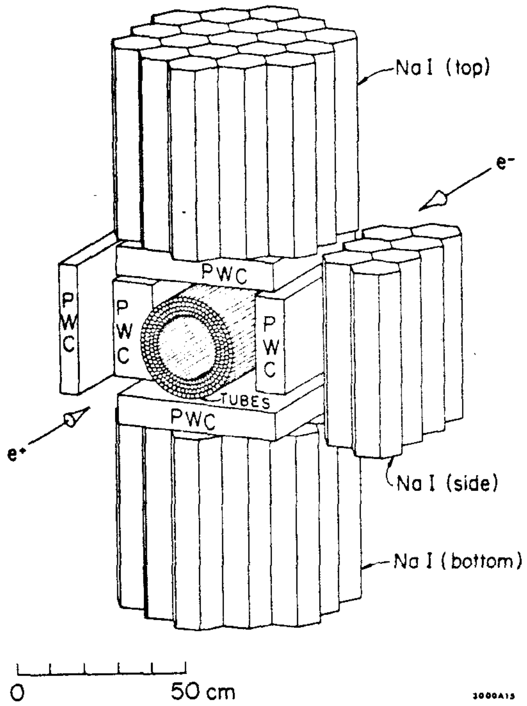

Fig. 44. Experimental setup for the NaI detector at SPEAR.[62]

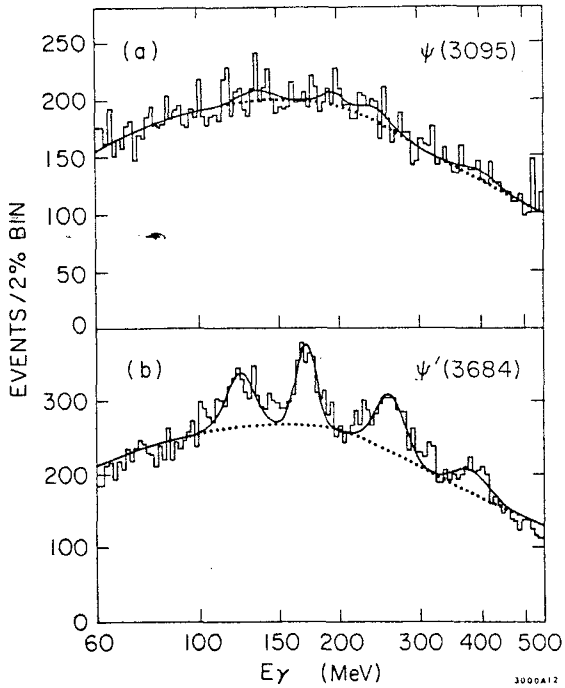

Fig. 45. Inclusive photon spectra measured at ψ(3095) and ψ(3684).[62]

3418 MeV, the peak at 383 MeV can be identified with the decay $\chi(3550) \rightarrow \gamma\psi(3095)$.

There are severe problems in extracting the branching ratios for these transitions. The observed widths of the peaks corresponding to monoenergetic photon lines are not the same. Whereas the signal at 168 MeV has the correct width, the lines at 121 MeV and 256 MeV are wider than expected from the resolution. This might indicate either unknown experimental problems or the presence of additional, unresolved photon lines. Secondly, the shape of background is unknown, and so far the authors have assumed a shape similar to the spectrum observed at the ψ(3095). This can be regarded only as a temporary solution. The fit designed to extract the branching ratio from the observed spectrum is dominated by large systematic uncertainties. Results are listed in Table VII. An upper limit of 5% for the decay $\psi(3095) \rightarrow \chi(2850)\gamma$ has been calculated from the ψ(3095) data.

2. Radiative Decays of the χ States

χ-states intermediate in mass to the ψ(3095) and ψ(3684) can decay to $\gamma\psi(3095)$. Such decays have been observed by the DASP group at DESY[63] and by the SLAC-LBL group at SPEAR.[61] Both groups identify the final state ψ(3095) by its decay to leptons. DASP measures the directions of both photons with the inner detector, the SPEAR group measures the energy and the direction of only one photon converted in the beam pipe. Kinematic fitting and simple cuts eliminate background from $\psi\pi^0\pi^0$ and $\psi\eta$ decay modes. The remaining events, 11 from DASP and 21 from SLAC, are plotted in Fig. 46. For each event there are two solutions for the mass of the intermediate state, as one does not know *a priori* which γ was emitted first.

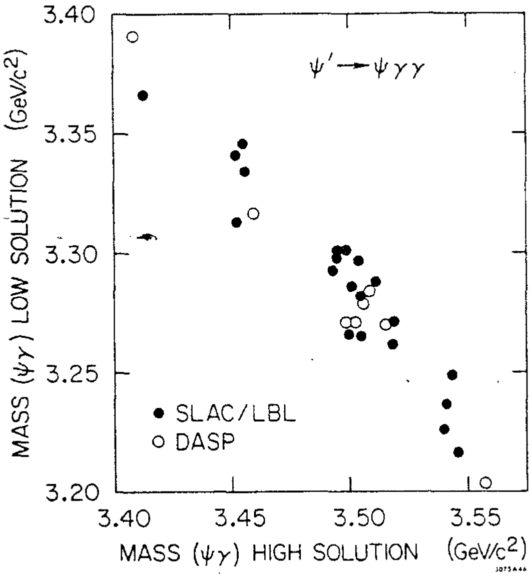

Fig. 46. Scatterplot of the two solutions for the mass of the intermediate states in decays $\psi(3684) \to \psi(3095)\gamma\gamma$ (Refs. (61,63)

There are three main clusters of events. The mass spread of each cluster projected on the axis for the high mass solution is consistent with the expected mass resolution. There is clear support for a state at 3.50 GeV, five events cluster at 3.45 GeV, and another five at 3.55 GeV. There is no other mass assignment for three states that fits the data. The branching ratio products for the decay sequence $\psi' \to \gamma\chi$, $\chi \to \gamma\psi$, as quoted by the SLAC group are $(1.2 \pm 0.6)\%$, $(3.7 \pm 1.1)\%$ and $(1.2 \pm 0.6)\%$ for the $\chi(3450)$, $\chi(3500)$, and $\chi(3550)$, respectively. These rather small transition rates are compatible with the observed monoenergetic photon lines. There is only one event from each of the two experiments compatible with the decay of the $\psi(3415)$. Its branching ratio to $\gamma\psi(3095)$ must therefore be considerably smaller than for the neighboring χ states.

3. Hadronic Decays of the χ States

It was the hadronic decay modes of the χ particles that first provided evidence for the existence of several states, intermediate in mass to the $\psi(3095)$ and the $\psi(3684)$.[64] The data sample for this study consists of 2-, 4- and 6-prong events with total charge zero, recorded at the $\psi(3684)$. The photon in the final state is undetected, its presence being inferred from the measurement of the missing energy and the missing momentum. To illustrate this, the square of the missing mass in 4-prong events is compared for decays of the $\psi(3095)$ and the $\psi(3684)$ in Fig. 47. In the case of the $\psi(3095)$, the distribution is consistent with the missing π^0, but inconsistent with the missing γ. For the $\psi(3684)$ the opposite is the case—the missing neutral is not a π^0, but it is consistent with being a photon. The case can actually be proven with the help of the shower counter information. In the rest system of the missing particle the angular distribution of the photons observed in the shower hodoscope is strongly peaked in forward direction, whereas for a π^0 this distribution should be flat. Events compatible with the hypothesis $\psi(3684) \to \gamma\chi$ and

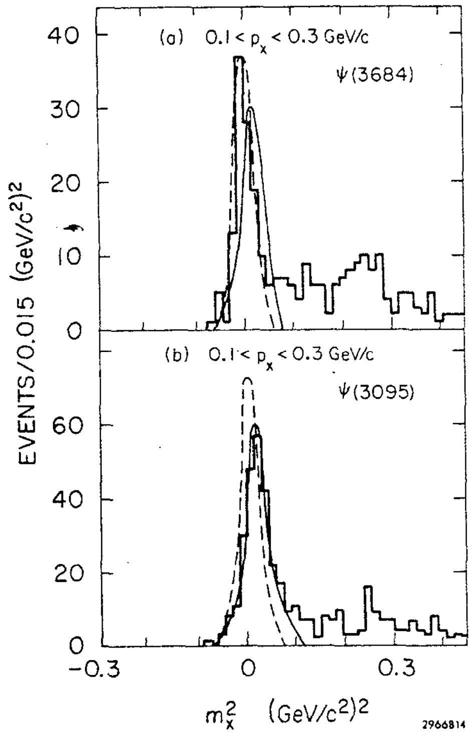

Fig. 47. The square of the missing mass for 4-prong events with missing momentum $0.1 < p_X < 0.3$ GeV/c (a) for $\psi(3684)$ and (b) for $\psi(3095)$. The solid and the dashed lines give the resolution functions for a missing π^0 and γ, respectively (Ref. (64)).

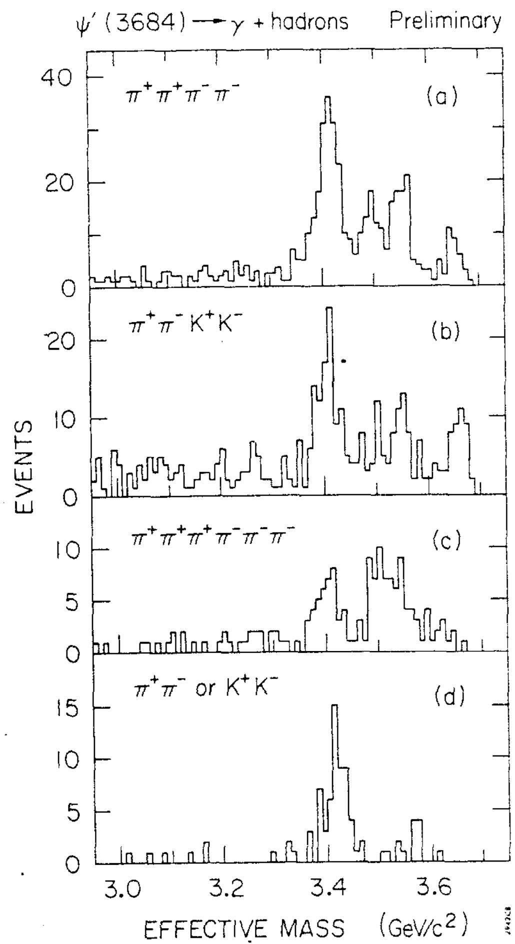

Fig. 48. Invariant mass spectra for events constraint to fit the reactions $\psi' \to \gamma +$ hadrons for various hadronic decay modes.[64]

the subsequent decays $\chi \to \pi^+\pi^+\pi^-\pi^-$, $\chi \to \pi^+\pi^+\pi^+\pi^-\pi^-\pi^-$, $\chi \to \pi^+\pi^+K^+K^-$, $\chi \to \pi^+\pi^-$ or K^+K^- are selected and submitted to a kinematic fitting procedure. Additional cuts are applied to remove background from the "cascade" decays $\psi \to \psi\pi^+\pi^-$ and to isolate the various decay modes. The shower counters and the muon chambers are used to suppress the enormous potential background in the two-body decays due to radiative electron or muon pairs. The invariant masses of all hadrons in the final states are presented in Fig. 48 for all decay modes under study. The four-body spectra show three clearly separated peaks at masses of 3415, 3500, and 3550 MeV/c^2 plus a fourth above 3600 MeV/c^2 corresponding to the nonradiative decays $\psi' \to 4\pi$ and $\psi' \to \pi\pi KK$. Except for the fortuitously narrow spike in $\pi^+\pi^-K^+K^-$ at 3.50 GeV/c^2, the observed widths are all similar and consistent with the experimental resolution. The 6π data appear to have a slightly worse resolution than the 4-prong data, and the two higher mass states are not resolved. The interpretation of the populations above 3.45 GeV/c^2 in terms of two distinct states is, however, supported by the analysis of the radiative decays discussed above.

For 2-prong events, the distinction between the $\pi^+\pi^-$ and K^+K^- final state has been made on the basis of the lowest χ^2 in the kinematic fit. These decays into two pseudoscalar mesons are particularly interesting because such a state has natural spin and parity and therefore only χ states with even spin and parity can decay to this mode. The strong signal at 3415 MeV/c^2 and a considerably weaker signal at 3550 MeV/c^2 confirm the earlier result.

In order to obtain some more information on the spin of the χ states, the angular distributions of the photon relative to the incident positron beam have been studied. In general, this distribution is of the form $1+a\cos^2\theta$ with $|a|\leq 1$. For spin J=0 the value is a=1, while predictions of a for other spins are not unique. The data for the three χ states are presented in Fig. 49. The distribution for $\chi(3415)$ suggests a J=0 assignment, the two other distributions are consistent with isotropy, but the statistical errors are too large to allow any definite conclusions (compare last column of Table VIII). The DESY-Heidelberg group at DORIS had demonstrated that the $\chi(3500)$ has nonzero spin.

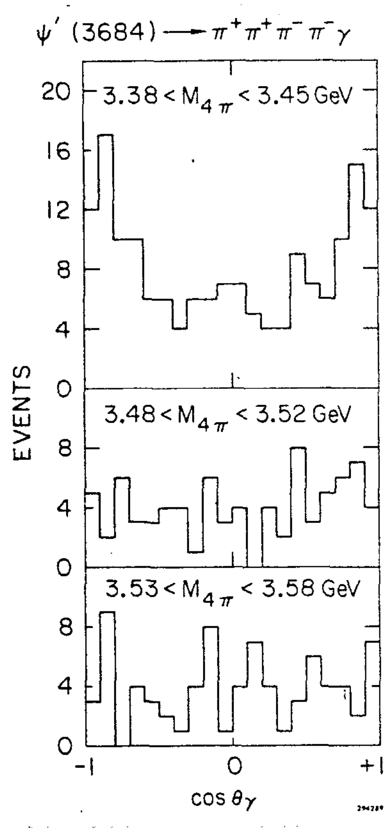

Fig. 49. Distribution of cos θ for 3 different bins of the 4π invariant mass. θ is the angle between the direction of the photon and the positron beam direction.[65]

A summary of the branching ratio products $B(\psi' \rightarrow \chi\gamma) \times B(\chi \rightarrow \text{hadrons})$ of various decay modes of the different states is given in Table VIII.[65] The data have been corrected for losses due to limited geometrical acceptance and cuts, as well as for decay in flight of $K^{\pm}$ mesons. The errors quoted reflect both statistical and systematic uncertainties. The branching ratio for $\psi(3684) \rightarrow \chi\gamma$ obtained from the inclusive photon spectrum have

Table VIII. Summary on the hadronic decay modes of the χ states.

Mass (MeV)	Decay mode f	$BR(\psi' \to \chi\gamma) \times BR(\chi \to f)$	$BR(\chi \to f)$	Coefficient a in $(1 + a\cos^2\theta)$
3414 ± 4	$\pi^+\pi^-\pi^+\pi^-$	$(3.2 \pm 0.6) \times 10^{-3}$	$(3.9 \pm 1.3) \times 10^{-2}$	1.4 ± 0.4
	$\pi^+\pi^-K^+K^-$	$(2.7 \pm 0.7) \times 10^{-3}$	$(3.3 \pm 1.2) \times 10^{-2}$	
	$\pi^+\pi^-\pi^+\pi^-\pi^+\pi^-$	$(1.4 \pm 0.5) \times 10^{-3}$	$(1.7 \pm 0.8) \times 10^{-2}$	
	$\pi^+\pi^- + K^+K^-$	$(1.4 \pm 0.4) \times 10^{-3}$	$(1.7 \pm 0.6) \times 10^{-2}$	
3508 ± 4	$\pi^+\pi^-\pi^+\pi^-$	$(1.1 \pm 0.4) \times 10^{-3}$	$(1.2 \pm 0.6) \times 10^{-2}$	0.25 ± 0.5
	$\pi^+\pi^-K^+K^-$	$(0.6 \pm 0.3) \times 10^{-3}$	$(0.7 \pm 0.3) \times 10^{-2}$	
	$\pi^+\pi^+\pi^+\pi^-\pi^-\pi^-$	$(1.3 \pm 0.4) \times 10^{-3}$	$(1.4 \pm 0.6) \times 10^{-2}$	
	$\pi^+\pi^- + K^+K^-$	$< 0.15 \times 10^{-3}$	$< 0.17 \times 10^{-2}$	
3552 ± 6	$\pi^+\pi^-\pi^+\pi^-$	$(1.6 \pm 0.4) \times 10^{-3}$	$(2.0 \pm 0.9) \times 10^{-2}$	0.22 ± 0.4
	$\pi^+\pi^-K^+K^-$	$(1.4 \pm 0.4) \times 10^{-3}$	$(1.8 \pm 0.7) \times 10^{-2}$	
	$\pi^+\pi^+\pi^+\pi^-\pi^-\pi^-$	$(1.3 \pm 0.4) \times 10^{-3}$	$(1.6 \pm 0.8) \times 10^{-2}$	
	$\pi^+\pi^- + K^+K^-$	$(0.23 \pm 0.12) \times 10^{-3}$	$(0.3 \pm 0.2) \times 10^{-2}$	
3454 ± 7	$\pi^+\pi^-\pi^+\pi^-$	$< 4 \times 10^{-4}$		
	$\pi^+\pi^-K^+K^-$	$< 5 \times 10^{-4}$		
	$\pi^+\pi^+\pi^+\pi^-\pi^-\pi^-$	$< 7 \times 10^{-4}$		
	$\pi^+\pi^- + K^+K^-$	$< 3 \times 10^{-4}$		

90% confidence level for all limits.

been used to calculate the actual branching fractions of the χ states. There is no evidence for a hadronic decay mode of a state at 3450 MeV that has only been seen in the study of $\psi' \to \psi\gamma\gamma$.[61] Upper limits at 90% confidence level are given.

4. Evidence for the χ(2850)

At the Lepton-Photon Symposium last summer, two experiments at DORIS[66] reported evidence for a new state with a mass of 2.85 GeV/c^2 decaying into two photons. The existence of this state has been reinforced by new data from DASP presented at the Tbilisi Conference.[1] Although $J \neq 1$ and $C=+1$ is all that is so far known, this state is generally interpreted as the pseudoscalar state with $J^{PC}=0^{-+}$. The evidence is based on an analysis of three photon final states recorded at the ψ(3095) resonance. Simple geometrical constraints allow a rather clean selection of such states. For each event there are three possible 2γ combinations, and clear signals for η and η' decay are visible in the effective mass spectra. The largest of all two photon masses is shown in Fig. 50a. A narrow peak, superimposed on a smooth background is observed between 2.8 and 2.9 GeV. The width is consistent with the experimental resolution. The background can be accounted for by the sum of the contributions from the strongly radiative QED process $e^+e^- \to \gamma\gamma$ and reflections from $\eta\gamma$ and $\eta'\gamma$ decays of the ψ(3095). The signal contains 29 events including 14 events background. Assuming that the observed enhancement of 15 events results from the decay of a narrow resonance with a mass of 2850 ± 50 MeV the product of the branching ratios for $\psi(3095) \to \chi(2850)\gamma$ and $\chi(2850) \to \gamma\gamma$ is

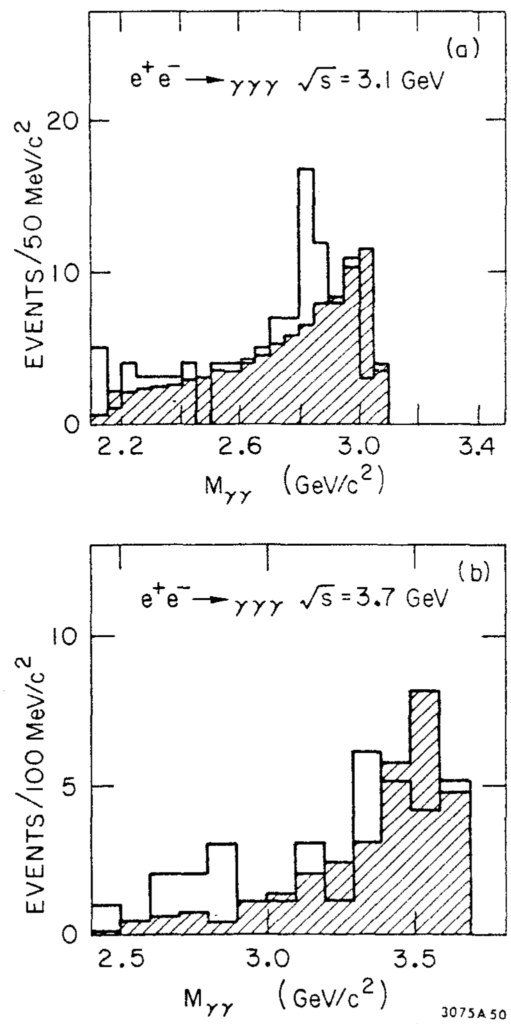

Fig. 50. Two-photon effective mass (highest mass combination) in three photon final states produced at (a) ψ(3095) and at (b) ψ(3684). The hatched areas show the background from QED plus reflections from $\eta\gamma$ and $\eta'\gamma$.

$(1.5 \pm 0.4) \times 10^{-4}$. The DESY-Heidelberg group, using the same method, finds an enhancement of 8 events above a background of 10 ± 4 events at a mass of roughly 2.7 GeV. If this excess is attributed to the same resonance the rate translates to $(1.4 \pm 0.8) \times 10^{-4}$.

Extensive searches for hadronic decay modes of the $\chi(2850)$ in radiative decays of the $\psi(3095)$ have so far not been successful. Special emphasis was placed on the decay $\chi(2850) \rightarrow p\bar{p}$, since two candidate events were reported last year. The SLAC-LBL group[57] has found no signal and places a 90% confidence limit of $B(\psi \rightarrow \chi\gamma) \times B(\chi \rightarrow p\bar{p}) < 4 \times 10^{-5}$. This is about a factor of 5 smaller than the upper limit reported from DASP.[1]

Three photon events observed at the $\psi(3684)$ resonance have been analyzed in the same way, the result is given in Fig. 50b. Between 2.7 GeV and 2.9 GeV there are 5 events observed compared to 1.3 events expected from radiative $\gamma\gamma$ final states. This translates to an upper limit of $B(\psi' \rightarrow \chi\gamma) \times B(\chi \rightarrow \gamma\gamma) < 3.7 \times 10^{-3}$.

5. The ψ Spectroscopy

A summary of all new states and their decay modes is presented schematically in Fig. 51. It clearly resembles the level scheme (Fig. 42) drawn from the idea that the new mesons are bound states of a new quark and its antiquark. One expects four levels of even charge conjugation between $\psi(3095)$ and $\psi(3684)$, one pseudoscalar $^1S_0$ with $J^{PC} = 0^{-+}$ and three ^3P_J states with $J^{PC} = 0^{++}, 1^{++}, 2^{++}$.

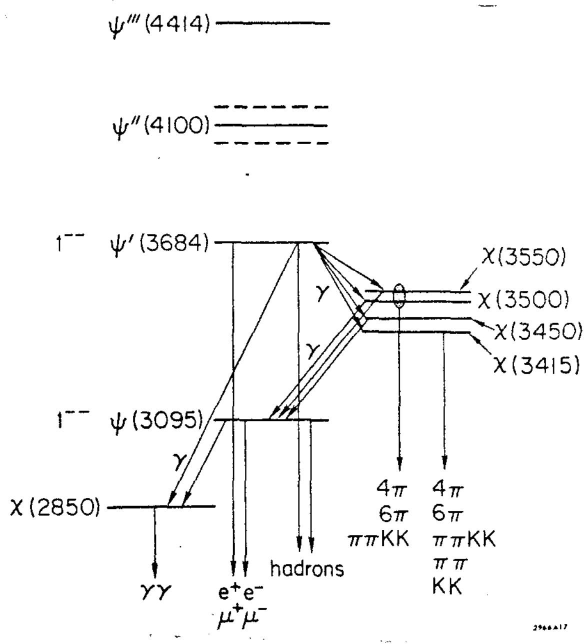

Fig. 51. Energy level diagram and decay modes of the new states.

Experimentally, there are four C-even states, namely $\chi(3415)$, $\chi(3450)$, $\chi(3500)$, and $\chi(3550)$:

1. The relatively strong decay mode to $\pi^+\pi^-$ and K^+K^- and the angular distribution of the $\chi(3415)$ highly suggest the quantum number assignment $J^{PC} = 0^{++}$.
2. The $\chi(3550)$ must have natural spin parity (based on the $\pi^+\pi^-/K^+K^-$ decay mode), and the observed value of $a = 0.2 \pm 0.4$ slightly favors $J \neq 0$.

3. The of $\pi^+\pi^-$ and K^+K^- decays for the $\chi(3500)$ is consistent with a state belonging to an unnatural spin-parity sequence, 0^-, 1^+, 2^-. The angular distribution requires $J \neq 0$.

4. Only five events of the decay $\chi(3450) \to \psi(3095)\gamma$ have been measured; there is no evidence for hadronic decay modes of this state, and no clear signal in the inclusive photon spectra. Thus, it requires confirmation.

This is all that can be deduced from the data above. However, comparing the available information with the predicted levels, one is lead to a unique assignment: It is $J^{PC}=0^{++}$, 1^{++}, 2^{++} for the states $\chi(3414)$, $\chi(3500)$, $\chi(3550)$, and the only level left for the $\chi(3450)$ is the pseudoscalar 0^{-+}. This assignment was suggested by Chanowitz and Gilman.(67)

There is evidence, though not fully convincing at this stage, for a state at 2.85 GeV, usually taken to be the pseudoscalar partner of the $\psi(3095)$. While the number of observed χ states is so far in agreement with the $c\bar{c}$ bound state hypothesis, some difficulties may arise if the 4.1 GeV enhancement turns out to be split into several substates. Furthermore, the relative mass splittings for the P states are in disagreement with general bounds computed(68) in a nonrelativistic model. However, satisfactory agreement with the data has been obtained both in a relativistic calculation(69) and in a model proposed by Schnitzer(70) that introduces a long-range spin dependence. The relative rates for electric dipole transitions $\psi(3684) \to \chi\gamma$ are proportional to $(2J+1)k^3$ and agree reasonably well with the data.

Identifying the $\chi(3450)$ with the $2\,^1S_0$ state leads to serious contradictions with the $c\bar{c}$ bound state model and the standard short range picture of the decays. The wave functions for the $^3S_1$ and the $^1S_0$ states supposedly are similar, while those for $2\,^3S_1$ and $1\,^3S_1$ or $2\,^1S_0$ and $1\,^1S_0$ should be almost orthogonal. This is in agreement with the small branching ratio for the transition $\psi(3684) \to \chi(2850)\gamma$. Likewise, one would expect transitions $2\,^1S_0 \to 1\,^3S_1$ to be suppressed. This turns out to be in contradiction with the lower limit of $B(\chi(3450) \to \psi(3095)\gamma) > 24\%$. Furthermore, this limit and the relation

$$\Gamma\left(2\,^1S_0 \to 1\,^3S_1 + \gamma\right) \lesssim \Gamma\left(2\,^3S_1 \to 1\,^3S_0 + \gamma\right) < 2.5 \text{ keV}$$

lead to a total width of less than 10 keV for the 2^1S_0 state. This turns out to be in strong disagreement with a predicted value of 2 MeV from the short range picture.

The above assignment of levels is based on the assumption that there are only four levels with C=+1 between $\psi(3095)$ and $\psi(3684)$. However, it is not unthinkable that the $^1D_2(J^{PC}=2^{-+})$ level is located below the $\psi(3684)$, due to large mass splitting.(71) In this case a complete assignment of levels in the framework of a $c\bar{c}$ bound state model would no longer be possible with the present experimental information.

VII. Summary on ψ Spectroscopy

A rich spectrum of new states with masses above 3 GeV has been discovered in the past two years. Some, notably the $\psi(3095)$ and the $\psi(3684)$, have been studied in detail, others are still largely unknown. The present experimental knowledge can be summarized as follows:

1. There are two extremely narrow and two or more broader resonances in e^+e^- annihilation above 3 GeV.
2. The $\psi(3095)$ and the $\psi(3684)$ are vector particles, pure states of odd parity and odd charge conjugation like the photon.
3. Both states couple directly to hadrons in a state of definite isospin and G-parity, $I^G=0^-$.
4. The ψ states do not seem to couple directly to leptons.
5. The decay rates of the $\psi(3095)$ favor an assignment as an SU_3 singlet.
6. The $\psi(3684)$ decays to $\psi(3095)$ with a branching ratio of almost 60%. The remaining decays proceed largely via photon emission to at least four C-even states.
7. There is some evidence for a C-even state with $J\neq 1$ below the $\psi(3095)$.

Clearly additional information is needed to implement the present knowledge, in particular on the intermediate states. All the data presently available can be explained by the existence of a fourth, heavy quark. It will be the subject of the fifth and final lecture to show that the properties of this new quark are similar to those conjectured by Glashow, Iliopoulos and Maiani(19) for the charmed quark.

LECTURE V. CHARM IN e^+e^- ANNIHILATION

I. Introduction

It was on the basis of symmetry among fermions that Bjorken and Glashow[19] proposed to introduce a fourth quark. The addition of a fourth hadron constituent carrying a new quantum number has immediate consequences for the spectrum of hadronic states. Multiplets with 8 and 9 members in SU_3 are enlarged to 15 or 16 members in SU_4. As an example the 0^- meson multiplet is given in Fig. 52. Since the additional states had not been observed, it was invoked that the new quark was considerably heavier than the other three. This plausibly pushed the masses of the new states into a relatively unexplored region of the mass scale.

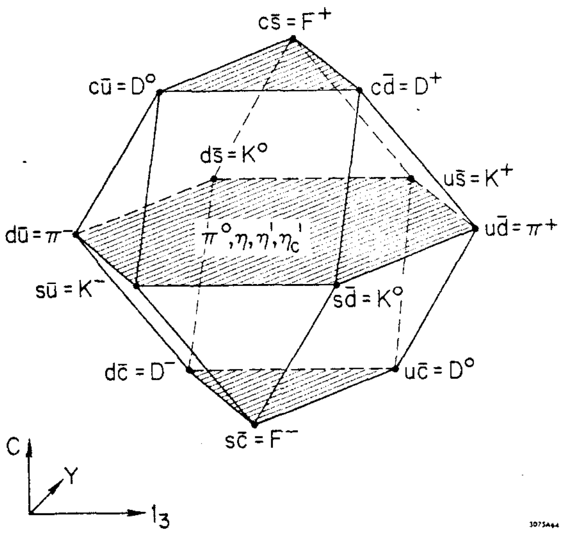

Fig. 52. Multiplet of pseudoscalar mesons in SU_4. The familiar $SU_3(C=0)$ multiplet is marked in the middle plane.

It was again a peculiarity of the neutral kaons that lead to the essential idea of Glashow, Iliopoulos and Maiani.[19] They used the charmed quark to cancel all strangeness changing neutral currents, that could contribute to the decay $K_L \rightarrow \mu^+\mu^-$ in first order weak interaction. Let us digress briefly to demonstrate this elegant theoretical mechanism.

The phenomenology of leptonic and semi-leptonic weak processes is based on V-A currents involving the four leptons (two isodoublets) and so far three quarks (isodoublet plus isosinglet),

$$\begin{pmatrix}\nu_\mu \\ \mu^-\end{pmatrix}_L \quad \begin{pmatrix}\nu_e \\ e^-\end{pmatrix}_L \quad \begin{pmatrix}u \\ d'\end{pmatrix} \quad (s')$$

The charged Cabbibo current has the quark structure

$$J_h^+ = \bar{u}d' = \bar{u}d \cos\theta + \bar{u}s \sin\theta$$

where

$$d' = d\cos\theta + s\sin\theta \quad , \qquad s' = -d\sin\theta + s\cos\theta \quad .$$

The weak interactions, which do not conserve strangeness, are free to mix d and s. These two quarks have the same electric charge, and differ only by strangeness. The weak coupling selects another pair of orthogonal states, d' and s', related to d and s by a rotation of $\theta \sim 15^{\circ}$, the Cabbibo angle.

The s' quark does not couple at all to the weak current, while u $\longleftrightarrow$ d' transitions are identical in strength to the $e^- \longleftrightarrow \nu_e$ and $\mu^- \longleftrightarrow \nu_\mu$ transitions.

The neutral hadronic current would be

$$
\begin{aligned}
j_h^o &= (u\bar{u} - d'\bar{d}') \\
&= u\bar{u} - d\bar{d}\cos^2\theta - s\bar{s}\sin^2\theta - (s\bar{d} + d\bar{s})\cos\theta\,\sin\theta
\end{aligned}
$$

and thus would include $|\Delta S|=1$ transitions. Such a scheme is in conflict with the smallness of the K_S-K_L mass difference and the observed rate for the decay $K_L \to \mu^+\mu^-$. This indicates that $|\Delta S|=1$ neutral currents must be absent in first and second order weak interactions. The introduction of a fourth quark solves this problem and at the same time provides an elegant theory of four quarks and four leptons with identical weak couplings. This is achieved by postulating a new quark c, with electric charge +2/3 and a new quantum number charm, that is not conserved by weak interactions. The c and s' quark are combined to a new isodoublet,

$$
\begin{pmatrix} \nu_\mu \\ \mu^- \end{pmatrix} \begin{pmatrix} \nu_e \\ e^- \end{pmatrix} \quad \begin{pmatrix} u \\ d' \end{pmatrix} \begin{pmatrix} c \\ s' \end{pmatrix}
$$

changing the quark structure of the charged current to

$$
\begin{aligned}
j_h^+ &= \bar{u}d' + \bar{c}s' \\
&= \cos\theta\,(\bar{u}d + \bar{c}s) + \sin\theta\,(\bar{u}s - \bar{c}d)
\end{aligned}
$$

and the neutral current to

$$
\begin{aligned}
j_h^o &= u\bar{u} - d'\bar{d}' + c\bar{c} - s'\bar{s}' \\
&= u\bar{u} - d\bar{d} + c\bar{c} - s\bar{s} \quad .
\end{aligned}
$$

Hence the weak neutral current is diagonal, allowing no exchange of strangeness, charm, and isospin. The assignment of the c-quark to the same isodoublet as s' has immediate consequences for the charm changing charged current. The c-quark is predicted to decay mostly ($\cos\theta$ in amplitude) to s-quarks with the selection rules

$$\Delta Q = \Delta S = \Delta C \qquad \Delta I = 0$$

The transition $c \longleftrightarrow d$ is Cabbibo suppressed ($\sin\theta$ in amplitude) with the selection

$$\Delta Q = \Delta C \qquad \Delta S = 0 \qquad \Delta I = 1/2$$

Consequently, the lowest lying charmed hadrons will preferentially decay to strange particles. For the pseudoscalar states this means that

$$D^o \rightarrow K^-\pi^+ \,, \qquad D^+ \rightarrow K^-\pi^+\pi^+$$

are Cabibbo favored,

$$D^o \rightarrow \pi^-\pi^+ \,, \qquad D^+ \rightarrow \pi^-\pi^+\pi^+$$

are Cabbibo suppressed, and

$$D^o \not\rightarrow K^+\pi^- \,, \qquad D^+ \not\rightarrow K^+\pi^+\pi^-$$

are absolutely forbidden. It should be noted here that the final state $K^-\pi^+\pi^+$ is exotic in terms of the quark picture; a meson of negative strangeness and positive charge cannot be formed from a single quark-antiquark pair. Thus the observation of a state decaying to this 'exotic' mode, but not to the 'nonexotic' $K^\pm\pi^+\pi^-$, is a rather strong proof for the weak decay of a charmed meson.

In addition to the charmed quark being a theoretical necessity, there has been more and more experimental evidence for the existence of a fourth quark, most of which comes from e^+e^- annihilation:

1. The extremely small width of the $\psi(3095)$ and the $\psi(3684)$ is commonly explained in terms of Zweig's rule for a state composed of a $c\bar{c}$ quark pair.
2. The four narrow C-even states, referred to by the generic name χ, show all the properties expected from a spectrum of $c\bar{c}$ states.
3. The threshold-like behavior of the total hadronic cross section in e^+e^- annihilation near 4 GeV can be interpreted as the onset of charmed particle production.
4. Dilepton events in high energy ν experiments could indicate the weak production and decay of charmed hadrons.

The most serious difficulty the charm hypothesis had encountered until recently was the lack of direct proof for the existence of particles carrying the proposed new quantum number and displaying the properties predicted by the GIM mechanism. If the behavior of the hadronic cross section near 4 GeV was somehow related to the threshold for the production of new mesons, their mass should lie between 1.84 GeV and 1.95 GeV. The lower limit is given by the narrow width of the $\psi(3684)$ while the upper limit is given by the rise in R near 3.9 GeV.

II. Discovery of Narrow States Near 1.86 GeV

The first direct observation of decays of 'new' mesons has recently been reported by the SLAC-LBL group.[73] In a sample of 29,000 hadronic events collected at c.m. energies between 3.90 GeV and 4.60 GeV a search for narrow peaks in invariant mass distributions of two, three, and four particles was performed. A signal of 110 ± 24 decays of a state decaying to $K^{\pm}\pi^{\mp}$, and 124 ± 21 decays to $K^{\pm}\pi^{\mp}\pi^{+}\pi^{-}$ have been observed at a mass of 1865 ± 15 MeV/c.

The evidence for this state is presented in Fig. 53. Invariant mass spectra for all possible combinations of two oppositely charged particles are plotted in the top row assuming both π and K masses for the particles. Through kinematic reflections, a signal appears near 1.74 GeV/c^2 for the $\pi^{+}\pi^{-}$ hypothesis, at 1.87 GeV/c^2 for $K^{+}\pi^{-}$ or $K^{-}\pi^{+}$, and at 1.98 GeV/c^2 for $K^{+}K^{-}$. To establish the correct choice of final-state particles associated with these peaks the measured flight time for each particle is used. Figure 54 illustrates that for momenta around 800 MeV/c the typical difference in flight time between a π and a K is comparable to the measurement resolution of 0.4 nsec, and therefore a separation can only be done on a statistical basis. The following technique is applied to extract maximum information on particle identity. Each track is assigned weights proportional to the probabilities that it is a π or K. These weights are determined from the measured momentum and time of flight assuming a Gaussian distribution with standard deviation 0.4 nsec. The relative π-K weights are normalized so that their sum is unity, and two-particle combinations are weighted by the joint probability that the particles satisfy the particular π or K hypothesis assigned to them. In this way, the total

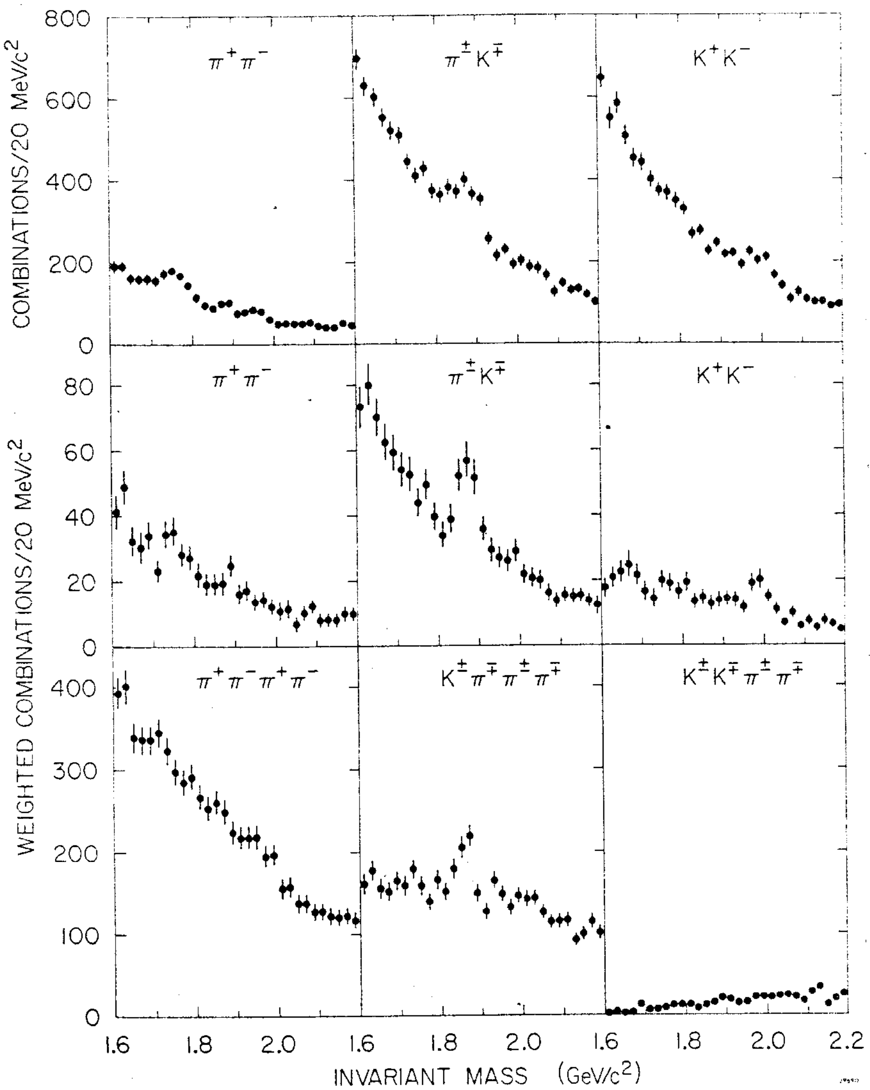

Fig. 53.

Invariant mass spectra for neutral combinations of two, and four charged particles; (a-c) arbitrary assignment of masses to both tracks; (d-f) same as above, but each pair is weighted by the probability for the particular mass assignment; (g-h) weighted four-particle masses.[73] Data recorded at c.m. energy of 3.9 - 4.6 GeV.

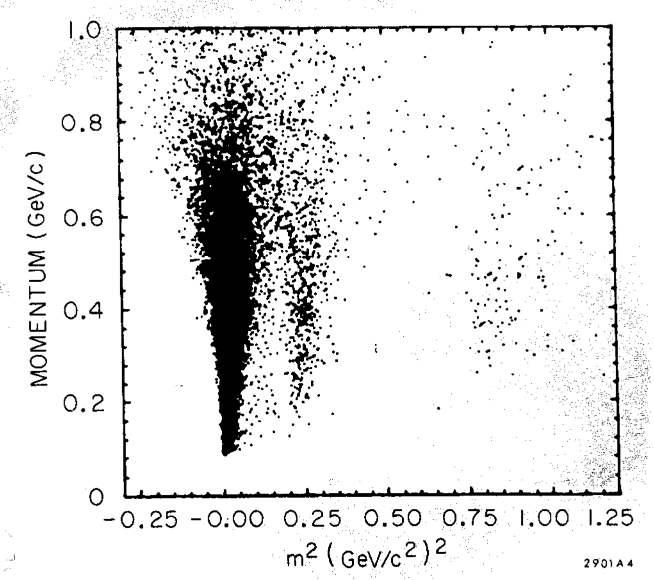

Fig. 54. Square of the particle mass as derived from the time of flight as a function of the particle momentum (SLAC-LBL magnetic detector).

weight assigned to all $\pi\pi$, $K\pi$, and KK combinations equals the number of two-body combinations and no double-counting occurs.

Invariant mass spectra weighted by the above procedure are presented in Fig. 53d-f. The $K\pi$ hypothesis with a peak at 1.87 GeV/c^2 is clearly preferred over either $\pi^+\pi^-$ or K^+K^-. The small peaks in the $\pi^+\pi^-$ and K^+K^- channels are consistent with the entire signal being $K\pi$ and the resulting misidentification expected from the flight time measurement. The estimated confidence level for the signal to arise only from $\pi^+\pi^-$ or K^+K^- is less than 1%. No signal occurs in the corresponding doubly charged channels. Figure 53g-i shows similarly weighted spectra for neutral combinations of a charged K and three charged pions. Here the K-π separation by time of flight is better because the particle momenta are smaller and consequently the only significant peak is observed in the $K^{\pm}\pi^{\mp}\pi^+\pi^-$ channel at a mass of 1.86 GeV/c^2. Again, there is no signal in the corresponding doubly charged channels.

To determine the masses and widths of the peaks in the Kπ and K3π mass spectra, the data were fitted to a Gaussian for the peak and linear and quadratic background terms under various conditions of bin size, event selection criteria, and kinematic cuts. Masses for the Kπ signal center at 1870 MeV/c^2; those for the K3π signal center at 1860 MeV/c^2. The widths obtained by these fits agree with those expected from experimental resolution alone. Systematic errors in momentum measurement are estimated to contribute a ±10 MeV/c^2 uncertainty in the absolute mass determination, and can account for the 10 MeV/c^2 mass difference between the Kπ and K3π systems; thus, both signals are consistent with being decays of the same state. The mass resolution leads to a 90% confidence level upper limit of 40 MeV/c^2 for the decay width of this state.

A study of the recoil mass spectra associated with these peaks shows evidence that this new state is produced in association with particles of comparable or even higher masses. The absence of any signal in the very large sample of data recorded at the ψ(3684) resonance indicates that there is a threshold for the production of these new states right below 4 GeV.[73]

In order to study this new state in more detail, the SLAC-LBL group has subsequently collected some 20,000 hadronic events at a fixed c.m. energy of 4.03 GeV. This particular energy was chosen because it corresponds to the maximum value of R in total hadron production. Preliminary results were presented at the Tbilisi Conference this summer,[74] others are ready for publication.[75, 76, 77]

For these new data the signal in the $K^{\pm}\pi^{\mp}$ mass distribution stands out very clearly above a small background as shown in Fig. 55. These new data revealed a third decay mode of the neutral state, namely to $K^o\pi^+\pi^-$. The evidence, 49 ± 13 events above

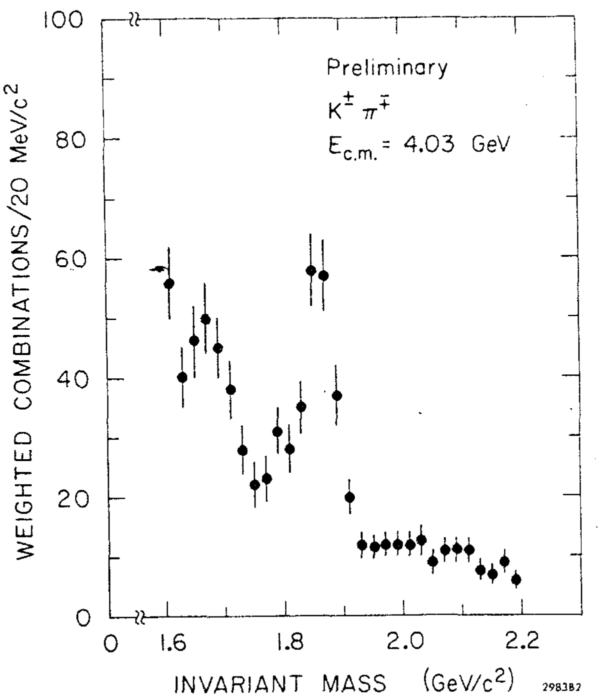

Fig. 55. Weighted invariant mass distribution for $K^{\mp}\pi^{\pm}$ for recent data recorded at 4.03 GeV.(74)

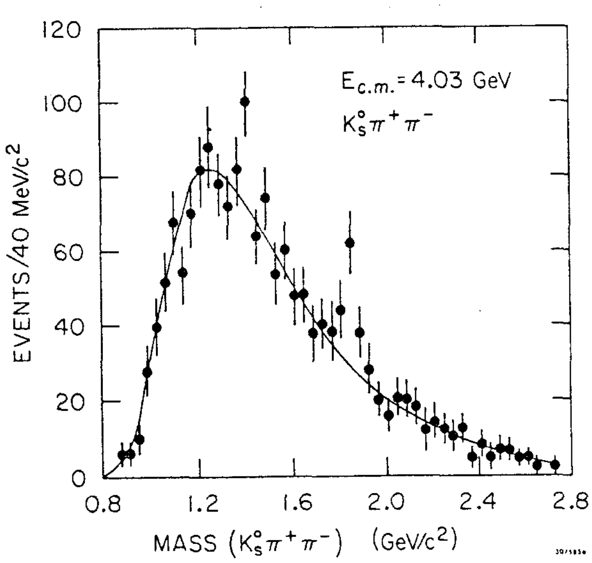

Fig. 56. Effective mass for $K^0\pi^+\pi^-$ at 4.03 GeV.

background, is presented in Fig. 56. In addition to the signal near 1.87 GeV, there appears to be an excess of events in the region of the K*(1420).

All properties of the neutral state at 1865 ± 15 MeV discussed so far—decay modes involving K mesons, the narrow widths, and the threshold near 4 GeV—are features expected for a meson carrying the new quantum number charm. However, if this state is taken to be the charmed pseudoscalar D^0 or the charmed vector D^{0*} it must have a charged partner $D^{\pm}$ or $D^{\pm *}$. In order to search for it the invariant mass spectra for systems of a charged kaon and two charged pions have been studied. $(K\pi\pi)^{\pm}$ states can be divided into two classes: 'nonexotic' combinations of the form $K^{\pm}\pi^+\pi^-$ (like K* decays) where the charge and strangeness is determined by the $K^{\pm}$, and 'exotic' combinations like $K^{\pm}\pi^{\mp}\pi^{\mp}$ that cannot be formed from a single quark-antiquark pair.

The invariant mass spectra for both $K\pi\pi$ states are given in Fig. 57. Again the distributions have been weighted by their time of flight likelihood, but contrary to the $K\pi$ spectra, the average momenta are sufficiently low to allow a much cleaner kaon identification. There is a significant ($>5\sigma$) peak in the $K^{\pm}\pi^{\mp}\pi^{\mp}$ spectrum, while no signal is present in the $K^{\pm}\pi^+\pi^-$ spectrum. A fit to the exotic mass distribution determines the mass of the state as 1876 ± 15 MeV/c^2 (systematic errors included) and sets an upper limit of 40 MeV/c^2 (90% confidence level) for the full

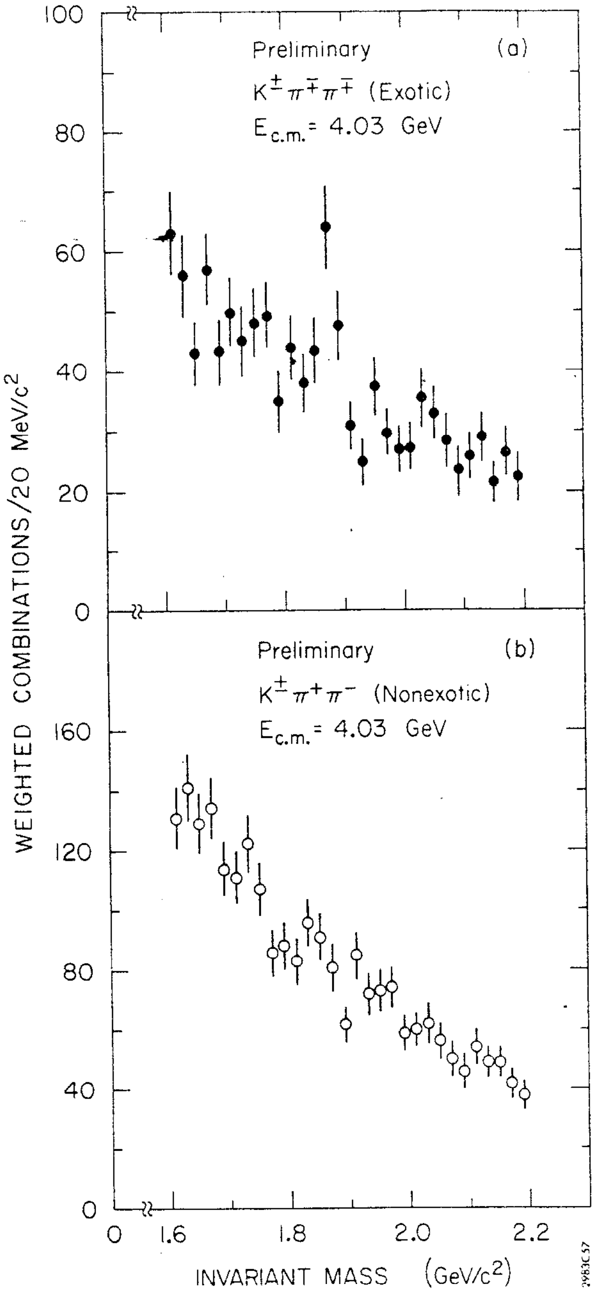

Fig. 57. Weighted distributions for invariant mass of (a) $K^{\pm}\pi^{\mp}\pi^{\mp}$ and (b) $K^{\pm}\pi^{+}\pi^{-}$ [75] at 4.03 GeV.

decay width. As pointed out above, this observation fits exactly the picture drawn by theory of weak interaction, and proves that the observed peaks cannot be interpreted as high mass K* resonances. We shall therefore use the nomenclature proposed for charmed mesons,[78] namely D^o, D^+ for the lowest lying states, and D^{o*}, D^{+*} for the first excited states, though experimentally the spins are still unknown.

At present, the systematic uncertainties in the measured rates are very large. Roughly speaking, the values for the product of the production cross section and branching ratio for the three observed decay modes of the neutral state and the 'exotic' decay of the charged state fall between 0.25 and 1.0 nb each. This is to be compared to a total hadronic cross section of 33 ± 5 nb at this energy.

III. Recoil Mass Spectra

Using the more recent data with increased statistics, the SLAC-LBL group has been studying the mass spectra recoiling against D^o and $D^{\pm}$.[74, 76] The earlier data had shown an enhancement, possibly with unresolved structure, at 2.0 - 2.2 GeV in the spectrum of the mass recoiling against the D^o. The interpretation of this was complicated by the fact that the data were collected over a wide range of c.m. energies. Now a substantial amount of data exists at 4.028 GeV and the results are presented in Figs. 58, 59. The spectrum of the mass recoiling against the D^o, $\bar{D}^o \rightarrow K^{\mp}\pi^{\pm}$ shows two large peaks above a smooth background, one near 2.01 GeV/c^2, the second centered at 2.15 GeV/c^2. There is only very marginal evidence, if any, for a peak at 1.87 GeV/c^2 corresponding to $D^0\bar{D}^0$ production. While the peak near 2.01 GeV/c^2 could most likely be due to the production of an excited state, usually referred to as $\bar{D}^{0*}$, in association with the $D^0(1865)$, the interpretation of the more impressive peak near 2.15 GeV/c^2 is ambiguous. It could represent another excited state at an even higher mass, or a kinematic reflection due to pair production of the D*(2010) object and the subsequent decay to $D^0(1865)\pi^0$. The recoil mass spectrum against $D^\pm \rightarrow K^\mp\pi^\pm\pi^\pm$ displays only a single peak near 2.01 GeV/c^2. The absence of the 2.15 GeV/c^2 enhancement could possibly be explained by phase space limitations caused by the larger mass of the charged D states.

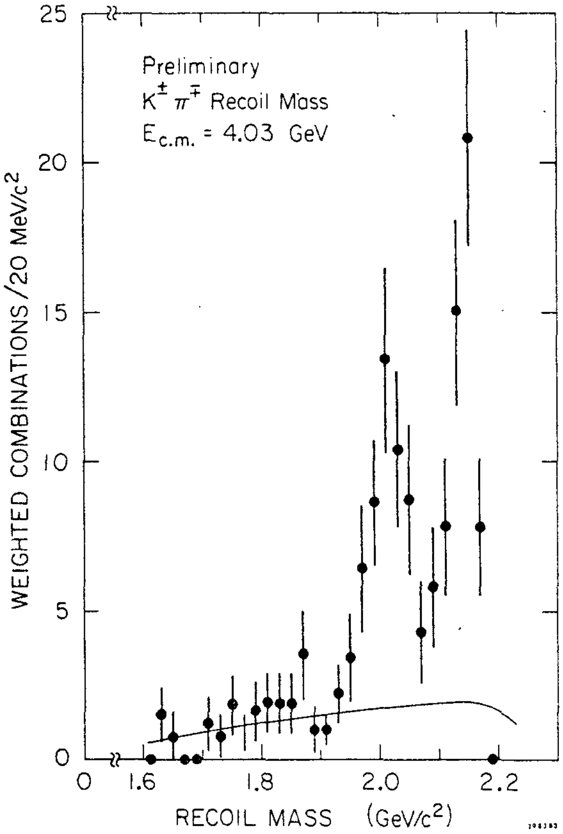

Fig. 58. Recoil mass against $K^\pm\pi^\mp$ peak data at 4.03 GeV.(74)

The key to the understanding of the observed recoil mass spectra is simple kinematics of a quasi-two-body system, including threshold, form factor, and spin effects, and the possibility of kinematic reflections.

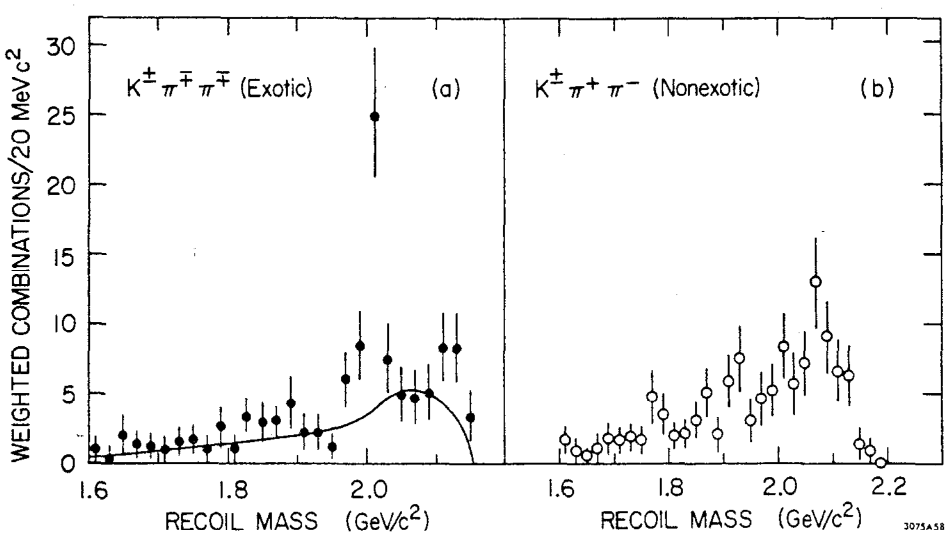

Fig. 59. Recoil mass at 4.03 GeV for $K^\pm\pi^\mp\pi^\mp$ and $K^\pm\pi^+\pi^-$ data.(74)

More explicitly, one assumes the existence of two states, D and D*, that can be produced in pairs at 4.028 GeV c.m. energy;

$$e^+e^- \rightarrow D\bar{D} \tag{1}$$

$$e^+e^- \rightarrow D\bar{D}^*\ , \quad \bar{D}D^* \tag{2}$$

$$e^+e^- \rightarrow D^*\bar{D}^*\ . \tag{3}$$

Furthermore, the D* state can decay to the D state via emission of a pion or a photon. There is a further possibility, the $D^o(1865)$ can arise from a charged D* through the decay $D^{\pm *} \rightarrow D^o\pi^{\pm}$. The kinematics of all these possible production mechanisms and decays are slightly different, allowing for a global analysis to determine the relative production rates of $D\bar{D}$, $D\bar{D}^*$, and $D^*\bar{D}^*$ and to accurately measure the masses of the D and D* mesons.

To be specific, let us consider a detected $D^o \rightarrow K^-\pi^+$ and study its recoil mass spectrum and, what is equivalent, its momentum spectrum. If the D^o is directly produced, it will have a unique momentum determined by the mass of the recoil particle. If the D^o originates from the decay of a D*, the observed D^o will have a spread in momentum, the width will depend on the Q-value in the decay of the D*. The Q-value is determined by the D*-D mass difference and the mass of the emitted particle, π or γ. Clearly, a small Q-value will lead to a very narrow spread in momentum, and likewise in the recoil mass. Schematic illustration of all possible systems recoiling against a detected D^o is given in Fig. 60. Here the decay mode $D^* \rightarrow \gamma D$ has not been taken into account. In Table IX the D^o momentum and the value of the mass recoiling against the observed D^o are calculated 4.028 GeV c.m. energy for the approximation of zero Q-value in the decay $D^* \rightarrow \pi D$. As can be seen from this table, the D^o momentum provides a better handle than the recoil mass to discriminate between the different sources of the observed D meson. The SLAC-LBL group is presently in the process of fitting the observed momentum spectrum to determine the masses of the D^o and D^{o*} and their relative production rates. Preliminary results indicate that the Q-value in the decay $D^{o*} \rightarrow \pi^o D^o$ is of the order of 3 MeV and the mass of the D* is approximately 2005 MeV/c^2. The decay rates for $D^* \rightarrow \gamma D^o$ and $D^* \rightarrow \pi^o D^o$ seem to be comparable. The uncertainty in the masses and the Q-value are

D°

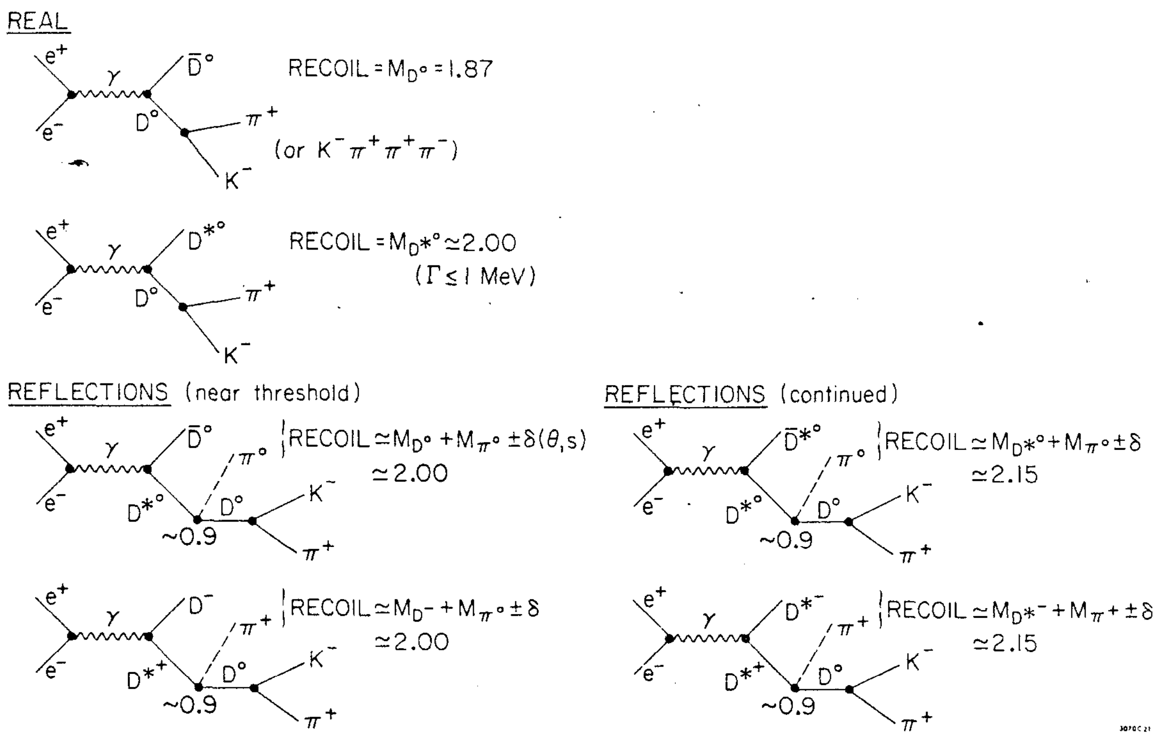

Fig. 60. Study of the mass recoiling against a D^0 meson produced according to reactions (1) - (3).

Table IX. Kinematics of D^0 production[79]
($M = 1.865$ GeV/c^2, $M^* = 2.005$ GeV/c^2, $\sqrt{s} = 4.028$ GeV)

Production	Momentum of D^0	Momentum (MeV/c)	Recoil Mass (GeV/c^2)
$D^0\bar{D}^0$	$p = \frac{1}{2}(s - 4M^2)^{1/2}$	760	1.865
$D^0\bar{D}^{0*}$	$p^{*2} = \frac{(s-(M^*+M)^2)(s-(M^*-M)^2)}{4s}$	558	2.005
$D^{*0}\bar{D}^0$ $\hookrightarrow \pi^0 D^0$	$\frac{M}{M^*} p^*$	519	2.027
$D^{*0}\bar{D}^{*0}$ $\hookrightarrow \pi^0 D^0$	$\frac{M}{M^*} \frac{(s-4M^{*2})^{1/2}}{2}$	177	2.148

presently of the order of a few MeV, most of the systematic uncertainties expected to be removed in the near future.[76]

IV. Parity Violation in D-Meson Decay

The proximity in mass and the decay properties of the charged and neutral state near 1870 MeV/c^2 suggest that they might be members of the same isospin multiplet. As such they are expected to have the same parity. In reminiscence of the famous θ-τ puzzle, one therefore looks for opposite parities in two decay modes. Since a $K\pi$ final state must have natural parity $P=(-1)^L$, a proof that the $K\pi\pi$ final state is inconsistent with natural spin parity implies a violation of parity in the decay. This then proves that the decay proceeds via weak interaction as expected for the lowest lying charmed mesons, the (D^+, D^o) isodoublet.

Recently, the SLAC-LBL collaboration[77] presented a study of the $K^{\pm}\pi^{\mp}\pi^{\mp}$ Dalitz plot. In this analysis a relatively clean sample of $K\pi\pi$ events was obtained by a cut on the recoil mass in addition to a cut on the invariant mass. Figure 61 shows the Dalitz plot (folded along the y-axis) for the exotic and the nonexotic $(K\pi\pi)^{\pm}$ final states selected by identical kinematical criteria. There are 126 events with an estimated background of 58 events in the $K^{\pm}\pi^{\mp}\pi^{\mp}$ data, compared to 112 events for the $K^{\pm}\pi^{+}\pi^{-}$ data. Both, the $K^{\pm}\pi^{\mp}\pi^{\mp}$ signal and the $K^{\pm}\pi^{+}\pi^{-}$ background, are consistent with a uniform population density.

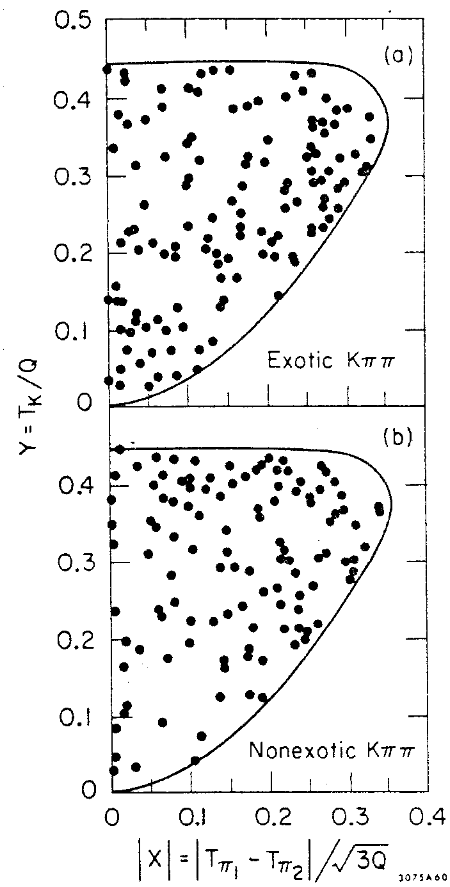

Fig. 61. Dalitz plots, folded around y-axis, for a cut in the $(K\pi\pi)^{\pm}$ mass in the region 1.86 - 1.92 GeV/c^2. Here Q is the sum of the kinetic energies (Ref. (77)).

To study the parity of the three particle system it is convenient to regard it as a dipion with angular momentum $\vec{\ell}$ and a kaon with angular momentum $\vec{L}$ relative to the $\pi\pi$ system. The total angular momentum is then $\vec{J} = \vec{\ell} + \vec{L}$, and the parity $P = -(-1)^J$. Consequently, for a spin zero system, one has $\vec{\ell} = -\vec{L}$ and $P=-1$, i.e., unnatural spin-parity. For $J \neq 0$, in general, all parity assignments are possible for a $K\pi\pi$ system. However, for natural spin-parity $(-1)^J$ of a state decaying to three pseudoscalars one expects a depopulation along the contour of the Dalitz plot. This follows from the fact that the kinematic boundary represents configurations where all three particles are emitted collinearly and their direction can therefore be specified by a single angle ϕ. The space wave function is given by the spherical harmonics $Y^J_m(\cos\phi)$, which has parity $(-1)^J$. Since the intrinsic parity of each particle is -1, the total parity for the collinear configuration is $(-1)^3(-1)^J = -(-1)^J$. Hence, a state of parity $(-1)^J$ cannot decay into a collinear configuration; in other words, the matrix element must vanish on the boundary of the Dalitz plot. For the case of a 1^- state one expects an additional zero along the y-axis, while in the case of 2^+ there is a higher order zero at the top.

In order to rule out the 1^- and 2^+ assignment for the $K\pi\pi$ final state, the observed distribution of events is compared to the matrix element calculated according to Zemach.(80) This analysis assumes that the distribution of events is not strongly influenced by rapidly varying form factors.

For $J^P=1^-$ the matrix element is constructed from an axial vector that is symmetric under exchange of the two pions. The intensity is essentially given by

$$I_{1^-} \propto |T_{\pi_1} - T_{\pi_2}|^2 \, |\vec{\pi} \times \vec{\pi}_2|^2$$

where $\vec{\pi}$ represents a pion momentum in the rest frame of the $K\pi\pi$ system, and T_π its kinetic energy. To compare the data with this distribution, the plot is divided by a contour of constant I_{1^-} into two regions, such that each of them would contain the same number of events for a phase space decay. Figures 62a, b show the $K^\pm\pi^\mp\pi^\mp$ invariant mass spectra for the two regions indicated by the shaded area in the respective inserts. A fit to a Gaussian resonance plus a background derived from the nonexotic events gives 34 ± 8 signal events in the peripheral region compared to 38 ± 9 in the central region. This is clearly consistent with a flat distribution (confidence level 75%) and rules out an enhancement of 8.2:1 of the central over the peripheral region as expected for a 1^- state.

For 2^+ decay the matrix element has the form of a traceless, second rank tensor which is symmetric under the exchange of the two pions. The intensity is given as

$$I_{2^+} \propto |\vec{\pi}_1 - \vec{\pi}_2|^2 \, |\vec{\pi}_1 \times \vec{\pi}_2|^2 \quad .$$

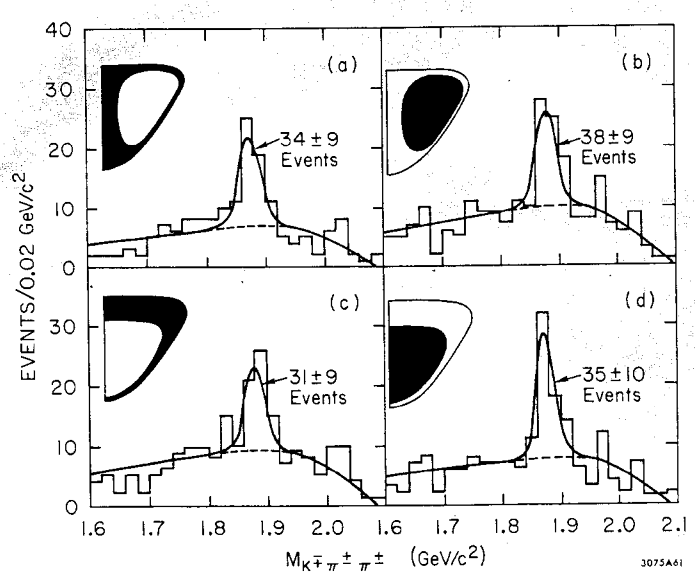

Fig. 62. Effective mass distributions for $K^{\mp}\pi^{\pm}\pi^{\pm}$ decays in (a) peripheral and (b) central region for a contour chosen by a 1^- matrix element; (c, d) same for 2^+ matrix element.[77]

Again, one chooses a contour of constant I_{2^+} to divide the Dalitz plot into two regions of equal population for a phase space decay. The matrix element for 2^+ depopulates the peripheral region relative to the central region by 1:5.6. The $K^{\pm}\pi^{\mp}\pi^{\mp}$ invariant mass spectra for the two Dalitz plot regions are given in Figs. 62c, d. The fits give 31 ± 9 events in the peripheral and 35 ± 10 events in the central region, again consistent with a flat distribution (confidence level 75%). The data prove the absence of a general depopulation along the kinematic boundary (confidence level 0.002) of the Dalitz plot.

In summary, the Dalitz plot distribution for the $K^{\pm}\pi^{\mp}\pi^{\mp}$ decay is incompatible with the zeros expected for spin parity 1^- and 2^+ and any state of natural spin parity. Since the decay $D^0 \rightarrow K^-\pi^+$ has a final state of natural spin parity, parity violation in the decay of the D is proven provided D^0 and $D^{\pm}$ are members of the same isospin multiplet. This implies that the decay occurs via weak interaction. The establishment of the spin of the D^0 as zero together with the observation of the decay modes $K^-\pi^+$ and $K_S^0\pi^+\pi^-$ would accomplish the proof of a weak decay without the assumption the D^0 and D^+ are in the same isomultiplet.

V. Evidence for Semileptonic Decays

Independent evidence for the fact that the D's decay weakly is provided by the observation of final states containing electrons and hadrons in the double-arm-spectrometer at DORIS.[1,54]

The DASP detector consists of two identical magnetic spectrometer arms covering a solid angle of 0.9 sr (cp. Lecture I). Electrons are identified twofold: a) by a signal from the freon-filled threshold Cerenkov counter mounted before the magnet and b) by the pulse height in the shower counters mounted in the rear. In addition to this minimum ionizing particle of at least 200 MeV/c momentum at least one additional non-showering charged particle in the central detector is required by the trigger. Data have been collected at c.m. energies between 3.9 GeV and 4.414 GeV, and below 3.68 GeV. There is a long list of conventional processes that can lead to final states containing electrons and hadrons. The following were considered by the DASP group:

1. Dalitz decays of π^o and η or pair conversion of photons,
2. misidentification of hadrons as electrons,
3. inelastic beam-gas scattering,
4. Compton scattering in the material in front of the Cerenkov counter,
5. semileptonic decays of pions and kaons,
6. two-photon processes of the form $e^+e^- \rightarrow e^+e^-$ + hadrons,
7. Cascade decay through an intermediate state with a large branching ratio to e^+e^- pairs.

Of the 28 electron-hadron events recorded in the interval 4.0 - 4.2 GeV at most 7 events can be accounted for by these sources, whereas below 3.68 GeV all observed events are consistent with this background. Aside from higher order electromagnetic processes (of which the 2γ interaction is the most likely), electron-hadron final states are produced only by weak interaction. The DASP group therefore interprets the data as evidence for the production of a new particle that decays via weak interaction. From the threshold-like behavior they conclude that the mass of this new particle must be between 1.8 GeV and 2.0 GeV.

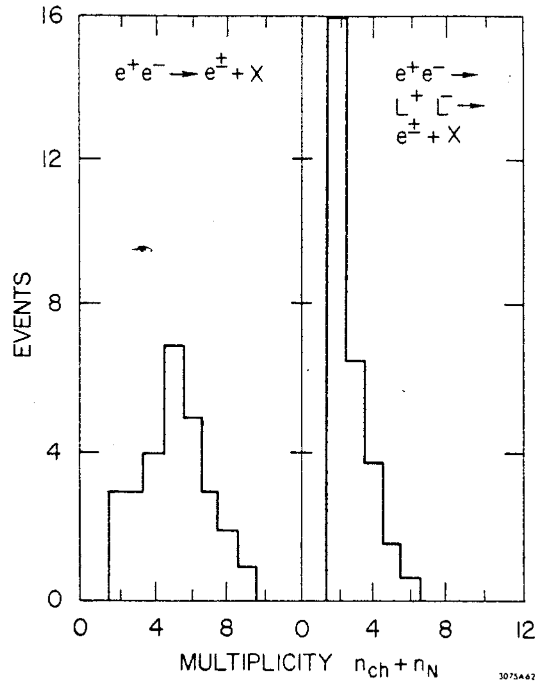

Fig. 63. Number of tracks per event in the reaction $e^+e^- \to e^\pm$ + hadrons; (a) measurement at 4.0 - 4.2 GeV,(1) (b) prediction from the decay of a heavy lepton using the same experimental acceptance.(81)

There are two different types of particles with large leptonic or semileptonic decay modes that could lead to final states containing leptons and hadrons, provided they are produced in pairs in e^+e^- annihilation. A heavy sequential lepton could decay either purely leptonically, $L^\pm \to \nu_e \nu_L e^\pm$, or semileptonically, $L^\pm \to \nu_L$ + hadrons. Alternatively, the production of a hadron that is inhibited by a conservation law for a new quantum number like charm from decaying via strong or electromagnetic interaction, would lead to electrons from semileptonic decays, $D^\pm \to e^\pm + \nu_e$ + hadrons. These two sources of events will give rise to different hadron and lepton multiplicities, and different lepton momentum spectra.

In Fig. 63a the number of detected particles, charged and neutral, per event is plotted. The distribution peaks at 5 tracks per events and only six events have less than four prongs. By comparison, the decay of a pair of heavy leptons would lead to much smaller multiplicities, as indicated by the result of a specific calculation(81) shown in Fig. 63b. The higher multiplicities are expected for the decay of a pair of heavy hadrons. Furthermore, inelastic production, contributing additional hadrons, is expected to be dominant at higher energies and should increase the multiplicity.

The difference in the decay modes is reflected as well in the momentum spectrum of the electrons. The corrected momentum spectrum for events with multiplicities $n \geq 4$ is given in Fig. 64a. This spectrum is very soft, in particular, there are no electrons with momenta above 700 MeV/c. For comparison, the distribution calculated from a (V-A) decay of a heavy lepton of mass 1.9 GeV/c^2 is presented. This curve has its average around 700 MeV/c, and is clearly inconsistent with the data.

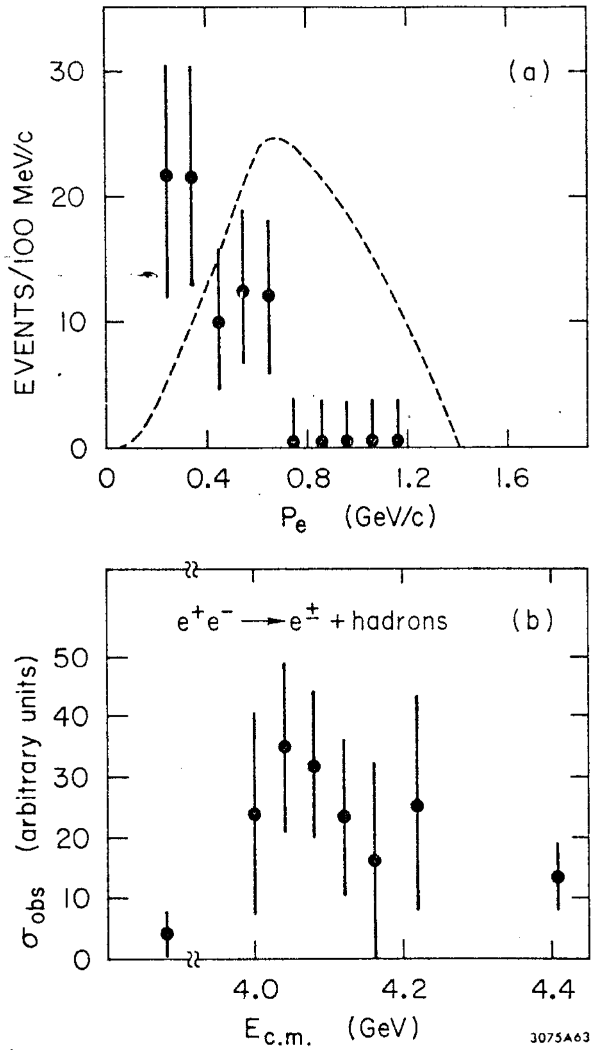

Fig. 64. $e^+e^- \to e$ + hadrons with multiplicity $n \geq 4$. (a) Acceptance corrected electron momentum spectrum. The curve illustrates the decay spectrum of a heavy lepton of 1.9 GeV mass. (b) Observed cross section vs. c.m. energy.[1]

The relative cross section for the production of electrons in large multiplicity events ($n \geq 4$) has been evaluated as a function of c.m. energy (Fig. 64b). There appears to be a threshold which coincides with the step in the total hadronic cross section around 4 GeV. Averaged over the interval 4.0 - 4.2 GeV the DASP group quotes a lower limit for the production of electron-hadron events of

$$\sigma(e^+e^- \to e^\pm + \text{hadrons})$$
$$= 2\,\text{BR}(D \to e^\pm + X) \cdot \sigma(e^+e^- \to D\bar{D})$$
$$> 1 \text{ nb}.$$

In summary, the soft electron spectrum and the high hadron multiplicity associated with the electron exclude the production and decay of a heavy lepton as the only source of these events. The measurements are at present in no way contradicting the observation of μe-events at SPEAR[28] at higher energies. These μe-events are characterized by a relatively hard lepton spectrum and hadron multiplicity zero, and fully agree with the features expected from the production of a heavy lepton. The most likely interpretation of the DASP data is in terms of a heavy hadron decaying semileptonically. It seems reasonable to associate these hadrons with the charmed mesons observed at SPEAR. This seems even more justified in the view of preliminary, though at this stage not fully convincing data on correlations between electrons and kaons. The DASP group observes an enhancement by two standard deviations of charged kaons in the electron data. The PLUTO group[82] confirms the soft electron spectrum near 4.05 GeV and claims a sharp peak in the inclusive $K_S e$ production rate at this energy.

VI. Summary

The study of hadron production by e^+e^- annihilation in the 4 GeV region, where the total hadron production increases dramatically, revealing rather prominent structures, is beginning to provide answers to some of the many questions it initially raised. New, narrow states, both charged and neutral, are produced with thresholds near and above 4 GeV. In particular, a charged state of mass 1876 ± 15 MeV/c^2 and a neutral state of 1865 ± 15 MeV/c^2 are now well established. Both states have narrow widths, consistent with decay rates typical for weakly decaying particles. All decay modes observed involve K mesons. The charged state is seen only in the exotic combination $K^{\pm}\pi^{\mp}\pi^{\mp}$ and not in the nonexotic combinations $K^{\pm}\pi^{+}\pi^{-}$ or any double charged mode. This strongly suggests that these states are the predicted isospin doublet of charmed mesons (D^+, D^o).

The observation of parity violation in the decay of these mesons proves that they decay weakly, as expected for states carrying the quantum number charm. The observation of electrons associated with large hadronic multiplicities is taken as evidence for semileptonic decays of these new states. All this is in striking agreement with the properties of charmed mesons proposed several years ago.[19]

But there are plenty of questions for the next generation of experiments. There is a whole new world of charmed particles to discover, starting with the F^+ meson, the $c\bar{s}$ state. All estimates place its mass near 2 GeV; it should decay to K^oK^+, $K^+K^-\pi^+$, etc. Its nonappearances may not yet be worrisome, but it would be nice to fill this gap in the spectroscopy of charmed mesons. The first charmed baryon with a mass of 2.25 GeV is presumably identified in the mode $\bar{\Lambda}\pi^+\pi^-\pi^-$. The study of charmed particles will open up new aspects of strong, electromagnetic and weak interactions of hadrons. In particular, the properties of the weak current, charged and neutral, are to be understood. An extremely interesting question that could be answered in the near future is the D^o-$\bar{D}^o$ mixing by study of the correlations between the charge of the K mesons observed in decays of D pairs.

Now that the existence of charm is no longer questioned, we are back to the question of how many basic hadronic constituents exist. Are four quarks and four leptons enough? There is already some evidence, though not completely convincing, for another charged lepton. How many more thresholds are waiting to be the uncovered as we go to higher and higher energies with the colliding beams of VEPP IV, PETRA and PEP?

Acknowledgments

I should like to express my gratitude to my Soviet colleagues and all members of the Organizing Committee of the Xth International School on High Energy Physics, in particular Dr. R. Mir-Kasimov, for making my visit to Baku such a pleasant experience.

I wish to thank all members of the SLAC-LBL collaboration who participated in the experiment at SPEAR for their many long hours and enthusiasm. All credit for the experimental data presented in these lectures should go to them. They designed and built the detector. They taught me most of the physics with its many interesting aspects during the past three years of my stay at SLAC. At present, the collaboration includes the following physicists: G. S. Abrams, M. S. Alam, A. M. Boyarski, M. Breidenbach, W. C. Carithers, W. Chinowsky, S. C. Cooper, R. G. DeVoe, J. M. Dorfan, G. J. Feldman, C. E. Friedberg, D. Fryberger, G. Goldhaber, G. Hanson, J. Jaros, A. D. Johnson, J. A. Kadyk, R. R. Larsen, D. Lüke, H. L. Lynch, R. J. Madaras, C. C. Morehouse, H. K. Nguyen, J. M. Paterson, M. L. Perl, I. Peruzzi, M. Piccolo, F. M. Pierre, T. P. Pun, P. Rapidis, B. Richter, B. Sadoulet, R. H. Schindler, R. F. Schwitters, J. Siegrist, W. Tanenbaum, G. H. Trilling, F. Vannucci, J. S. Whitaker, and J. E. Wiss. This list does not include the many people who maintained and operated the equipment; I cannot possibly thank them all individually, but I should like to commend the SPEAR operating staff for their excellent support.

I gratefully acknowledge the professional expertise and exceptional patience of the people in the group for illustrations and text editing at SLAC. They made this report possible.

REFERENCES

1. B. H. Wiik, Rapporteur's talk at the Int. Conf. on High Energy Physics, Tbilisi, 1976.
2. C. Bernardini et al., Nuovo Cim. 18, 1213 (1960).
3. M. Sands, Proc. Int. School of Physics, "Enrico Fermi", Course XLVI (Academic Press, New York, London, 1971), p. 257.
4. C. Pellegrini, Ann. Rev. Nucl. Sci., Vol. 22, 1 (1972).
5. A. N. Skrinsky, Particle Accelerator Conference, San Francisco, 1973, IEEE Trans. Nucl. Sci., NS20.3, 756.
6. Orsay Storage Ring Group, Proc. V. Int. Conf. High Energy Accel., Frascati, 1965, p. 271.
7. F. Amman et al., Proc. Int. Conf. High Energy Accel., Dubna, 1963, p. 249.
8. SPEAR Storage Ring Group, Proc. VIII Int. Conf. High Energy Accel., Geneva, 1971, p. 145.
9. DESY Storage Ring Group, Proc. IX Int. Conf. High Energy Accel., Stanford, 1974, p. 43.
10. D. Marin, Proc. IX Int. Conf. High Energy Accel., Stanford, 1974, p. 49.
11. PETRA Storage Ring Group, Proposal. DESY Internal Report (1974).
12. SLAC-LBL PEP Study Group, Stanford Linear Accelerator Center Report SLAC-171 (1975).
13. J.-E. Augustin et al., Phys. Rev. Lett. 34, 233 (1975).
14. B. H. Wiik, Proc. Int. Sym. on Lepton and Photon Interactions at High Energies, Stanford, 1975, p. 69.
15. R. P. Feynman, Photon-Hadron Interactions (W. A. Benjamin Inc., New York, 1972).
16. S. D. Drell and T. M. Yan, Phys. Rev. 187, 2159 (1969); Phys. Rev. D 1, 1617 (1970).
17. N. Cabbibo, G. Parisi, and M. Testa, Nuovo Cim. Lett. 4, 35 (1970).
18. M. Gell-Mann, Phys. Lett. 8, 214 (1964); G. Zweig, CERN preprint TH 401, 412 (1964).

19. J. D. Bjorken and S. L. Glashow, Phys. Lett. 11, 255 (1964); S. L. Glashow et al., Phys. Rev. D 2, 1285 (1970).

20. R. F. Schwitters and K. Strauch, Ann. Rev. Nucl. Sci., Vol. 26 (1976).

21. F. Ceradini et al., Phys. Lett. 42B, 401 (1972).

22. G. Cosme et al., Phys. Lett. 40B, 685 (1972).

23. L. M. Kurdadze et al., Phys. Lett. 42B, 515 (1972).

24. A. Litke et al., Phys. Rev. Lett. 30, 1189 (1973); G. Tarnopolsky et al., Phys. Rev. Lett. 32, 432 (1974).

25. R. F. Schwitters, Proc. 1975 Int. Symposium on Lepton-Photon Interactions at High Energies, Stanford, 1975, p. 5.

26. J.-E. Augustin et al., Phys. Rev. Lett. 34, 764 (1975).

27. J. Siegrist et al., Phys. Rev. Lett. 36, 700 (1975).

28. M. L. Perl et al., Phys. Rev. Lett. 35, 1489 (1975); M. L. Perl et al., Phys. Lett. 63B, 466 (1976).

29. J. Whitmore, Phys. Reports 10C, 273 (1974).

30. J. D. Bjorken, Phys. Rev. 179, 1547 (1969).

31. V. N. Baier, Proc. Int. School of Physics, "Enrico Fermi", Course XLVI (Academic Press, New York, London, 1971).

32. J. D. Jackson, Rev. Mod. Phys. 48, 417 (1976).

33. J. D. Bjorken, private communication.

34. G. Hanson et al., Phys. Rev. Lett. 35, 1609 (1975); G. Hanson, Invited talk at the Int. Conf. High Energy Physics, Tbilisi, 1976.

35. J. D. Bjorken and S. J. Brodsky, Phys. Rev. D 1, 1416 (1970).

36. A. M. Boyarski et al., Phys. Rev. Lett. 34, 1764 (1975).

37. V. Lüth et al., Phys. Rev. Lett. 35, 1124 (1975).

38. D. R. Yennie, Phys. Rev. Lett. 34, 239 (1975); Y. S. Tsai, Stanford Linear Accelerator Center preprint SLAC-PUB-1515 (1975).

39. W. Braunschweig et al., Phys. Lett. 56B, 491 (1975); L. Criegee et al., DESY preprint 75-32 (1975).

40. R. Baldini-Celio et al., Phys. Lett. 58B, 471 (1975); B. Esposito et al., Lett. Nuovo Cim. 14, 73 (1975).

41. A. M. Boyarski et al., Phys. Rev. Lett. 34, 762 (1975); M. Breidenbach et al., to be published.

42. V. M. Aulchenko et al., Novosibirsk 75-65; V. A. Siderov, Invited talk at the Int. Conf. on High Energy Physics, Tbilisi, 1976.

43. C. Bacci et al., Phys. Lett. 58B, 481 (1975); B. Esposito et al., Phys. Lett. 58B, 478 (1975).

44. D. C. Hom, Phys. Rev. Lett. 36, 1236 (1976); D. Eartly et al., Phys. Rev. Lett. 36, 1355 (1976).

45. H. D. Snyder et al., Phys. Rev. Lett. 36, 1415 (1976).

46. J. D. Jackson, Lectures given at the SLAC Summer Institute, 1976.

47. B. Jean-Marie et al., Phys. Rev. Lett. 36, 291 (1976).

48. W. Braunschweig et al., Phys. Lett. 63B, 487 (1976).

49. W. Bartel et al., DESY preprint 76-40 (1976); W. Bartel et al., Contribution to Int. Conf. High Energy Physics, Tbilisi, 1976.

50. SLAC-LBL Collaboration, unpublished. V. Lüth, Proc. of Int. Conference for High Energy Physics, Palermo, 1975, p. 54.

51. V. Gupta and R. Kögerler, Phys. Lett. 56B, 473 (1975).

52. F. Vannucci et al., to be published in Phys. Rev, SLAC-PUB-1862 (1976).

53. S. Okubo, Phys. Lett. 5, 165 (1963); G. Zweig, CERN preprint TH 401, 412 (1964).

54. H. U. Martyn, Contribution to the Int. Conf. High Energy Physics, Tbilisi, 1976.

55. H. Harari, Phys. Lett. 60B, 172 (1976); T. F. Walsh, Nuovo Cim. Lett. 14, 290 (1975); R. N. Cahn and M. S. Chanowitz, Phys. Lett. 59B, 277 (1975).

56. I. M. Shmushkevich, Dokl. Akad. Nauk. SSSR 103, 235 (1955).

57. I. Peruzzi et al., to be published.

58. G. S. Abrams et al., Phys. Rev. Lett. 34, 1177 (1975).

59. W. Tanenbaum, J. S. Whitaker et al., Phys. Rev. Lett. 35, 1328 (1975).

60. W. Tanenbaum et al., Phys. Rev. Lett. 36, 402 (1976).

61. J. S. Whitaker, W. Tanenbaum et al., submitted to Phys. Rev. Lett. (1976).

62. D. H. Badtke et al., submitted to Int. Conf. High Energy Physics, Tbilisi, 1976.

63. W. Braunschweig et al., Phys. Lett. 57B, 407 (1975).

64. G. J. Feldman et al., Phys. Rev. Lett. 35, 821 (1975).

65. G. H. Trilling et al., to be published; F. Pierre et al., submitted to Int. Conf. High Energy Physics, Tbilisi, 1976.

66. B. H. Wiik, Proc. 1975 Int. Symposium on Lepton-Photon Interactions at High Energies, Stanford, 1975, p. 69; J. Heintze, ibid., p. 97.

67. M. S. Chanowitz and F. J. Gilman, Stanford Linear Accelerator Center preprint SLAC-PUB-1746 (1976).

68. J. Pumplin, W. Repko, and A. Sato, Phys. Rev. Lett. 35, 1538 (1975); H. J. Schnitzer, Phys. Rev. Lett. 35, 1540 (1975).

69. A. B. Henrigues, B. H. Kellett, and R. G. Moorhouse, Phys. Lett. 64B, 85 (1975).

70. H. J. Schnitzer, Brandeis University preprint (1976).

71. H. Harari, CERN TH 2222 (1976).

72. E. B. Hughes et al., Phys. Rev. Lett. 36, 76 (1976).

73. G. Goldhaber, F. Pierre et al., Phys. Rev. Lett. 37, 255 (1976).

74. R. F. Schwitters, Rapporteur's talk at the Int. Conf. on High Energy Physics, Tbilisi, 1976 (SLAC-PUB-1832).

75. I. Peruzzi, M. Piccolo et al., Phys. Rev. Lett. 37, 569 (1976).

76. R. F. Schwitters, Talk presented at the APS Conference at BNL (1976).

77. J. E. Wiss, G. Goldhaber et al., submitted to Phys. Rev. Lett. (1976).

78. M. K. Gaillard, B. W. Lee, and J. L. Rosner, Rev. Mod. Phys. 47, 277 (1975).

79. F. J. Gilman, Talk presented at the APS Conference at BNL (1976).

80. C. Zemach, Phys. Rev. B 133, 1201 (1964).

81. Y. I. Azimov, L. L. Frankfurt, and V. A. Khose, Leningrad Nucl. Phys. Inst. Preprint 245 (1976).

82. J. Burmester et al., DESY report 76/50 (1976).